




Deliverable 2.4: Algorithms providing effects of array changes on economics

Lead partner:	WavEC Offshore Renewables
Contributing partners:	Aalborg University, IT Power Ltd., University College Cork, University of Edinburgh, France Energy Marines, Sandia National Labs
Authors:	Marta Silva, Alex Raventos, Boris Teillant (WavEC) Francesco Ferri (AAU) Thomas Roc, Ned Minns (IT Power) Chris Chartrand, Jesse Roberts (Sandia) Jean François Filipot (FEM)

	<p>DTOcean - "Optimal Design Tools for Ocean Energy Arrays" is funded by the European Commission's 7th Framework Programme.</p> <p>Grant agreement number: 608597</p>
---	--

D2.4: Algorithms providing effects of array changes on economics

Project: DTOcean - Optimal Design Tools for Ocean Energy Arrays

Code: DTO_WP2_ECD_D2.4

	Name	Date
Prepared	WavEC	17/09/15
Checked		
Approved		

The research leading to these results has received funding from the European Community's Seventh Framework Programme under grant agreement No. 608597 (DTOcean).

No part of this publication may be reproduced, stored in a retrieval system, or transmitted in any form – electronic, mechanical, photocopy or otherwise without the express permission of the copyright holders.

This report is distributed subject to the condition that it shall not, by way of trade or otherwise, be lent, re-sold, hired-out or otherwise circulated without the publishers' prior consent in any form of binding or cover other than that in which it is published and without a similar condition including this condition being imposed on the subsequent purchaser.

DOCUMENT CHANGES RECORD			
<i>Edit./Rev.</i>	<i>Date</i>	<i>Chapters</i>	<i>Reason for change</i>
A/0	15/07/2015	All	New Document – Outline
A/1	17/09/2015	All	Full document sent to Quality Review
A/2	24/09/2015	All	Full document prepared for EC submission

ABSTRACT

This report presents Deliverable 2.4 (Algorithms providing effects of array changes on economics) which details the algorithms for implementation of the effects of array changes on device cost. It also describes the overall methodology to determine the LCOE as calculated in the DTOcean tool.

The main findings of Deliverable 2.3 (Algorithms providing effects of array changes on performance) are also presented in this deliverable as the energy production has an important role on the LCOE calculation.

This document strongly focuses on the impact of array changes on the LCOE.

Two case studies are also presented to illustrate these interactions.

TABLE OF CONTENTS

<i>Chapter</i>	<i>Description</i>	<i>Page</i>
Abstract		4
1	Introduction	9
2	State-of-the-art analysis of economic assessment of marine renewable energy arrays	10
2.1	The choice of the LCOE indicator for DTOcean	10
2.2	Economic assessment in the energy industry	15
2.2.1	Economic assessment of wave energy converters	18
2.2.2	Economic assessment of tidal energy converters	20
3	Methodology for the LCOE calculation in the DTOcean tool	22
3.1	Overview of the LCOE calculation in the DTOcean tool	22
3.2	Methodology for the cost calculation in the DTOcean tool	25
3.2.1	Cost variations due to array changes	26
3.3	Methodology for the energy output calculation in the DTOcean tool	29
3.3.1	Optimization routine	30
3.3.2	Wave hydrodynamics and array energy output calculation	32
3.3.3	Tidal hydrodynamics and array energy output calculation	43
3.3.4	Functionality testing and verification	61
3.3.5	Note on the losses across WP3-6 to apply on the results from WP2	61
4	Simplified analysis of energy output and LCOE variation with array changes	63
4.1	Wave: Scenario 3: Aegir Shetland Wave Farm	63
4.1.1	Scenario Description	63
4.1.2	Energy output variations due to array changes	67
4.1.3	Simplified LCOE variations due to array changes	70
4.2	Tidal: Scenario 5: Sound of Islay	72
4.2.1	Scenario Description	72
4.2.2	Energy output variations due to array changes	76
4.2.3	Simplified LCOE variations due to array changes	79
5	Summary	82
	References	83

TABLES INDEX

<i>Description</i>	<i>Page</i>
Table 2.1: Estimated discount rates for different technologies and perceived risk	13
Table 2.2: Summary of economic data for ocean energy arrays averaged for each stage of deployment	17
Table 3.1 Cost and energy production implications in the DTOcean computational modules	23
Table 3.2: Array layout types and descriptive parameters	30
Table 3.3: Limitations on the wave submodel stemming from the assumptions made on the theoretical formulation.....	41
Table 3.4: Weighting values for Figure 3.17	53
Table 3.5: Thrust coefficients measured by experimentalists compared to the velocity backed out value.	55
Table 4.1: Pelamis dimensions	64
Table 4.2. Power produced in kW by the Pelamis for different sea state conditions defined by T_e and H_s	65
Table 4.3. Coordinates of the 5-nodes delimiting the lease area for Scenario 3.....	65
Table 4.4: Energy output for all cases in Scenario 3	69
Table 4.5. HS1000 turbine's dimensions.	73
Table 4.6. Coordinates for the 5-nodes delimiting the lease area for Scenario 5.	74
Table 4.7: Energy output for all cases in Scenario 5	79

FIGURES INDEX

<i>Description</i>	<i>Page</i>
Figure 2.1: Relative LCOE for different project durations	11
Figure 2.2: Range of discount rates for different company and project profiles	12
Figure 2.3: Risk component of the discount rate	12
Figure 2.4: U.S. Average Levelized Costs for Plants Entering Service in 2020.....	15
Figure 2.5. Observed learning curves in energy Technologies	16
Figure 2.6: LCOE predictions for wave and tidal energy, starting at 10MW arrays after 10MW have been previously installed	16
Figure 2.7: LCOE evolution at the three stages based on developer responses and reference international analysis	18
Figure 2.8: Wave LCOE Percentage Breakdown by Cost Centre Values at Current Stage of Deployment (Left) and the Commercial Target (Right)	19
Figure 2.9: Trade-off between cost of energy and distance to shore for a specific example in the UK	19
Figure 2.10: Tidal energy LCOE Ranges at Differing Stages of Deployment.....	20
Figure 2.11: Tidal LCOE Percentage Breakdown by Cost Centre Values at Current Stage of Deployment (Left) and the Commercial Target (Right).	20
Figure 3.1: Flow-chart structure of the DTOcean software environment	22
Figure 3.2: Schematic overview of the LCOE calculation in the DTOcean tool.....	24
Figure 3.3: Global Spot Steel Price Index Jan '05-Oct '09.....	26
Figure 3.4: Equipment Price Index	27
Figure 3.5: WP2 algorithm overview.....	29
Figure 3.6: Sketch of the array layout parameters listed in Table 3.2.....	31
Figure 3.7: Theoretical directional spectrum for the ISSC spectrum with 0.1 m significant wave height and 1.0 s peak period.	33
Figure 3.8: ketch of the local cylindrical coordinates for two WECs and the geometrical relationships between them (39) ..	36
Figure 3.9: Wave submodel algorithm	40
Figure 3.10: Software architecture for the WP2 Tidal model - conceptual diagram	43
Figure 3.11: u and v time series (18.55 days) from ADCP data collected over a French tidal site.....	45
Figure 3.12: Probability density function $p(u,v)$ corresponding the time series displayed in Figure 3.11.....	46
Figure 3.13: The 10 probability density functions $p(u,v)$ used to estimate the velocity v_s as described in.	47
Figure 3.14: CEC wake results from OpenFOAM.	51
Figure 3.15: CEC wake results using OpenFOAM.	51
Figure 3.16: CEC wake results using OpenFOAM.	52
Figure 3.17: Example of the parametric interpolated solution.	53
Figure 3.18: Parametric CFD model results.	54
Figure 3.19: C_T vs. wake velocity/velocity deficit according to momentum theory.	55
Figure 3.20: Iso-lines where wake velocity equals 95% of inflow velocity from axi-symmetric CFD simulations.....	56

Figure 3.21: Second order curve fit for 95% recovery distance vs. blockage ratio.	57
Figure 3.22: Normalized second order fit of 95% recovery vs blockage ratio.	57
Figure 3.23: Iso-lines where wake velocity equals 90% of inflow velocity from 3D CFD simulations.....	58
Figure 4.1: (Top) Pelamis in operation at the EMEC test site. (Bottom) simplified model of the Pelamis with description of the generalised degree of freedom.....	63
Figure 4.2: Lease area for Scenario 3. The lease area corresponds to the inner region delimited by the red line.....	66
Figure 4.3: Bathymetry for Scenario 3. 3D representation of the seabed surface.	67
Figure 4.4: Array layouts for Scenario 3	68
Figure 4.5: Device Production Variation, normalized to the average production	69
Figure 4.6: Average energy output per device	69
Figure 4.7: Total lifetime costs for Scenario 3	70
Figure 4.8: Capex and Opex distribution for Scenario 3.....	70
Figure 4.9: LCOE variation	71
Figure 4.10: LCOE variation for different availability/energy output cases	71
Figure 4.11: Andritz Hydro Hammerfest HS1000	72
Figure 4.12: Sound of Islay lease area.....	74
Figure 4.13: Sound of Islay lease area.....	75
Figure 4.14: Array layout for Scenario 5.....	76
Figure 4.15: Wake distribution (left) and energy production per device (right), with layout representation for Scenario 5, case 20 devices	77
Figure 4.16: Device Production Variation, normalized to the average production	78
Figure 4.17: Average energy output per device.....	78
Figure 4.18: Total Lifecycle costs for Scenario 5.....	79
Figure 4.19: Capex and Opex distribution for Scenario 5.....	80
Figure 4.20: LCOE variation	80
Figure 4.21: LCOE variation for different availability/energy output cases	81

1 INTRODUCTION

DTOcean is a European funded research project that aims to develop a suite of shared-access numerical design tools for wave and tidal energy arrays. Within the framework of Work Package 2 a module simulating the hydrodynamic interactions between devices in an array is being programmed. This module primary aim is to find the optimal number of devices to be deployed while minimising the losses due to hydrodynamic interactions. Constraints associated with the leasing agreement typically shape the optimization domain, although other work packages/modules will be able to provide further no-go areas to the lease area.

Deliverable 2.4 reports the key outcomes of two tasks necessary towards the delivery of WP2 module: task 2.4 concerns the development of algorithms providing the effects of array changes on the power production, and task 2.5 deals with the development of algorithms providing the device cost dependency on array changes.¹

The main goal of the present document is to disclose the key aspects underlying the development of the algorithms providing the power production and cost device dependency on array changes. In other words, it consists of describing the methodology for the implementation of these algorithms as well as illustrating their use through simple case studies.

While preliminary results generated by WP2 algorithms are included in this report, advanced functional testing and verification of the whole WP2 module is outside the scope of Deliverable 2.4. The overriding objective of the case studies is limited to having initial sensitivity analysis allowing the measure of the impacts of device costs and energy production due to array changes.

Deliverable 2.4 kicks off with a state-of-the-art analysis of the economic assessment of Marine Renewable Energy (MRE, which includes wave and tidal energy converters) arrays in chapter 2. Subsequently, chapter 3 details the methodology for the development of the algorithms carried out in tasks 2.4 and 2.5 on the one hand, and expose the preliminary results provided by these algorithms, on the other hand.

¹ It should be noted here that Deliverable 2.4 partially depicts the algorithms that form Deliverable 2.3. Since the latest Deliverable 2.3 actually corresponds to the code itself, it was decided to keep record of these algorithms in a written format inside Deliverable 2.4, which ultimately forms a more comprehensive overview of WP2 module than just focusing on the device costs issue.

2 STATE-OF-THE-ART ANALYSIS OF ECONOMIC ASSESSMENT OF MARINE RENEWABLE ENERGY ARRAYS

2.1 THE CHOICE OF THE LCOE INDICATOR FOR DTOCEAN

The electricity generated by marine energy arrays will be fed into the main grid and can be bought, sold and traded as any other commodity. Prices in the electricity markets are based on the marginal cost, which is the cost of dispatching an additional unit of energy (usually in terms of €/MWh). Like other renewable energy technologies such as wind and solar, marine energy has low marginal costs (in fact, close to zero). Renewable energy resources are seemingly free when compared to fuel powered power plants, as there are no fuel expenditures associated. However, marine technologies require a higher initial investment and, in order to obtain an adequate return on investment, it is required to sell electricity at a higher average price than their marginal cost. Therefore, the marginal cost is not a good indicator to assess and compare the costs of energy technologies over their lifetime.

As indicated by the International Energy Agency (IEA), *the notion of levelized costs of electricity (LCOE) is a handy tool for comparing the unit costs of different technologies over their economic life. It would correspond to the cost of an investor assuming the certainty of production costs and the stability of electricity prices* (1).

Concretely, LCOE is defined as the total lifecycle costs (i.e., the sum of all capital costs and lifetime operation and maintenance costs, discounted to present value) divided by the electricity generation to grid accumulated throughout the technology's lifetime (also discounted to present value) (2). A common representation of this is shown in (2.1).

$$LCOE = \frac{\sum_{t=0}^n \frac{(Investment_t + O\&M_t + Fuel_t + Carbon_t + Decommissioning_t)}{(1+r)^t}}{\sum_{t=0}^n \frac{AEP_t}{(1+r)^t}} \quad (2.1)$$

LCOE = Levelized Cost of Energy

AEP_t = Annual electricity production (at year *t*)

r = Discount rate

n = Lifetime of the system

t = Project year, from the start of the project (year 0) to the final year of the project (year *n*)

This equation can be used for different energy systems, and other cost centres can be added as needed. For renewable energy systems, which have no fuel or carbon costs, it is common to simplify the equation down to:

- Investment costs, commonly called **CAPEX**: these are assumed to happen all in year 0, for the simplicity of the calculation. However this value can be adjusted to account the time it takes to develop a project. Investment costs can also be divided into procurement costs (cost of purchasing the elements in a project), installation costs and administrative costs.
- Operational costs, commonly called **OPEX**: all the cost incurred during the operational lifetime of the project. For more simple calculations these can be assumed as fixed rate throughout the lifetime of the project, sometimes expressed as a percentage of the CAPEX in less mature

technologies for which the operational costs are still subject to high uncertainty. However, operational costs are not fixed. There will be a part of fixed costs related to administrative and other recurrent costs, but maintenance operations, especially corrective ones, will have a variable element to the operational costs. Mid-life refit contribution to OPEX is comparable to that of planned or corrective maintenance (3), but happens once during the lifetime of the project. This means that there will be a period with significantly higher costs (and lower production).

- Decommissioning costs are sometimes included in the OPEX. However, like operational costs, in the case of less mature technologies, it may be hard to estimate the actual values for decommissioning, meaning that it is also common for these costs to be expressed as a percentage of CAPEX or of Installation costs. It is also common that decommissioning costs are not included, as due to the nature of the present value calculation, its impact on the LCOE is very small.

The impact of these cost centres in the LCOE is also a function of the lifetime of the project and the discount rate.

The chosen lifetime of the project has a big influence on the relative contribution of CAPEX and OPEX to the LCOE, as well as the value of LCOE itself. Shorter projects, such as prototype and technology demonstration ones, will have fewer production years to offset the high initial costs². Furthermore, the balance between CAPEX and OPEX will be skewed towards CAPEX. Typical values used in LCOE analysis for wave and tidal energy are between 15-25 years. First arrays are assumed to have a shorter duration, but the most common value found is 20 years (1; 3; 4; 5; 6; 7; 8).

To illustrate the influence of the project duration on the LCOE, the graph below shows the relative change in LCOE by changing the project duration, compared to a generic 20-year project³.

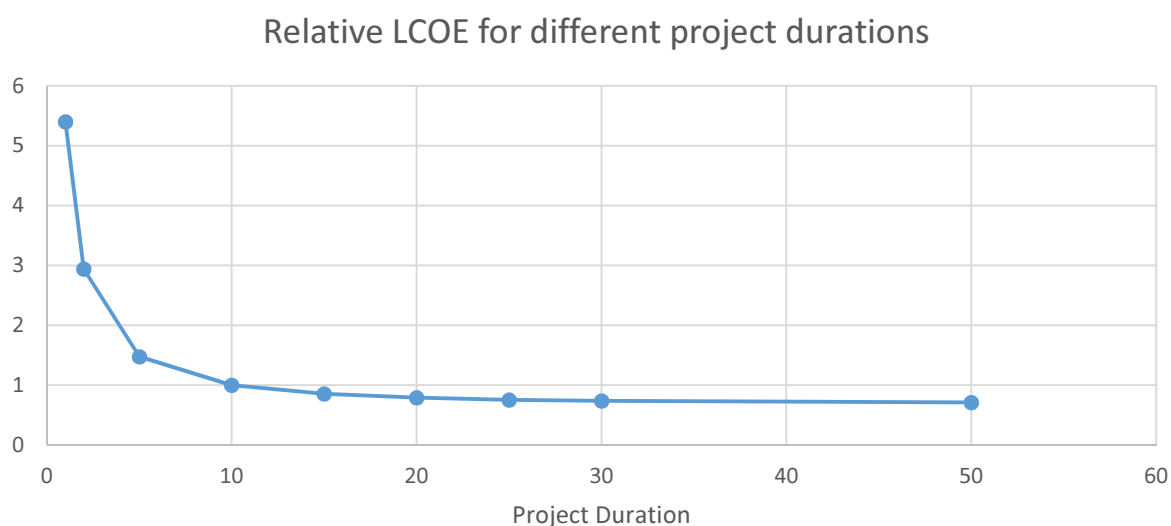


Figure 2.1: Relative LCOE for different project durations

² Even when neglecting that these projects have higher costs and lower efficiencies than what is expected for array projects.

³ Assuming a 10% discount rate

The discount rate is a measure of time-value, which is the price put on the time that an investor waits for a return on an investment. Furthermore, the discount rate is also used to account for the risks and uncertainties of an investment. For a specific project, the discount rate will be a product of the project developer's (or investors) desired return on investment⁴ (Figure 2.2) and the inherent risks of the project that will not only be related to the technology being deployed but also to the market it will be deployed in (see Figure 2.3) (2; 9; 10).

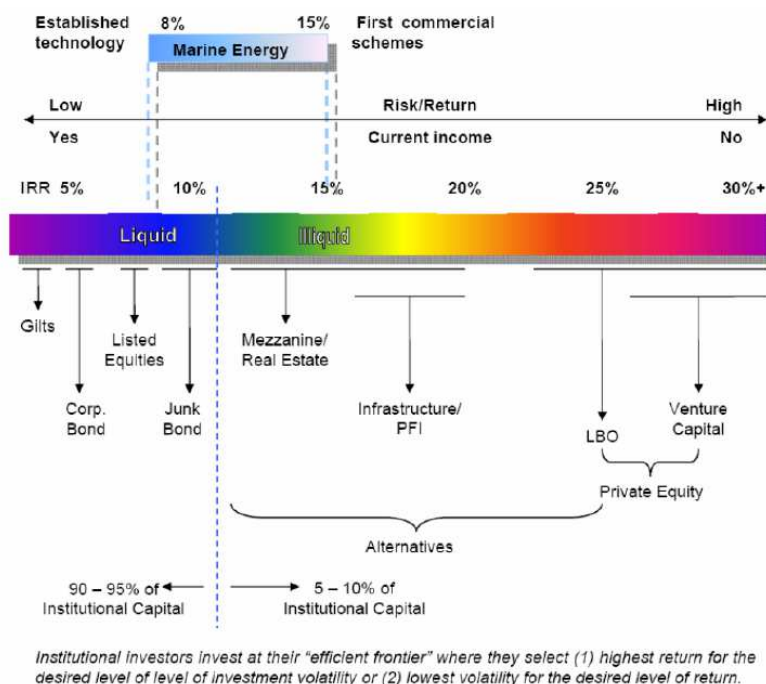


Figure 2.2: Range of discount rates for different company and project profiles (9)

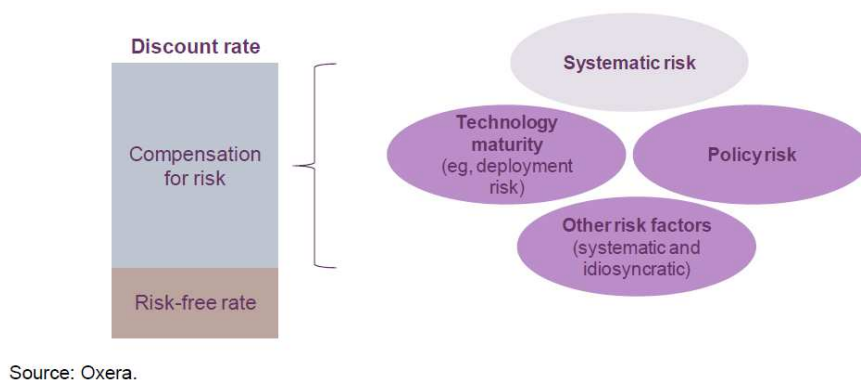


Figure 2.3: Risk component of the discount rate (10)

⁴ This is associated with the weighted average cost of capital (WACC), which determines how much the developer has to pay for others to supply the funds to advance the project. This can come from debt (the cost of capital is the interest rate), equity (with varying costs of capital depending on company profile) and from public funding (which may have a 0 cost of capital).

Higher discount rates penalise more heavily capital-intensive, low-carbon technologies due to their high upfront investment costs, and comparatively favour fossil-fuel technologies with higher operating costs but relatively lower investment costs (1). In terms of choosing a discount rate for a marine energy project, it means that the higher this rate is, the higher will be the CAPEX contribution to LCOE.

The table below shows estimates of discount rates for different technologies, as well as the perceived risk.

Table 2.1: Estimated discount rates for different technologies and perceived risk (10)

		Discount rate (real, pre-tax) (%)	
Technology	Risk perception	Low	High
Conventional generation			
CCGT	Low	6	9
Low-carbon and renewable generation			
Hydro ROR	Low	6	9
Solar PV	Low	6	9
Dedicated biogas (AD)	Low	7	10
Onshore wind	Low	7	10
Biomass	Medium	9	13
Nuclear (new build)	Medium	9	13
Offshore wind	Medium	10	14
Wave (fixed)	Medium	10	14
Tidal stream	High	12	17
Tidal barrage	High	12	17
CCS, coal	High	12	17
CCS, gas	High	12	17
Wave (floating)	High	13	18

Note: This table presents indicative ranges for the discount rate based on the assumptions and methodology described in this report.

Typical values of discount rate for marine energy projects range between 8-15% (4; 7; 9; 11; 12; 13), but in LCOE evolution analysis is typical to use values between 10% and 12% (3; 5; 14).

The different LCOE values for different energy technologies are due to not only different discount rates and inherent risk, but also because these have different cost breakdowns. While large conventional fossil-fuelled power plants require a relatively low initial investment (CAPEX) per MW installed compared to most renewable energy technologies, the operational costs (OPEX) are higher as they need to burn fuel to operate while wind, sun, wave or tides are free. Also, there are significant differences in the annual energy production per MW installed (depending on the plant capacity factor and availability). All these indicators are important but provide only partial information while the LCOE provides a better understanding of the overall economics of energy technologies.

Ultimately, in order to invest in a power plant and decide which is the best technology to install or optimize the array configuration, (private or public) investors will ask a certain level of return on investment⁵. This is achieved when the price at which the electricity is sold is equal or higher than the LCOE of the project they are investing on.

However, that is a simplified approach that disregards elements such as debt and taxes payments. To fully assess the financial attractiveness of a project, there are different metrics that can be used, such as:

- Net Present Value (NPV): The net present value is the sum of all the discounted cash-flows, throughout the lifetime of the project. It adds an element of revenues that is missing from the LCOE analysis, but uses the same principles of present value calculation. A NPV equal to 0 indicates that the project is at its break-even point, a positive value indicates it is an attractive investment.
- Internal Rate of Return (IRR): The internal rate of return is the value of the discount rate that needs to be used to achieve a NPV equal to 0. In other words, it's the discount rate necessary for the project to break even.
- Payback Period (PBP): The payback period is the time needed for the project to break even. It can be a simple PBP that does not use the discount rate (and thus ignores the time value of money), or a discounted PBP, using the discount rate.

To assess the attractiveness of a project, investors will look to have a positive NPV (and when comparing different opportunities, will choose the higher NPV), and shorter payback periods.

These metrics are not only dependent on the technology and array configuration but on national regulations (e.g. energy prices, feed-in tariffs, capital support, tax regimes, etc.) as well as how the project is financed.

DTOcean aims to develop a set of tools to optimize the design of marine energy arrays. In order to provide a simpler and more transparent tool it has been decided that the decisions should be based on the technology and site characteristics, but independently on regulatory and financial aspects, which vary for different countries, companies, etc. The relative neutrality of the LCOE with regards to the uncertain and volatile market environmental conditions can be seen as very attractive feature for array design optimisation purposes. Therefore LCOE has been selected as the objective function for DTOcean.

Nevertheless, in the context of a project feasibility assessment, these financial indicators can be readily computed by making use of the ingredients forming the LCOE calculation (annual costs and energy yield). The solutions that minimize the LCOE (assuming the desired return in terms of discount rate), will also be the ones providing higher NPV and IRR.

The DTOcean tool should also allow the user to export detailed annual information on both CAPEX, OPEX and energy production which can be input in the company's own models for detailed financial assessment.

⁵ Return on investment is the amount an investor requires to gain in order to consider an investment attractive. This value will influence the discount rate, as is a part of the WACC

2.2 ECONOMIC ASSESSMENT IN THE ENERGY INDUSTRY

In the large electricity markets, marine renewables will compete with large conventional power plants with low costs of energy and it is required some level of support in order to enable the progressive deployment of new technologies with higher LCOE in the market, and enable learning and cost reduction until grid parity is achieved.

At an early stage, prototypes and pilot projects usually require capital support mechanisms such as R&D and capital grants, while as the technology gets closer to the market, the market support mechanisms such as feed-in tariffs enter in place, filling the gap between the LCOE of the new energy technologies and the average market prices. There are also smaller markets and off-grid applications with higher energy costs such as running with diesel generation where may be used as an intermediate step before feeding electricity into the main grids at a competitive price.

The energy sector is very dynamic and the cost of energy is in constant evolution. Recent analyses show that some renewable energy technologies have achieved grid parity with conventional power plants. The following graph has been extracted from the most recent report from the Annual Energy Outlook 2015 published by the U.S (15), which provides similar outlooks as other reference reports published by other international reference institutions (1; 16; 17; 18).

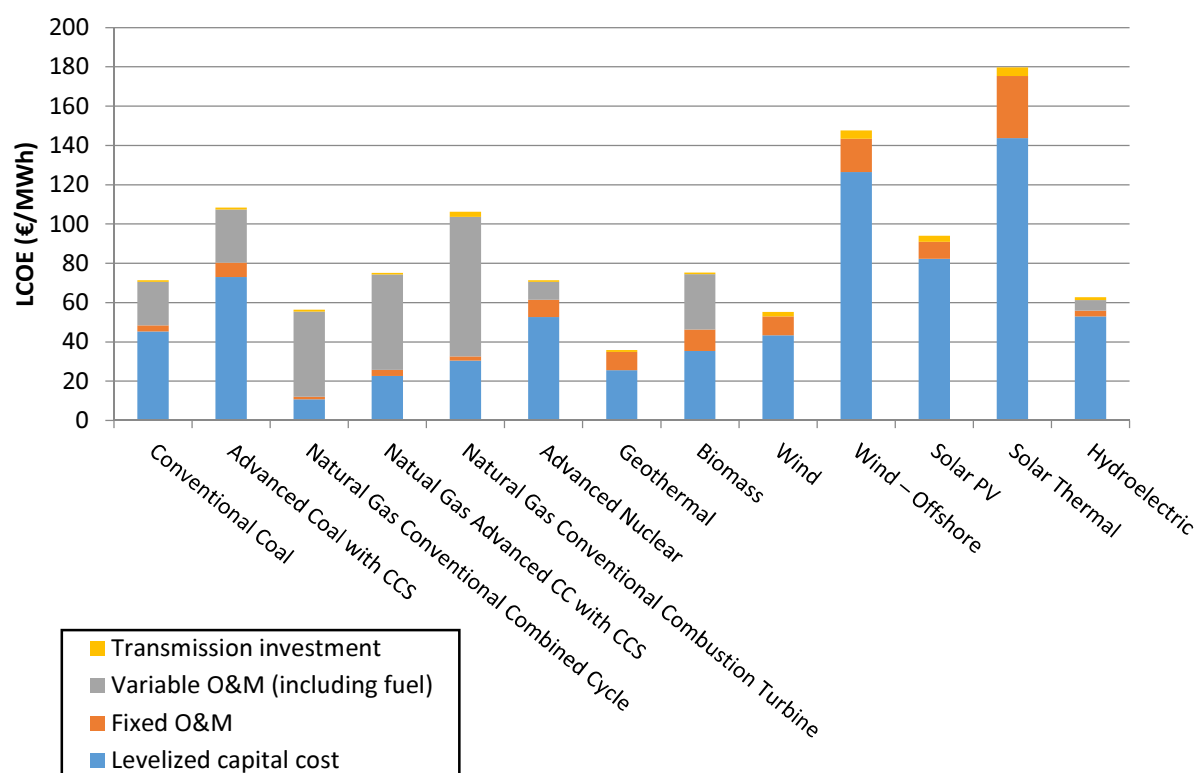


Figure 2.4: U.S. Average Levelized Costs for Plants Entering Service in 2020 (19)
Original costs in 2013 \$/MWh have been converted to Euros by applying avg. 0.75 EUR/US\$.

It can be observed that renewable energy technologies such as geothermal, biomass, onshore wind, hydropower or solar PV are already competing with the conventional coal, gas or nuclear power plants.

However, the first arrays of wind and solar power plants had significantly higher prices, only a few decades ago. New energy technologies typically offer higher energy prices at the start of the learning curve, which typically decrease over time after learning and experience is gained with the manufacture, deployment, and production, as well as with R&D effort. This cost reduction is also expected for the marine energy industry and arrays will follow a similar path as explained in the following sections.

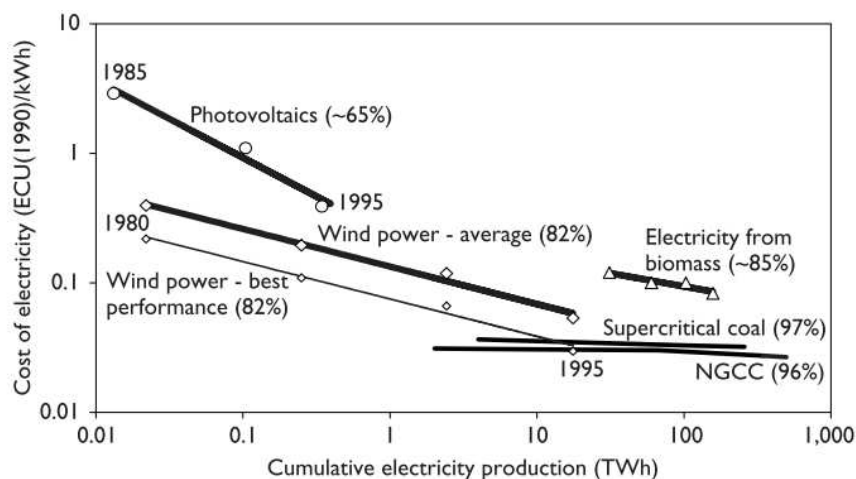


Figure 2.5. Observed learning curves in energy Technologies (20)

It is also important to mention that LCOE varies from project to project, especially depending on the site resource levels and characteristics that influence the energy production as well as some of the costs (e.g. installation). Many of these factors can only be fully understood at array level and this is why DTOcean is an important step towards the assessment and optimization of the energy economics of the first ocean energy arrays.

A number of reports have been published in the last years showing the expected costs of the first ocean arrays, as well as the expected cost reduction in the future (4; 6; 8; 9; 11; 14; 21; 22; 23).

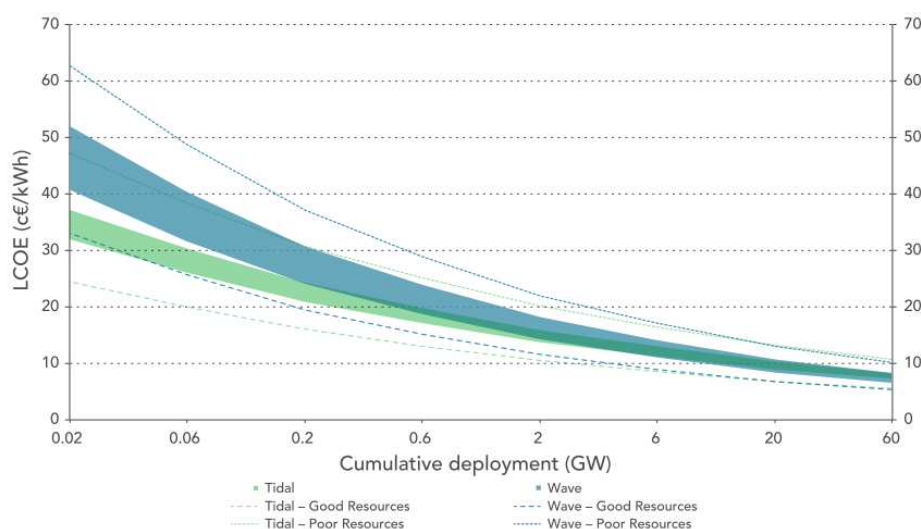


Figure 2.6: LCOE predictions for wave and tidal energy, starting at 10MW arrays after 10MW have been previously installed (14), (24)

The following table summarizes the expected economics for the first wave and tidal energy arrays based on the most recent study published in May 2015 by the IEA-OES. This study analysed previous reports from Europe and the US and adding an international context, by including responses from questionnaires sent to leading developers across the world (5).

Table 2.2: Summary of economic data for ocean energy arrays averaged for each stage of deployment (5).
Values converted to Euros (0.75 EUR/US\$ 2014)

Deployment Stage	Variable	Wave		Tidal	
		Min	Max	Min	Max
First array/First Project	Project Capacity (MW)	1	3	0.3	10
	CAPEX (€/kW)	3000	13575	3825	10950
	OPEX (€/kW per year)	105	1125	120	870
Second array/Second Project	Project Capacity (MW)	1	10	0.5	28
	CAPEX (€/kW)	2700	11475	3225	6525
	OPEX (€/kW per year)	75	375	112,5	397,5
	Availability (%)	85%	98%	85%	98%
	Capacity Factor (%)	30%	35%	35%	42%
	LCOE (€/MWh)	157,5	502,5	157,5	352,5
First Commercial Scale Project	Project Capacity (MW)	2	75	3	90
	CAPEX (€/kW)	2025	6825	2475	4200
	OPEX (€/kW per year)	52,5	285	67,5	300
	Availability (%)	95%	98%	92%	98%
	Capacity Factor (%)	35%	40%	35%	40%
	LCOE (€/MWh)	90	352,5	97,5	210

The following sections will describe in more detail the economics for both wave and tidal energy converters.

2.2.1 ECONOMIC ASSESSMENT OF WAVE ENERGY CONVERTERS

Results from wave energy developers in the study provide a very high range for the first pre-commercial array, due to the variety of concepts as well as large uncertainties and different assumptions in costs but especially in capacity and availability factors for different developers. The expected costs in the future reduce significantly and tend to converge between developers. In the long term, forecasts indicate that the LCOE of wave energy could achieve 100€/MWh or lower as shown in the forecasts from SI Ocean (see Figure 2.6).

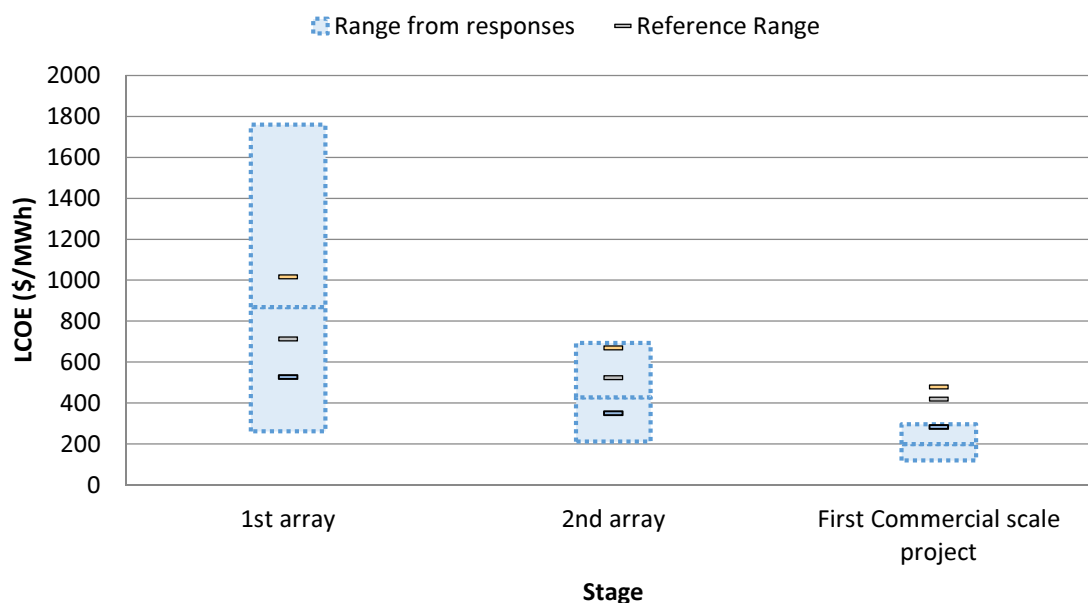


Figure 2.7: LCOE evolution at the three stages based on developer responses and reference international analysis (5). Values in US dollars.

A large share of the LCOE is related to the device CAPEX (both structural and PTO)⁶. Estimates of device CAPEX are based on developers' responses as well as on the historical costs of wave energy prototypes published in the OES report. The CAPEX of these prototypes ranged between 7.500-40.000 € per kW installed, depending on the type and scale (the higher the scale the lower the cost per kW). In addition to the device CAPEX, the balance of plant CAPEX (other array sub-component such as moorings & foundations and electrical infrastructure), the installation CAPEX as well as the O&M costs typically represent more than 50% of the overall LCOE (4). Furthermore, the energy production (both capacity factor and availability) is the most critical factor for which there are more differences and uncertainties among developers.

⁶ However, the average may not be representative of some technology types, and significant differences in the breakdown will appear for different devices (e.g. floating vs. near shore bottom mounted devices: bottom mounted devices have significantly higher foundation and installation costs, but may offer lower connection costs and O&M costs).

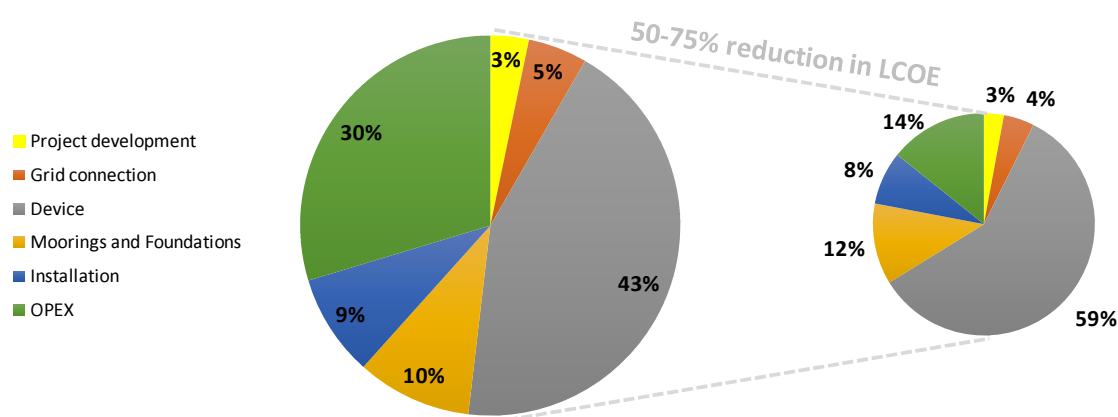


Figure 2.8: Wave LCOE Percentage Breakdown by Cost Centre Values at Current Stage of Deployment (Left) and the Commercial Target (Right) (5)

Note: the area of the chart represents the LCOE

The LCOE of ocean energy arrays depend in fact on many factors and vary from project to project depending on the type and number of device in the array, level of resource, water depth, type of seabed, distance to shore and ports, etc. (see illustration from the Carbon Trust on the trade-off between cost of energy and distance to shore for a particular example in the UK). DTOcean tool will help understanding how these factors affect the economics of ocean energy arrays in order to design optimal layouts.

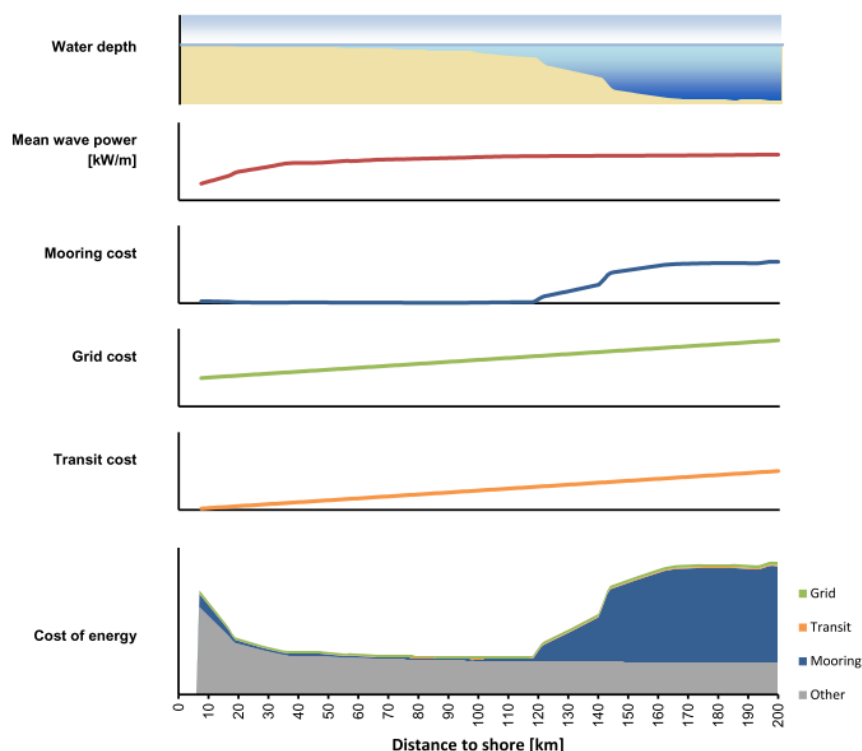


Figure 2.9: Trade-off between cost of energy and distance to shore for a specific example in the UK (22).

Results will differ from site to site and for different technologies.

2.2.2 ECONOMIC ASSESSMENT OF TIDAL ENERGY CONVERTERS

For tidal energy converters, LCOE ranges are also diverse for first array deployment (200-750 €/MWh, with a mid-range around 300-525€/MWh), but clear convergence is seen across the tidal energy sector as progression is made towards commercial scale projects. The costs for the second array published in the report are lower (~160-340€/MWh) than those predicted by the SI Ocean project (LCOE range of 250-470 €/MWh for the second 10MW arrays) (5; 14).

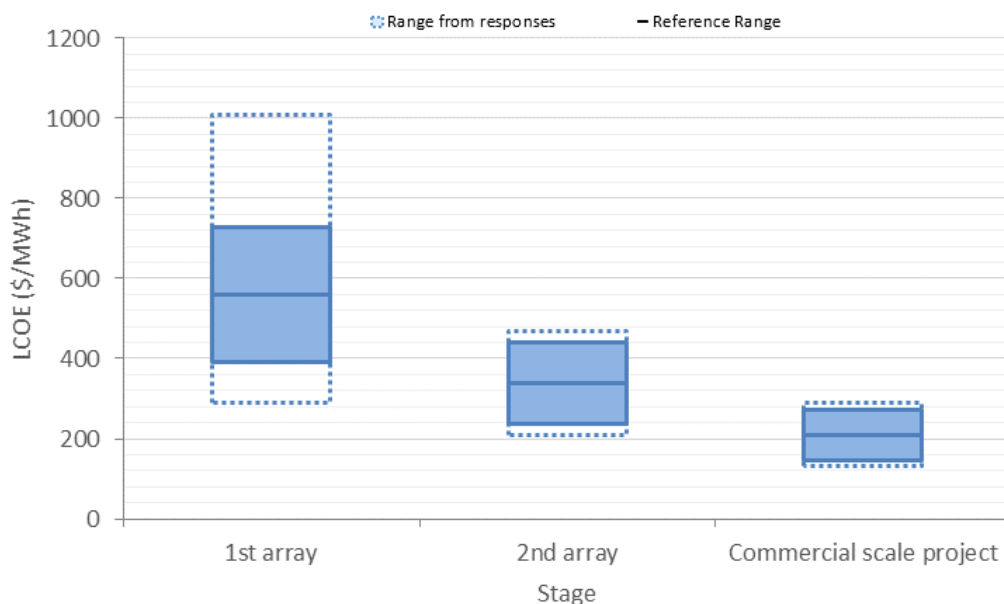


Figure 2.10: Tidal energy LCOE Ranges at Differing Stages of Deployment (5).
Values in US dollars.

A breakdown of CAPEX (by specific cost centre) and OPEX contributions to the LCOE is presented in the figure below. In the case of tidal, the costs of the device are expected to represent a lower share of the LCOE, while the costs of moorings and foundations, installation and O&M could be higher, especially for the fixed devices.

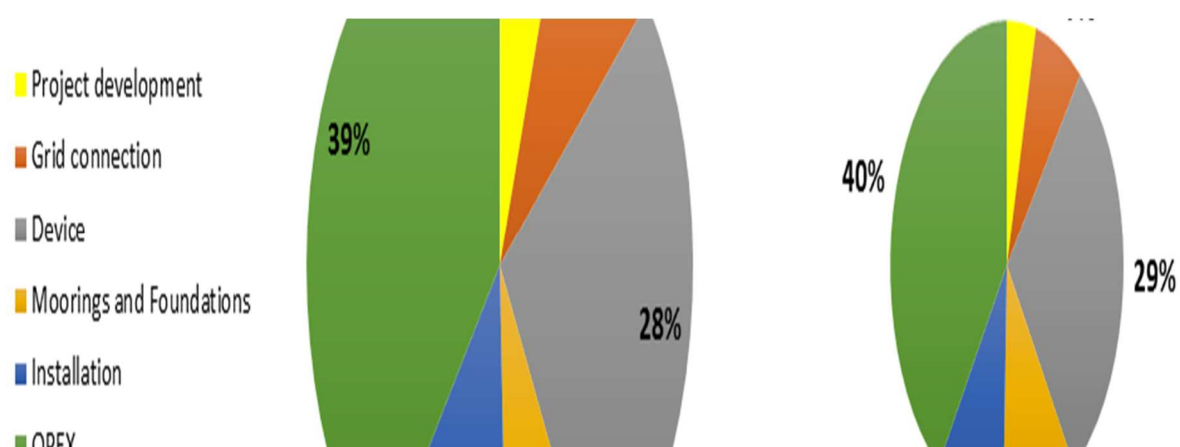


Figure 2.11: Tidal LCOE Percentage Breakdown by Cost Centre Values at Current Stage of Deployment (Left) and the Commercial Target (Right). (5)

All the previous estimates are based on prototype costs for single devices but there are still large uncertainties in the costs and performance of tidal energy arrays. A number of factors such as the hydrodynamic interaction between devices are not well understood and decisions in the array layout design are difficult.

As indicated in the OES report (5), *it is difficult to provide a single or a narrow band of LCOE estimates for the sector given the diversity of technologies and uncertainties involved. An in-depth collaborative effort could help the sector to move forward, sharing non-commercially sensitive information to build knowledge, help to reduce uncertainties and costs, and improve reliability, availability and performance, which could ultimately understand what the real cost drivers are and advance through the cost reduction path.*

By using an integrated and common set of tool as DTOcean, it is expected to see an important reduction in the levels of uncertainties as well as a much higher level of convergence among the sector.

3 METHODOLOGY FOR THE LCOE CALCULATION IN THE DTOCEAN TOOL

3.1 OVERVIEW OF THE LCOE CALCULATION IN THE DTOCEAN TOOL

Understanding how the LCOE calculation is performed within the DTOcean tool requires knowledge of the structure of the software environment. To compute the different ingredients forming Equation (2.1), commercial cost information stored in the global DTOcean database and tailored cost functions aggregate the relevant information throughout the different modules of the software. Figure 3.1 displays the high-level schematic view of the DTOcean software environment illustrating how the flow of data inputs and outputs (I/O) is constructed.

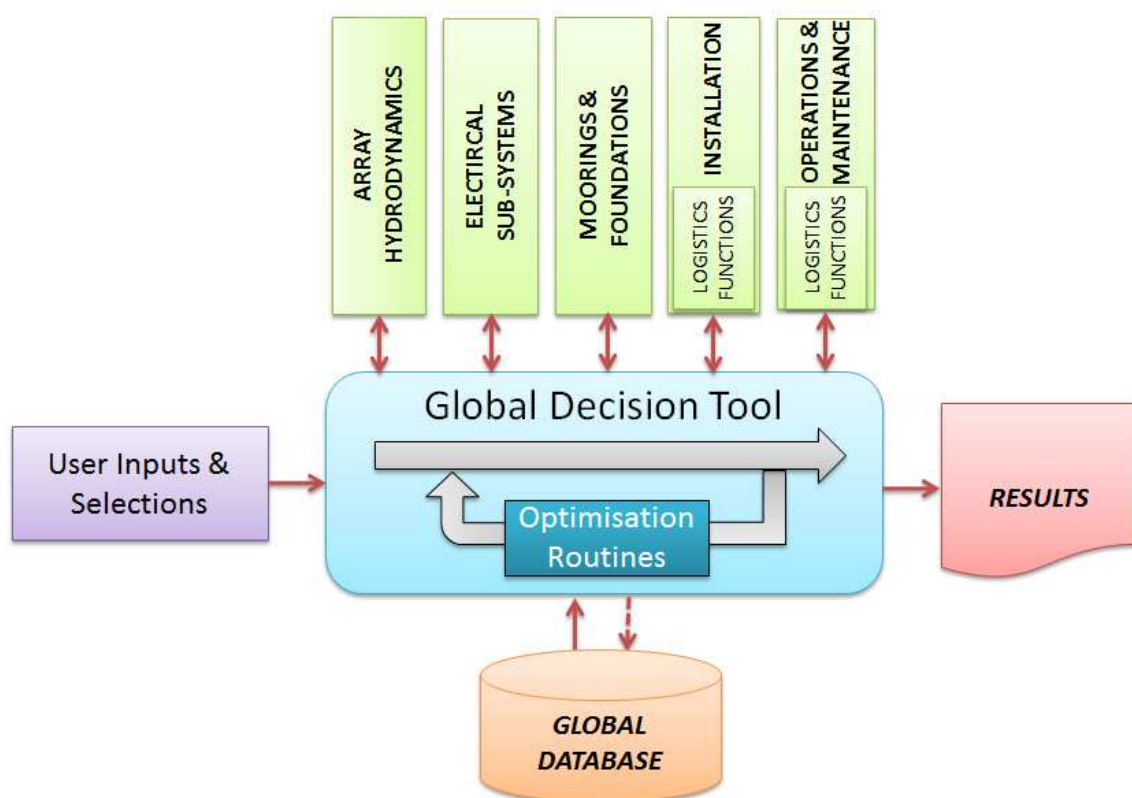


Figure 3.1: Flow-chart structure of the DTOcean software environment

The green blocks in the figure correspond to computational modules solving a particular physical or technical problem towards the realization of an optimum wave or tidal energy array design. From this modular functional structure represented by the green blocks, it transpires that there exists an implicit hierarchy dictating the inherent relationship between the modules.

From left to right, the green blocks of Figure 3.1 translates the fact that each block relies upon the outputs produced by the upstream computational module (i.e. other block green(s) located on the left on-side, if any). This hierarchy has implications in the step-wise calculation of the LCOE throughout the DTOcean tool.

In addition to the I/O communication between computational modules, the end-user inputs and selection also “indirectly” impacts the LCOE by driving decisions such as: the device type, the site selection (including location, bathymetry, met-ocean data and soil conditions) and the lifetime of the project.

Furthermore, the global database serves as a pool of information which contains relevant input parameters to both the costs calculation and the energy production prediction. For instance, the price of items such as mooring system components feeds simple cost functions to estimate a subset of the overall cost associated with the mooring systems. Similarly, the physical characteristics of the power cables selected from the global database influence the losses calculation due to the electrical infrastructure layout.

Adapted cost functions on the one hand, and energy production functions, on the other hand, communicate with the computational modules via the global design tool. Table 3.1 summarizes the main ingredients influencing the cost and energy production calculations generated by the respective computational modules.

Table 3.1 Cost and energy production implications in the DTOcean computational modules

DTOcean computational module	Cost implications	Energy production implications
WP2 – Array Hydrodynamics	Number of devices	Hydrodynamic interactions between devices
WP3 – Electrical Sub-Systems	Type and length of cables, cable route, collection point and substation types and number, electrical connectors types and number	Electrical losses throughout the transmission chain, electrical array layout and redundancy
WP4 – Moorings And Foundations	Type, dimension, position and number of foundations/ anchors/mooring lines	
WP5 – Installation	Number and type of vessels/port/equipment, estimated durations of marine operations	Predicted commissioning time of the wave or tidal energy converters
WP6 – Operation & Maintenance	Number and type of vessels/port/equipment, estimated durations of marine operations, type and number of parts, labour and insurance	Downtime estimation based on the reliability assessment, the maintenance strategy & type of actions, the electrical network implications & the duration of the maintenance operations

Beyond the collection of all cost contributions and the estimation of the energy production throughout the lifetime of the project, the user will have to provide two parameters of the *LCOE* equation:

- the project discount rate r
- the project lifetime n

As previously mentioned in section 2.1, typical values of discount rate for marine energy projects range between 8-15%, and project lifetime between 15 and 25 years.

```

graph LR
    WP1[(WP1 Database of costs:  
Unitary cost of components  
Cost of devices)] --> BM[/Bill of Materials/]
    WP2[/WP2 Bill of Materials inputs:  
Number of devices/] --> BM
    WP3[/WP3 Bill of Materials inputs:  
Chosen Electrical Components and quantity/] --> BM
    WP4[/WP4 Bill of Materials inputs:  
Chosen Moorings and Foundations  
Components and quantity/] --> BM
    WP5[/WP5 Bill of Materials inputs:  
Vessels, Ports and Equipment Required and  
quantities  
Year of purchase/Installation/] --> BM
    WP6[/WP6 Bill of Materials inputs:  
Components Required for O&M and quantity  
Year of O&M operation/] --> BM
    WP6 <--> WP5
    WE[/WP6 Energy Input:  
Total energy Output/] --> BM
    UI[/User Input:  
Discount Rate  
Project Duration/] --> BM
    BM --> CC[Cost calculation:  
Function: item_total_cost  
Requirements:  
• Number of items  
• Item Unitary Cost  
Output:  
• Total cost]
    CC -- "Total Cost" --> PVP[Present Value Calculation  
Function: present_value  
Requirements:  
• Cost/energy output  
• Year  
• Discount Rate  
Output:  
• Present Value]
    CC -. "Year of Cost" .-> PVP
    PVP -- "Costs" --> LCE[Levelized Cost of Energy:  
Function: simple_lcoe  
Requirements:  
• Sum of all Present Value Costs  
• Sum of all Present Value Energy Output  
Output:  
• LCOE]
    PVP -- "Energy" --> LCE
    WE --> LCE
    UI --> LCE
    LCE --> LCOE([LCOE])
  
```

The flowchart illustrates the Economic Assessment Module, which calculates the Levelized Cost of Energy (LCOE) for a power plant project. The process begins with data inputs from various sources, which are then processed through a series of modules to arrive at the final LCOE output.

Inputs:

- WP1 Database of costs:** Unitary cost of components, Cost of devices.
- WP2 Bill of Materials inputs:** Number of devices.
- WP3 Bill of Materials inputs:** Chosen Electrical Components and quantity.
- WP4 Bill of Materials inputs:** Chosen Moorings and Foundations Components and quantity.
- WP5 Bill of Materials inputs:** Vessels, Ports and Equipment Required and quantities, Year of purchase/Installation.
- WP6 Bill of Materials inputs:** Components Required for O&M and quantity, Year of O&M operation.
- WP6 Energy Input:** Total energy Output.
- User Input:** Discount Rate, Project Duration.

Processing Flow:

- The inputs from WP1 through WP6 and the User Input are fed into the **Bill of Materials** module.
- The **Bill of Materials** module outputs data to the **Cost calculation** module.
- The **Cost calculation** module (Function: *item_total_cost*) requires the Number of items and Item Unitary Cost. It outputs the **Total cost**.
- The **Total cost** is then passed to the **Present Value Calculation** module (Function: *present_value*). This module also receives the **Year of Cost** (indicated by a dashed arrow) and the **Discount Rate** from the User Input. It outputs the **Present Value**.
- The **Present Value** is then split into **Costs** and **Energy**, which are fed into the **Levelized Cost of Energy** module (Function: *simple_lcoe*). This module also receives the **Sum of all Present Value Costs** and **Sum of all Present Value Energy Output** from the **Present Value Calculation** module.
- The **Levelized Cost of Energy** module outputs the final **LCOE**.

In summary, one can say that the methodology for the LCOE calculation in the DTOcean tool is based on the aggregation of customized cost and energy production functions agglomerating progressively all the ingredients of the LCOE equations through the computational modules from WP2 to WP6. Further details on the cost functions and the energy production functions is provided below with special emphasis on the computational module – array hydrodynamics (WP2).

3.2 METHODOLOGY FOR THE COST CALCULATION IN THE DTOCEAN TOOL

The cost calculation in the DTOcean can be divided into two standard categories: the CAPEX and the OPEX. While WP2 to WP5 contribute to the CAPEX, WP6 is almost only recording OPEX – some equipment for condition based maintenance will be a CAPEX input, if it is present. Therefore, one can write the following CAPEX breakdown Equation (3.1):

$$CAPEX = CAPEX_{WP2} + CAPEX_{WP3} + CAPEX_{WP4} + CAPEX_{WP5} [+CAPEX_{WP6}] \quad (3.1)$$

The details of the CAPEX contributions from WP3 to WP5 is documented in the respective deliverables 3.4 (25), 4.6 (26) and 5.6 (27). Nevertheless, it should be noted that the cost calculation in WP3 and WP4 follows a similar approach consisting of straightforwardly multiplying the unit cost per component selected (electrical infrastructure components in the case of WP3; moorings and foundations components in the case of WP4) by the quantity of components.

Additional economic factors such as economies of scale and progress ratio can be readily implemented. All these economic factors together with the unitary price per item are stored in the global database. The global database contains a large list of components, with detailed specifications and, when available, commercial prices. If prices are not available, best estimates can be derived from similar components, from cost functions developed specifically for each module/component, or the user can input their own values⁷.

WP5 approach differs somewhat from that of previous modules, in which the deciding factor is not just quantity, but the product between quantity and time. For a specific port, vessel or equipment, the module will assess how many will be needed and for how long, with this last part being also a complex assessment of operation time, waiting time (as a function of weather windows), and mobilization times. Furthermore, the functions developed in WP5 will be used for both CAPEX and OPEX, as these deal with the logistics of maritime operations – in the installation phase and during the farm operation.

Similar to Equation (3.1), the OPEX breakdown in DTOcean is represented by Equation (3.2).

$$OPEX = OPEX_{WP5} + OPEX_{WP6} \quad (3.2)$$

WP6 will access the maintenance strategy, which will result in a schedule of operations during the project lifetime, each with associated costs based on:

- Replacement parts
- Labour
- Ports (provided by WP5)
- Vessels (provided by WP5)
- Equipment (provided by WP5)

⁷ As commercial prices of components are volatile and subject to changes due to commodity markets, inflation, exchange rates, choice of suppliers and, in many cases of energy projects, subject to negotiation and private quotations from suppliers, for best accuracy it is always better for the user to evaluate the values presented on the tool. With that in mind, DTOcean uses industry trends, and the solutions provided will reflect that.

Each of the costs elements detailed so far and associated quantities are recorded in each module and aggregated through the core in a Bill of Materials (BoM). Once all models are run, the core will call in the LCOE calculation functions, which will use the Bill of Materials and the final energy production⁸ to output the LCOE for the chosen design. To be developed in task 7.4, are the optimization routines that will ensure that final solution is the most economical one at array level, as opposed to sub-system level, as each module delivers a local optimum to the core.

3.2.1 COST VARIATIONS DUE TO ARRAY CHANGES

3.2.1.1 IMPACT ON DEVICE COSTS DUE TO ARRAY CHANGES

The cost of wave and tidal energy devices is a product of the development of such technology, as well as the cost of fabrication and assembly of its parts.

On the fabrication side, the cost of the device will be influenced by the mass and materials the device is made of, the complexity of the structure for fabrication, and the cost of the mechanical and electric components to be included. The needed raw materials and components, and the fabrication and assembly contracts may be subject to price negotiation depending on the amount being contracted. Furthermore, raw materials such as steel are prone to price changes, which will in turn affect the cost of devices and its components, as it can be seen in Figures 3.3 and 3.4, showing the increase in steel prices and its effect in equipment prices (28).

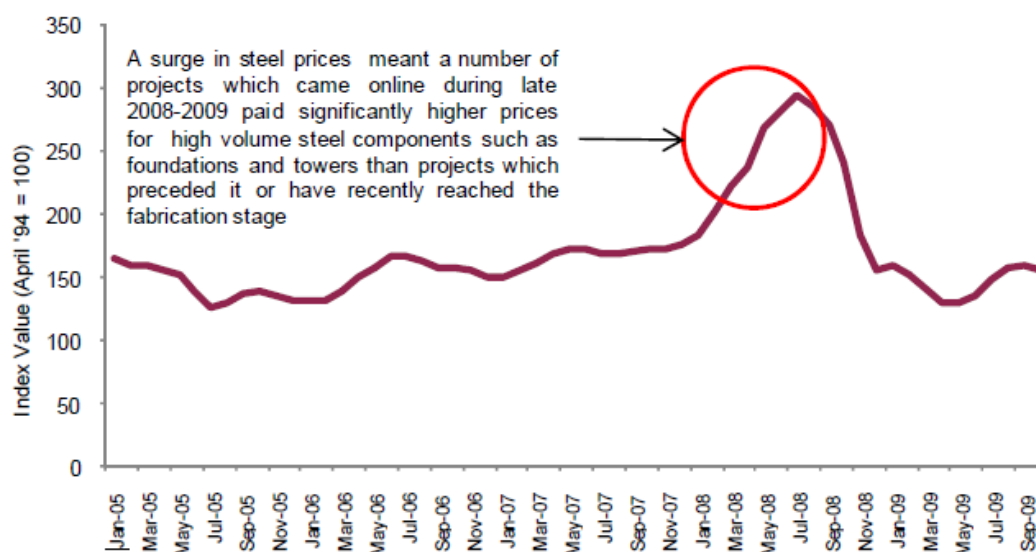


Figure 3.3: Global Spot Steel Price Index Jan '05-Oct '09 (28)

⁸The annual energy output figure used will be the power metered at the point of connection, provided by work package 6, which includes the effects of hydrodynamic losses, electrical losses and availability.

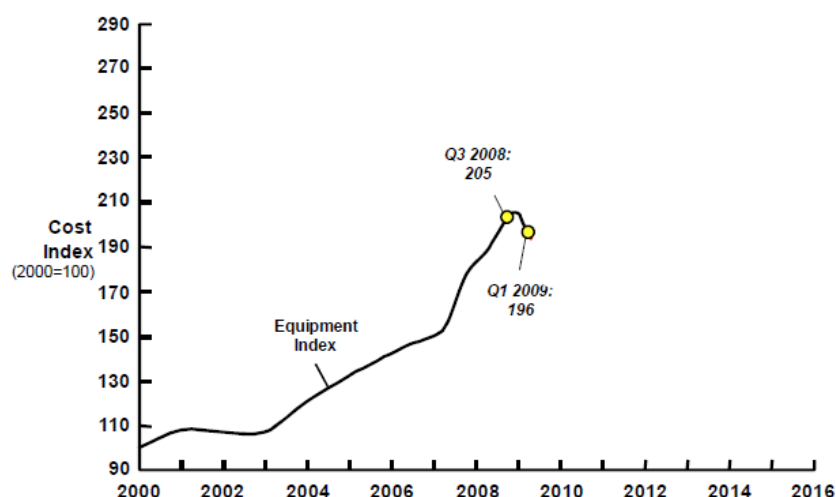


Figure 3.4: Equipment Price Index (28)

While the cost of specific devices can be subject to supplier's offers and market variations, the design is expected to remain constant across projects – especially so when moving to array projects. Wave and tidal developers, like wind developers currently, may offer different solutions for different resource and geophysical characteristics, but in order to reduce the overall costs of devices, developers will focus in serializing the production of devices (14).

The methodology used in DTOcean for project costing can also be applied for device costing – with a component breakdown, including also IP costs and overheads, and associated prices, the cost of one device can be assessed. However, within the context of DTOcean, devices are treated as black boxes – not only on its technical aspects but also to their costs. The commercial price of a device, while dependent on the cost of its components, is also subject to profit margins from the developers that will be providing these to array projects.

At this stage of development of the sector there isn't a commercial offer of devices - these are still prototypes, fabricated for testing proposes. However, it is expected that the market will move similarly to that of wind energy, with developers establishing product lines, that while not truly 'off-the-shelf', will have defining characteristics which are unlikely to be changed to match a specific project. It will be the developer's choice to pass on to the project developers any cost savings and/or discounts that come from high volume orders.

Therefore, in the context of the DTOcean tool, the possible variations of array configurations have no impact in device unitary costs. While different models, with different characteristics, may exist for the same technology family from a specific developer, these are an initial user input and are not changed by the tool during its analysis. The contribution of devices towards the LCOE will be the product of its unitary cost, and the number of units determined in WP2.

3.2.1.2 NOTE ON THE COSTS OF OTHER ARRAY COMPONENTS DUE TO ARRAY CHANGES

While device costs will not be affected by array changes in this tool, their distribution and layout in the array area, as well as the chosen site area itself, will have implications on the choice of components downstream on the array design process within DTOcean. The way the economics of the different sub-systems in an array project change based on the different configurations is dealt in the specific work packages and detailed on the corresponding Deliverables (25; 26; 27). However it is important to stress that many of the decisions made in the other work packages will be constrained by the outputs of WP2.

As an example, the impact on costs of the addition of one extra device is not simply the added cost of another unit. Further procurement costs are incurred, as this extra unit needs also moorings or foundations and an electrical connection to the farm collecting system. All these components will also need to be installed, which will increase the installation costs, especially if it is impossible to include the extra installation in the schedule for the base case. Finally, this new device will also have an associated reliability figure – no system is fault-free, so there will also be an added O&M cost.

Further costs can also be added if, for instance, the electrical system has to be redefined to deal with the extra power output from the farm, or the location of the devices changes to locations with less favourable seabed conditions.

These extra elements will also have an impact on the energy production side of the LCOE equation – different hydrodynamic interactions between devices, and possible changes to transmission losses and availability figures. It is one of the aims of the DTOcean project to evaluate these project-wide interactions, and within the context of WP7, these layout changes will be analysed and optimized to deliver a low LCOE array design.

3.3 METHODOLOGY FOR THE ENERGY OUTPUT CALCULATION IN THE DTOCEAN TOOL

The main objective of the WP2 tool is to generate a (fast) optimised array layout of marine renewable energy devices, taking into account the complex hydrodynamic interaction between bodies. The devices used in the array will be either wave or tidal converters.

The main structure of the algorithm is shown in Figure 3.5.

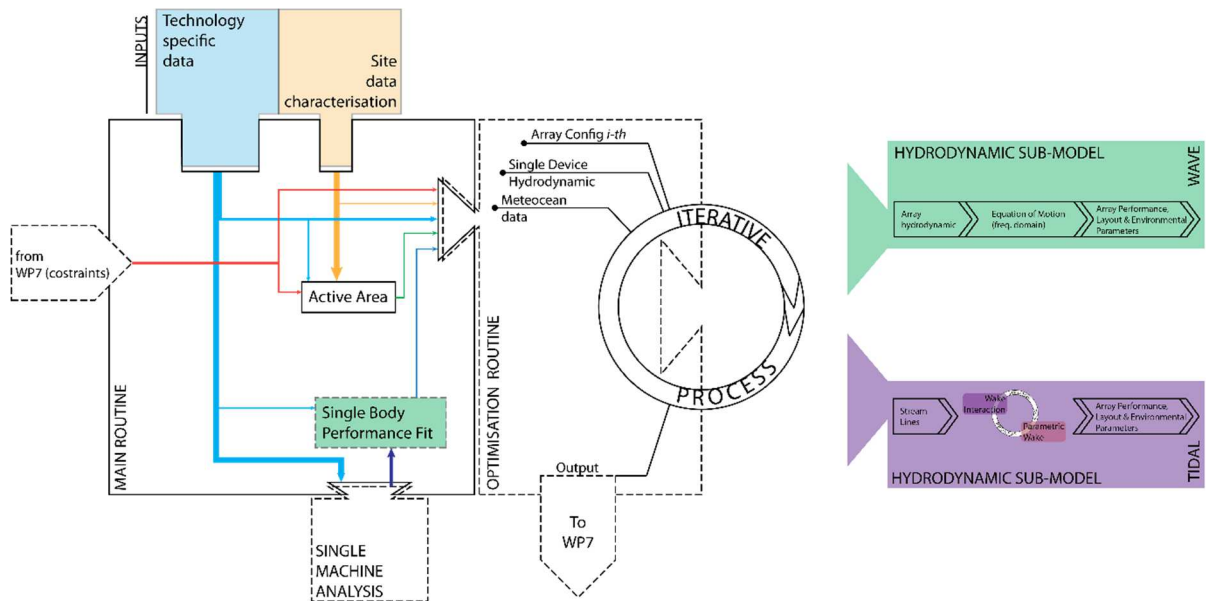


Figure 3.5: WP2 algorithm overview

On a macroscale the algorithm is divided into blocks:

- The main routine (left side) is the place where the user input and WPs constraints are loaded, modified if needed and checked. Further, in the main block the performance of a single WEC are assessed. This process takes place in the main block because it is required one time only, and can be seen as an initialisation of the WP2 tool.
- The optimisation loop (right side) is where the hydrodynamic interaction of the array is assess and the array layout is iteratively optimised in order to achieve the best device positioning.

The optimisation loop calls in turn the wave and tidal sub-modules, which retain the core of the whole process.

The optimisation loop and the two submodels are described in details hereafter.

3.3.1 OPTIMIZATION ROUTINE

The final goal of the WP2 tool can be efficiently described in mathematical notation as:

$$\max_{\mathbf{x}} \{P_{yr}(\mathbf{x}) : q > q_u\}, \quad (3.3)$$

with

$$q = \frac{(P_{yr})_{array}}{N(P_{yr})_{single}}. \quad (3.4)$$

for an array of $N_b - 1$ WECs. Here, P_{yr} is the annual power production, \mathbf{x} is the array layout and q is the so called q-factor of the array defined in (2). Further, the array layout (\mathbf{x}) needs to fulfill additional constraints, such as minimum distance between devices, membership of a feasible region, etc.

In other words, the optimization algorithm is used to find the array layout \mathbf{x} , which maximizes the yearly averaged power production of the array P_{yr} subjected to:

- Minimum allowable hydrodynamic losses,
- Minimum distance between devices and
- Unfeasible areas.

The hydrodynamic losses are quantified by means of the q-factor, which is defined as the ratio between the power produced by the array and the power produced by the same array but with no interacting WECs (3.2). The power produced by the array is obtained by calling either the wave or tidal submodules, with a given array layout; this last being updated at each optimisation loop. The wave and tidal submodules will be described in Section 3.3.2 and Section 3.3.3.

The parameters used for array layout description, and so the arguments \mathbf{x} of the objective function $P_{yr}(\mathbf{x})$ to be maximized, are given below. For further details see deliverable D2.2 (29).

Table 3.2: Array layout types and descriptive parameters

Type	Parameter #	Parameter ID	Parameter Description
Linear	1	iR	Devices inter-distance
Staggered	2	iR	Devices' rows inter-distance
		iC	Devices' column inter-distance
General	4	iR	Devices' rows inter-distance
		iC	Devices' column inter-distance
		β	Devices' rows angle with respect to the main direction
		ψ	Devices' column angle with respect to the main direction

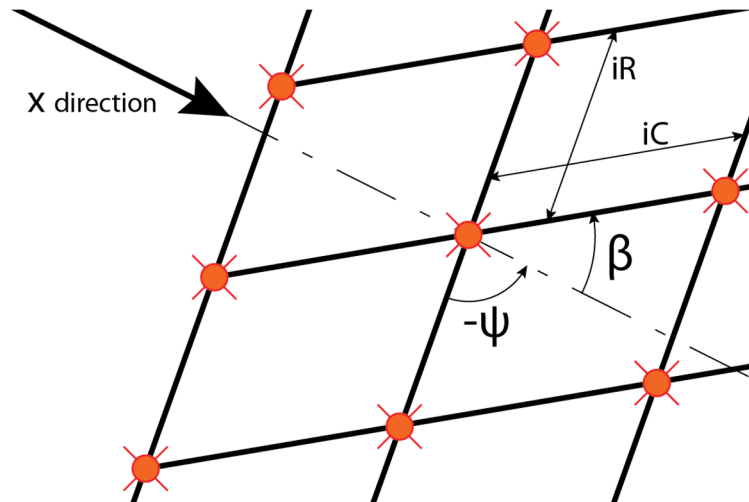


Figure 3.6: Sketch of the array layout parameters listed in Table 3.2

In addition to the array layout types given in Table 3.2, the user will also be able to include his/her own array layout. In such case, the given array layout will be optimized by simple homogeneous shrink/stretch scale factor.

In order to select the best optimisation algorithm to be used into the WP2 tool, a short survey of the different methods is given hereafter.

The optimization algorithms can be divided into gradient based and gradient free algorithms. The first have a quicker convergence than the last, as they use the information of the gradient to foresee the next iteration step. Besides, gradient based usually have a clear convergence criterion, based on the magnitude of the gradient. However, the main disadvantages of the gradient based algorithms are the high development cost, the low intolerance to gradient inaccuracy and the identification of local than rather global minimums.

The gradient free algorithms stands on the other side, since they have a low development cost, they search for global minimums (even if not ensured), and all this comes in terms of higher computational cost.

The work presented by (30) shows the utilisation of a gradient based method, using an adjoint approach for the calculus of the gradient. Even though using the adjoint approach reduces the development complexity, the method is still far more complex than a gradient free approach.

One possible approach is the one proposed by (31), where they make use of a simplified shape of the wave-body interaction (parabolic) to optimize the position of the devices in the array. The devices are positioned at the parabolic intersection to maximize the q-factor of the array. This method shows good results for the case of array with large device inter-distance, while it will be inaccurate for packed array due to the simplistic assumption of the wave field shape. In addition, if short crested waves are used, the assumed parabolic shape becomes less accurate, unless many parabolas are used to account for the spreading function. This type of approach is a gradient-free approach but it requires a moderate to high development cost.

On the other hand, the approach presented by (32) requires a moderate to low development cost by implementing a greedy-algorithm. In this case the algorithm recursively reconstruct the array starting

from placing the first device and then, using a concentric circle approach, will place other devices and so on until all the devices have been placed. In the article the position is based on the maximum constructive interference between devices, for the case of regular wave, and therefore neither spectral shape in frequency nor in direction is assumed. As in the parabolic intersection case this may cause inaccurate results.

Another intermediate approach to solve non-linear global optimisation problems is the one proposed by (33) and (34)). Both documents describe the potential usage of hypersurfaces, fitted to few simulation results, to search for global minimums. In order to increase the method's reliability the hypersurface is checked at the minimum point and if the solution is not correct a new hypersurface is fitted to an extended results space. This methodology seems to be a good alternative for a future development, but at the time of writing its applicability to the wave, tidal or wind sectors; it is too limited.

The work presented by (35) is based on a genetic algorithm approach. In this case the solution is sought by allowing mutation in the child generations. The approach mimics the evolution model proposed by Darwin. In this case, the system is considered as a black-box and the best solution is sought by letting the parent configuration to mutate and generate a new set of possible solutions randomly. This type of approach is well in line with the more mature wind sector as shown in (36), (37) and (38).

For WP2 tool and at the actual stage of development, the gradient free approach is envisaged as the first applicable solution. In addition to the small development complexity, the gradient free approaches are less type dependent, that is, it can be applied on both wave and tidal cases, and are adopted by more mature sectors, such as the wind energy sector. Moreover, it is worth mentioning that PeraWatt project, which developed a similar code, choose a genetic algorithm as optimisation baseline.

Listed below several gradient free based optimization methods are listed:

- Coordinate Descent,
- Cuckoo Search,
- Genetic Algorithm,
- Nelder-Mead Method,
- Particle Swarm Optimisation and
- Pattern Search.

The genetic algorithm is the main candidate to be implemented in WP2, and it will be discussed hereafter.

Description Missing due to the uncertainties on the method implemented.

3.3.2 WAVE HYDRODYNAMICS AND ARRAY ENERGY OUTPUT CALCULATION

The wave submodule solves the hydrodynamic interaction between WECs, given their spatial disposition and orientation.

At the time of writing only few methods are capable to run a large number of simulation in a relative short amount of time. Since this is a sensible parameter in the DTOcean tool, it has been chosen to use a BEM solver as a base model. BEM solver, such as WAMIT, WADAM or Nemoh are commonly used to estimate the motion of a floating body in operational condition, because the method provide relatively accurate result, keeping the computation cost at the minimum.

But even BEM solvers with the actual calculation power of a standard computer will require too much time to assess the interaction into an array of floating bodies

Therefore a reduced method has been selected. The method solves the interaction between floating bodies, by first characterising the single body behaviour and reducing the order of the problem and then by applying the reduced order model of the single body to the array.

Two main considerations underpin the wave submodel:

1. The wave submodel deals with the plane wave diffraction and radiation of an array of WECs, under the assumptions of:

- Linearized potential flow,
- Constant water depth h ,
- Small WEC motions compared with the wave length and
- Harmonic time variation with angular frequency ω , time factor $e^{i\omega t}$, time t and $\tilde{t} = \sqrt{-1}$.

All time dependent quantities are then written in the domain of frequencies through

$$x(t) = \Re(\tilde{X}(\omega)e^{i\omega t}), \quad (3.5)$$

where $\Re(\tilde{Z})$ returns the real part of the complex number \tilde{Z} .

2. The sea states are characterized by a significant wave height H_s , a peak period T_p , a predominant wave direction α_p and a user-defined wave energy spectrum S [$\text{m}^2 \text{s rad}^{-1} \text{deg}^{-1}$] (variance spectrum, see Figure 3.7).

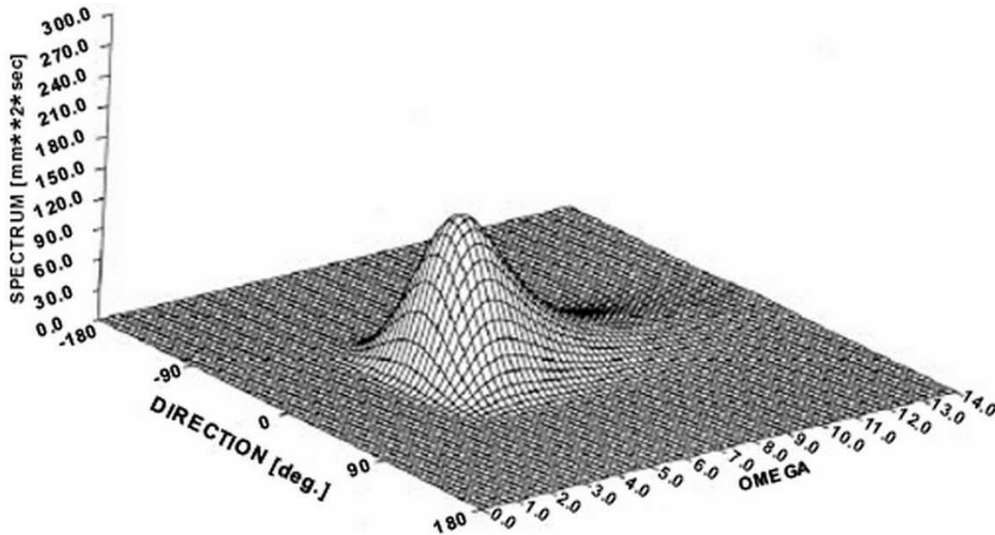


Figure 3.7: Theoretical directional spectrum for the ISSC spectrum with 0.1 m significant wave height and 1.0 s peak period.

The 0 deg. direction corresponds to the predominant wave direction, α_p , of this particular sea state.

Each sea state is then decomposed into a superposition of plane waves with wave frequency ω , wave direction θ and amplitude $A^2 = 2S(\omega, \theta)\Delta\theta\Delta\omega$, with the operator Δ used as the difference between two consecutive elements of a discretized quantity.

Hereafter, the following discretization of sea states and plane wave components apply:

- $(H_S, T_p, \alpha_p)_l$ with $l = 0, 1, \dots, L - 1$,
- ω_m with $m = 0, 1, \dots, M - 1$ and
- θ_n with $n = 0, 1, \dots, N - 1$.

3.3.2.1 POWER PRODUCTION

Let's first consider the equation of motion of an array of interacting WECs, excited by a unit-amplitude plane wave with angular frequency ω_m and wave direction θ_n :

$$[-\omega_m^2(\mathbf{M} + \mathbf{M}_m^R) + i\omega_m(\mathbf{C}_l^{PTO} + \mathbf{C}_m^R + \mathbf{C}_l^A) + (\mathbf{K}^H + \mathbf{K}_l^A)]\tilde{\mathbf{X}}_{lmn} = \tilde{\mathbf{F}}_{mn}^D, \quad (3.6)$$

with:

- $\tilde{\mathbf{X}}_{lmn}$ the vector of complex amplitude displacements of the whole array per unit of wave amplitude,
- \mathbf{M} the mass matrix of the array,
- \mathbf{K}^H the hydrostatic stiffness of the array,
- $\tilde{\mathbf{F}}_{mn}^R = -(-\omega_m^2\mathbf{M}_m^R + i\omega_m\mathbf{C}_m^R)\tilde{\mathbf{X}}_{lmn}$ the complex amplitude of the radiation force, \mathbf{M}_m^R the added mass matrix, \mathbf{C}_m^R the radiation damping matrix,
- $\tilde{\mathbf{F}}_{mn}^D$ the complex amplitude of the excitation force per unit of wave amplitude.
- \mathbf{C}_l^{PTO} the damping matrix associated with the action of the linear damping PTOs and for the sea state $(H_S, T_p, \alpha_p)_l$,
- \mathbf{C}_l^A and \mathbf{K}_l^A damping and stiffness matrices respectively associated with the action of other external forces than that of the PTO for the sea state $(H_S, T_p, \alpha_p)_l$.

The algorithms to estimate $(\mathbf{M}_m^R, \mathbf{C}_m^R, \tilde{\mathbf{F}}_{mn}^D)$ and $(\mathbf{C}_l^A, \mathbf{K}_l^A)$ are described in the sections 3.3.2.2 and 3.3.2.3 respectively.

Once the WECs motion is known, the average power absorbed by the WEC array out of the ambient plane wave (ω_m, θ_n) can be calculated through

$$p_{lmn} = \frac{1}{2}\omega_m^2 \left(\Re(\tilde{\mathbf{X}}_{lmn})^T \mathbf{C}_l^{PTO} \Re(\tilde{\mathbf{X}}_{lmn}) + \Im(\tilde{\mathbf{X}}_{lmn})^T \mathbf{C}_l^{PTO} \Im(\tilde{\mathbf{X}}_{lmn}) \right), \quad (3.7)$$

where $\Im(\tilde{Z})$ returns the imaginary part of the complex number \tilde{Z} .

Moreover, for the sea state $(H_S, T_p, \alpha_p)_l$, the average power absorbed by the WEC array will come from the contribution of each plane wave component weighted by their respective spectral density value:

$$P_l = \sum_{m=0}^{M-1} \sum_{n=0}^{N-1} S_{lmn} p_{lmn} \Delta\theta \Delta\omega. \quad (3.8)$$

Finally, the annual averaged power production of the array is calculated from the contribution of each sea state weighted by their respective probability of occurrence f_l :

$$P_{yr} = \sum_{l=0}^{L-1} f_l P_l. \quad (3.9)$$

3.3.2.2 HYDRODYNAMICS

The diffraction and radiation potentials are calculated from the interaction theory presented by (39) to further calculate wave forces through the recent method presented in (40).

Interaction theory

The scatter (or radiation) complex amplitude of the velocity potential representing the scatter wave field in an immediate neighbourhood of WEC i in local cylindrical coordinates can be written as

$$\tilde{\phi}_i^{S,R}(r_i, \theta_i, z) = \frac{\cosh k(z+h)}{\cosh kh} \sum_{u=-\infty}^{\infty} a_{u_i}^{S,R} H_u^{(2)}(kr_i) e^{iu\theta_i} + (\text{evanescent}), \quad (3.10)$$

where $H_u^{(2)}$ is the u th order Hankel function of the second kind and $a_{u_i}^{S,R}$ is the amplitude coefficient for the scatter wave mode $\Psi_{u_i}^{S,R} = \frac{\cosh k(z+h)}{\cosh kh} H_u^{(2)}(kr_i) e^{iu\theta_i}$. Evanescent modes are not implemented since these are only relevant at surrounding distances from WEC i . The wave number k is calculated through the linear dispersion relationship:

$$gk \tanh kh = \omega^2, \quad (3.11)$$

where g is the acceleration of gravity.

Graf's addition theorem (41),

$$H_u^{(2)}(kr_i) e^{iu\theta_i} = \sum_{v=-\infty}^{\infty} H_{u-v}^{(2)}(kL_{ij}) e^{i(u-v)\alpha_{ij}} J_v(kr_j) e^{iv\theta_j}, \quad (3.12)$$

enables to transform scatter wave modes in local coordinates of WEC i into incident travelling wave modes in local coordinates of WEC j , $\Psi_{v_j}^I = \frac{\cosh k(z+h)}{\cosh kh} J_v(kr_j) e^{iv\theta_j}$, so that the total scatter wave field can be rewritten as

$$\tilde{\phi}_i^{S,R}(r_j, \theta_j, z) = \frac{\cosh k(z+h)}{\cosh kh} \sum_{u=-\infty}^{\infty} \sum_{v=-\infty}^{\infty} a_{u_i}^{S,R} H_{u-v}^{(2)}(kL_{ij}) e^{i(u-v)\alpha_{ij}} J_v(kr_j) e^{iv\theta_j}, \quad (3.13)$$

where J_v is the v th order Bessel function of the first kind.

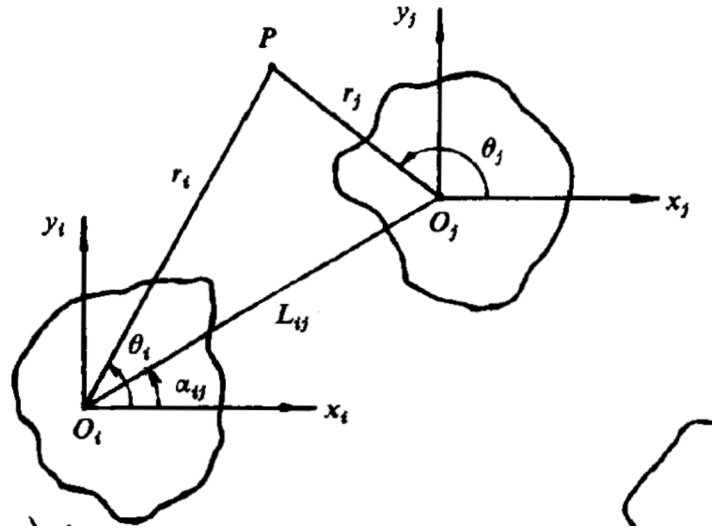


Figure 3.8: ketch of the local cylindrical coordinates for two WECs and the geometrical relationships between them (39)

Furthermore, the ambient plane wave can also be expressed by incident wave modes in local coordinates of WEC j ,

$$\tilde{\phi}_j^P(r_j, \theta_j, z) = \frac{\cosh k(z+h)}{\cosh kh} \sum_{v=-\infty}^{\infty} a_{v_j}^P J_v(kr_j) e^{iv\theta_j}, \quad (3.14)$$

with

$$a_{v_j}^P = \tilde{t} \frac{gA}{\omega} e^{-ik(X_j \cos \theta + Y_j \sin \theta)} e^{-iv(\theta + \pi/2)}. \quad (3.15)$$

Therefore, the total incident wave field around WEC j can be written from the contribution of the ambient plane wave, (3.14), and the waves scattered by the other WECs, (3.13), so that fully accounting for WEC interactions:

$$\tilde{\phi}_j^I = \frac{\cosh k(z+h)}{\cosh kh} \sum_{v=-\infty}^{\infty} \left(a_{v_j}^P + \sum_{i=0}^{N_b-1} \sum_{u=-\infty}^{\infty} a_{u_i}^S H_{u-v}^{(2)}(kL_{ij}) e^{i(u-v)\alpha_{ij}} \right) J_v(kr_j) e^{iv\theta_j}, \quad (3.16)$$

where a total number of $N_b - 1$ WECs has been considered.

On the other hand, diffraction transfer matrices exist, such that

$$a_{w_j}^S = \sum_{v=-\infty}^{\infty} B_{wv_j} a_{v_j}^I, \quad (3.17)$$

leading to the linear system of equations

$$a_{w_j}^S = \sum_{v=-\infty}^{\infty} B_{wv_j} \left(a_{v_j}^P + \sum_{i=0}^{N_b-1} \sum_{u=-\infty}^{\infty} a_{u_i}^S H_{u-v}^{(2)}(kL_{ij}) e^{i(u-v)\alpha_{ij}} \right) \quad w = -\infty, \dots, \infty, \quad (3.18)$$

to be solved for scatter wave amplitude coefficients.

Assuming a proper truncation order N_m for the infinite series, the system of equations in (3.18) can be written for the whole array, in matrix notation, as

$$(I - BT)a^S = Ba^P, \quad (3.19)$$

where

- $a^{S,P} = [a_0^{S,P} \quad \cdots \quad a_{N_b-1}^{S,P}]^T$, with $a_j^{S,P} = [a_{-N_m}^{S,P} \quad \cdots \quad a_{N_m}^{S,P}]^T$.
- $B = \begin{bmatrix} B_0 & 0 & 0 \\ 0 & \ddots & 0 \\ 0 & 0 & B_{N_b-1} \end{bmatrix}$, with $B_j = \begin{bmatrix} B_{-N_m-N_mj} & \cdots & B_{-N_mN_mj} \\ \vdots & \ddots & \vdots \\ B_{N_m-N_mj} & \cdots & B_{N_mN_mj} \end{bmatrix}$.
- $T = \begin{bmatrix} 0 & T_{10}^T & \cdots & T_{(N_b-1)0}^T \\ T_{01}^T & 0 & \cdots & T_{(N_b-1)1}^T \\ \vdots & \vdots & \ddots & \vdots \\ T_{0(N_b-1)}^T & T_{1(N_b-1)}^T & \cdots & T_{(N_b-1)(N_b-1)}^T \end{bmatrix}$, with $(T_{ij})_{uv} = H_{u-v}^{(2)}(kL_{ij})e^{i(u-v)\alpha_{ij}}$.
- I is the identity matrix.

The radiation problem due to the motion of body i in its degree of freedom d is similarly solved through

$$(I - BT)a^R = Ba_{d_i}^A, \quad (3.20)$$

with the ambient wave now being the wave radiated by body i in its degree of freedom d .

The complex amplitude velocity potential (3.10) representing such wave can be rewritten into incident waves to each WEC within the array by use of Graf's addition theorem (3.12), as seen before. Therefore, the amplitude coefficients for such ambient wave can be expressed as

$$a_{d_i}^A = [T_{0i}^T a_{d_i}^R \quad \cdots \quad T_{(N_b-1)i}^T a_{d_i}^R]^T, \quad (3.21)$$

with $a_{d_i}^R = [a_{-N_{md_i}}^R \quad \cdots \quad a_{N_{md_i}}^R]^T$.

$a_{d_i}^R$ is to be determined for the isolated WEC i moving in its degree of freedom d (see "Cylindrical wave amplitude coefficients").

Excitation and radiation forces

Similarly than the diffraction transfer matrix, the force transfer matrix is defined such that

$$\tilde{F}_{d_j}^D = \sum_{v=-\infty}^{\infty} G_{dvj} a_{vj}^I. \quad (3.22)$$

Assuming again a proper truncation order N_m for the infinite series, the complex amplitude of the excitation force vector $\tilde{\mathbf{F}}^D$ can be directly computed from

$$\tilde{\mathbf{F}}^D = \mathbf{G}(\mathbf{a}^P + \mathbf{T}\mathbf{a}^S), \quad (3.23)$$

where

- $\tilde{\mathbf{F}}^D = [\tilde{\mathbf{F}}_0^D \quad \cdots \quad \tilde{\mathbf{F}}_{N_b-1}^D]^T$, with $\tilde{\mathbf{F}}_j^D = [\tilde{F}_{0j}^D \quad \cdots \quad \tilde{F}_{D_j-1j}^D]^T$.
- $\mathbf{G} = \begin{bmatrix} \mathbf{G}_0 & \mathbf{0} & \mathbf{0} \\ \mathbf{0} & \ddots & \mathbf{0} \\ \mathbf{0} & \mathbf{0} & \mathbf{G}_{N_b-1} \end{bmatrix}$, with $\mathbf{G}_j = \begin{bmatrix} G_{0-N_{mj}} & \cdots & G_{0N_{mj}} \\ \vdots & \ddots & \vdots \\ G_{(D_j-1)-N_{mj}} & \cdots & G_{(D_j-1)N_{mj}} \end{bmatrix}$.
- D_j is the total number of degrees of freedom of WEC j .

In a similar manner, the complex amplitude of the radiation force $\tilde{\mathbf{F}}_{d_i}^R$ due to a unit displacement of WEC i in its degree of freedom d , $\tilde{X}_{d_i} = 1$, can be computed from the contribution of the excitation force at each not moving WEC and the radiation force experienced by WEC i when moving in d :

$$\tilde{\mathbf{F}}_{d_i}^R = \mathbf{G}(\mathbf{a}_{d_i}^A + \mathbf{T}\mathbf{a}^S) + \tilde{\mathbf{F}}_{d_i}^A, \quad (3.24)$$

where

- $\tilde{\mathbf{F}}_{d_i}^R = [(\tilde{\mathbf{F}}_{d_i}^R)_0 \quad \cdots \quad (\tilde{\mathbf{F}}_{d_i}^R)_{N_b-1}]^T$, with $(\tilde{\mathbf{F}}_{d_i}^R)_j = [(\tilde{F}_{d_i}^R)_{0j} \quad \cdots \quad (\tilde{F}_{d_i}^R)_{D_j-1j}]^T$.
- $\tilde{\mathbf{F}}_{d_i}^A = [(\tilde{\mathbf{F}}_{d_i}^A)_0 \quad \cdots \quad (\tilde{\mathbf{F}}_{d_i}^A)_{N_b-1}]^T$, with $(\tilde{\mathbf{F}}_{d_i}^A)_j = \begin{cases} \mathbf{0} & j \neq i \\ -(-\omega^2 \mathbf{M}_{:d_i}^R + i\omega \mathbf{C}_{:d_i}^R) & j = i \end{cases}$.

The radiation force experienced by WEC i when moving in all its degrees of freedom, $\tilde{\mathbf{F}}_i^R = -(-\omega^2 \mathbf{M}_i^R + i\omega \mathbf{C}_i^R)$, can be calculated by means of any boundary element method (BEM) software.

Cylindrical wave amplitude coefficients

The orthogonality of the system of functions $(e^{i-N_m\theta_i}, \dots, e^{iN_m\theta_i})$ in the interval $\theta_i \in [0, 2\pi]$ and $(\cosh k(z+h), \text{evanescent})$ in $z \in [-h, 0]$, used to represent the scatter wave field around WEC i (3.10), allow us to separate each wave mode through:

$$a_{u_i}^{S,R} = -\frac{i\omega}{2\pi g} \frac{2 \cosh kh}{h \left(1 + \frac{\sinh 2kh}{2kh}\right)} \frac{1}{H_u^{(2)}(kR_i)} \int_{-h}^0 \int_0^{2\pi} \tilde{\phi}_i^{S,R} e^{-iu\theta_i} \cosh k(z+h) d\theta_i dz \quad (3.25)$$

Thus, field points $\tilde{\phi}_i^{S,R}$ must be known over a cylinder of radius R_i around WEC i prior calculation of $a_{u_i}^{S,R}$.

The double integral in (3.25) is solved numerically so that a proper discretization of the cylinder is assumed. The required field points over the cylinder can then be computed by means of a BEM solver, such as Nemoh or WAMIT.

Diffraction and force transfer matrices

The diffraction and force transfer matrices for the isolated WEC j are defined as

$$\mathbf{a}_j^S = \mathbf{B}_j \mathbf{a}_j^P \quad (3.26)$$

and

$$\tilde{\mathbf{F}}_j^D = \mathbf{G}_j \mathbf{a}_j^P \quad (3.27)$$

respectively.

Then, diffraction and force transfer matrix coefficients can be solved from scatter wave amplitude coefficients (see “*Cylindrical wave amplitude coefficients*”), plane wave amplitude coefficients (see equation (3.15)) and excitation forces (computed from Nemoh or WAMIT) due to at least $2N_m + 1$ plane waves, going from $\theta = 0$ to $\theta = 2\pi$ directions of propagation, through

$$\begin{bmatrix} a_{u_j}^S(0) \\ \vdots \\ a_{u_j}^S(2\pi) \end{bmatrix} = \begin{bmatrix} a_{-N_{m_j}}^P(0) & \cdots & a_{N_{m_j}}^P(0) \\ \vdots & \cdots & \vdots \\ a_{-N_{m_j}}^P(2\pi) & \cdots & a_{N_{m_j}}^P(2\pi) \end{bmatrix} \begin{bmatrix} B_{u-N_{m_j}} \\ \vdots \\ B_{uN_{m_j}} \end{bmatrix}, \quad (3.28)$$

for $u = -N_m, \dots, N_m$, and

$$\begin{bmatrix} \tilde{F}_{d_j}^D(0) \\ \vdots \\ \tilde{F}_{d_j}^D(2\pi) \end{bmatrix} = \begin{bmatrix} a_{-N_{m_j}}^P(0) & \cdots & a_{N_{m_j}}^P(0) \\ \vdots & \cdots & \vdots \\ a_{-N_{m_j}}^P(2\pi) & \cdots & a_{N_{m_j}}^P(2\pi) \end{bmatrix} \begin{bmatrix} G_{d-N_{m_j}} \\ \vdots \\ G_{dN_{m_j}} \end{bmatrix}, \quad (3.29)$$

for $d = 0, \dots, D_j - 1$.

Normally, the systems of equations (3.28) and (3.29) are overdetermined by considering more than $2N_m + 1$ plane waves. This is strongly recommended in order to get a better estimate of the diffraction and force transfer matrices.

3.3.2.3 POWER FITTING

The power matrix fitting methodology has been introduced into the wave submodel in order to increase the reliability of the numerical model. In facts, the number of assumption embedded into the linear theory, can easily bring to an unrealistic behaviour of the system if compared with the physical machine behaviour.

The key concept of the method is to reduce the error between the synthetic power matrix, built using the linear theory, and the power matrix associated (and certified) to the real machine. The error is attributed to two linear parameters, being a damping \mathbf{C}^A , and a stiffness term \mathbf{K}^A . In this way, additional friction and stiffness, as well as hydrodynamic viscous damping and other losses are linearized and fed into the model.

The error is calculated and minimised for each sea state, $(H_S, T_p, \alpha_p)_l$, so that there will be additional damping and stiffness matrices for each sea state, (C_l^A, K_l^A) .

The error is minimised using a heuristic optimisation routine, in particular a quasi-Newton's method. The method uses a local approximation of the trend with a quadratic function, estimate the Jacobian and the Hessian and search for a local minimum and maximum. The implemented method is a low memory usage method called L-BFGS-B algorithm. For further details see (42).

3.3.2.4 RESOURCE REDUCTION

Compute mechanical energy per unit area.

3.3.2.5 SUMMARY OF THE ALGORITHM

The steps to calculate the yearly averaged power production and the q-factor are summarized in the following flow chart:

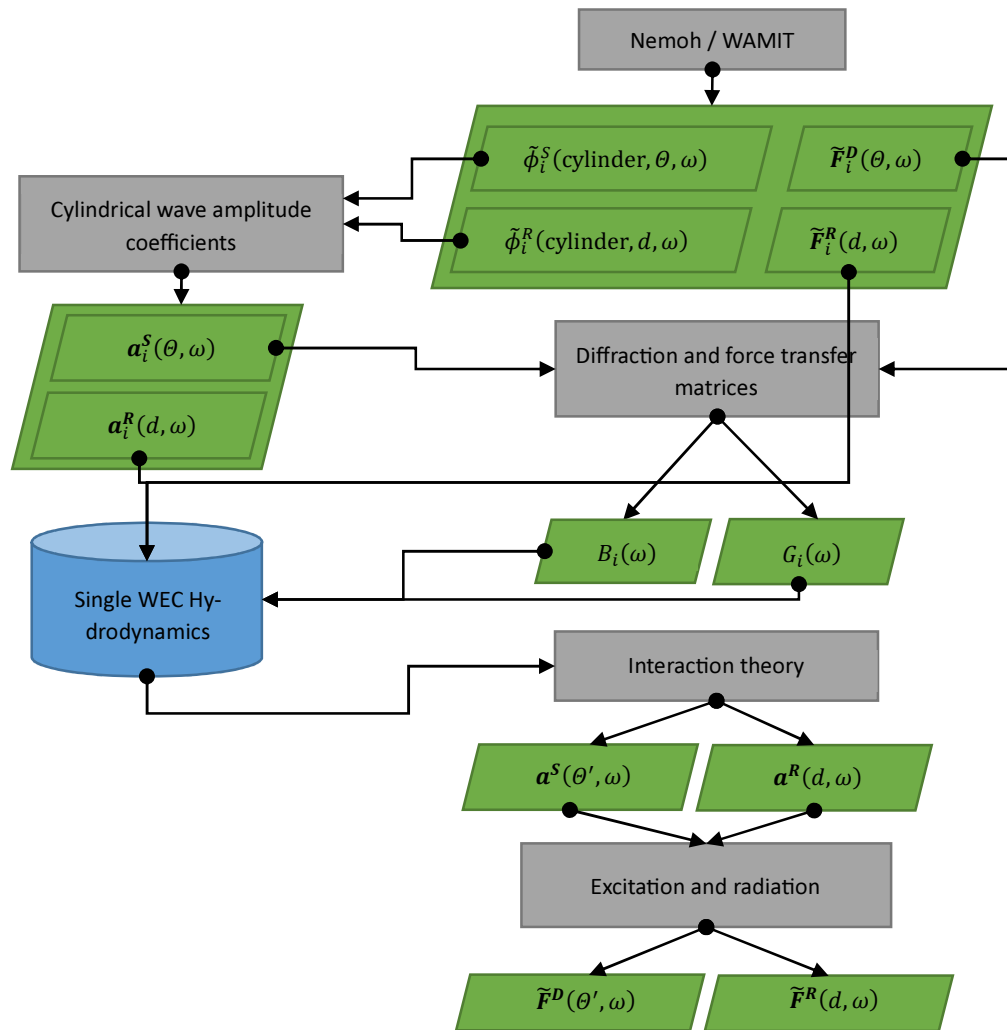


Figure 3.9: Wave submodel algorithm

It follows:

1. Power fitting to get C^A and K^A .
2. Solve equation of motion in frequency domain for ω frequencies and θ' directions.
3. Solve AEP for l sea states.

3.3.2.6 ASSUMPTIONS AND LIMITATIONS

There are some limitations on the wave submodel due to the assumptions made on the theoretical formulation. These are listed here below:

Table 3.3: Limitations on the wave submodel stemming from the assumptions made on the theoretical formulation.

Assumption	Limitation
Inviscid flow.	Viscous forces are disregarded (only gravity forces).
Irrotational flow.	Vorticity is zero (thin boundary layer in good agreement with inviscid flow).
Constant water depth.	The bathymetric changes are disregarded.
Linearization of the boundary conditions on the free surface.	Amplitudes of the waves are much smaller than the wave length.
Linearization of the boundary condition on the WEC surface.	Amplitude of the WECs motion is much smaller than the wave length.
Wave field representation outside and immediate neighbourhood of a WEC in the array.	The wave field inside the enclosing cylinder is not valid. The cylinders enclosing the WECs do not overlap vertically
Frequency domain analysis.	The PTO system is a linear damper. Nonlinear forces are disregarded.

Inviscid and irrotational flow

The viscosity of the water is known to be low compared to other Newtonian fluids such as honey, oil or gasoline. Therefore, treating the flow of water as inviscid is usually well-accepted, which makes the wave-WEC array interaction problem easier to solve. However, since the water does have some viscosity, assuming inviscid flow will invariably introduce some inaccuracy on the results.

The viscous effects are confined within a region called boundary layer, close to the fluid boundaries. In this region shear stresses will arise between fluid-fluid and fluid-solid contact surfaces with the consequent development of vortices (rotational flow) and a resultant integrated drag (friction drag) and lift forces on the solid.

For water-waves the boundary layer is known to remain thin and thus the developed flow is usually modelled as inviscid and irrotational. However, when water-waves interact with an array of WECs such assumption might be no longer valid.

The viscous effects on the WECs are usually taken into account by means of a quadratic drag force approximation which involves a drag coefficient determined from experimental data. Hence, the user might decide the convenience of inviscid and irrotational flow assumption by comparing the approximated drag force against the hydrodynamic forces from linearized potential flow theory (excitation and radiation forces).

It must also be mentioned that since the drag force is quadratic with the fluid-solid velocity and WP2 tool solves the equation of motion in frequency domain, the quadratic drag force is not herein considered.

Constant water depth

The bathymetric changes are not considered. This assumption is well agreed for deep water waves but it might not be valid when dealing with WECs set up in intermediate-shallow water wave conditions. Therefore, the user might decide the convenience of constant water depth assumption by assessing the deviation between the inputted water depth and the actual bathymetry in the cases of intermediate-shallow water waves.

Linearized wave-structure interaction problem

The linearization of the problem requires the waves and the WECs motion amplitude to be small compared with the wave length. The validity of this assumption can only be decided by the user. He or she might decide the convenience of the assumption of linearity by comparing the actual waves he or she want to use for the analysis with a linear wave. In other words, if the actual waves are not well represented by cosine waves, the WP2 tool will produce inaccurate results.

Wave field representation

The wave field solution used in WP2 tool to further compute wave forces on WECs is valid outside a virtual cylinder enclosing each WEC of the array. Therefore, the WECs throughout the array must not overlap vertically; otherwise the interaction forces between the intersecting WECs will come from an invalid wave field representation. Therefore, the user should take into account that the virtual cylinders enclosing the WECs cannot intersect at any point.

3.3.3 TIDAL HYDRODYNAMICS AND ARRAY ENERGY OUTPUT CALCULATION

Figure 3.10 **Error! Reference source not found.** represents the latest software architecture for the WP2 Tidal model.

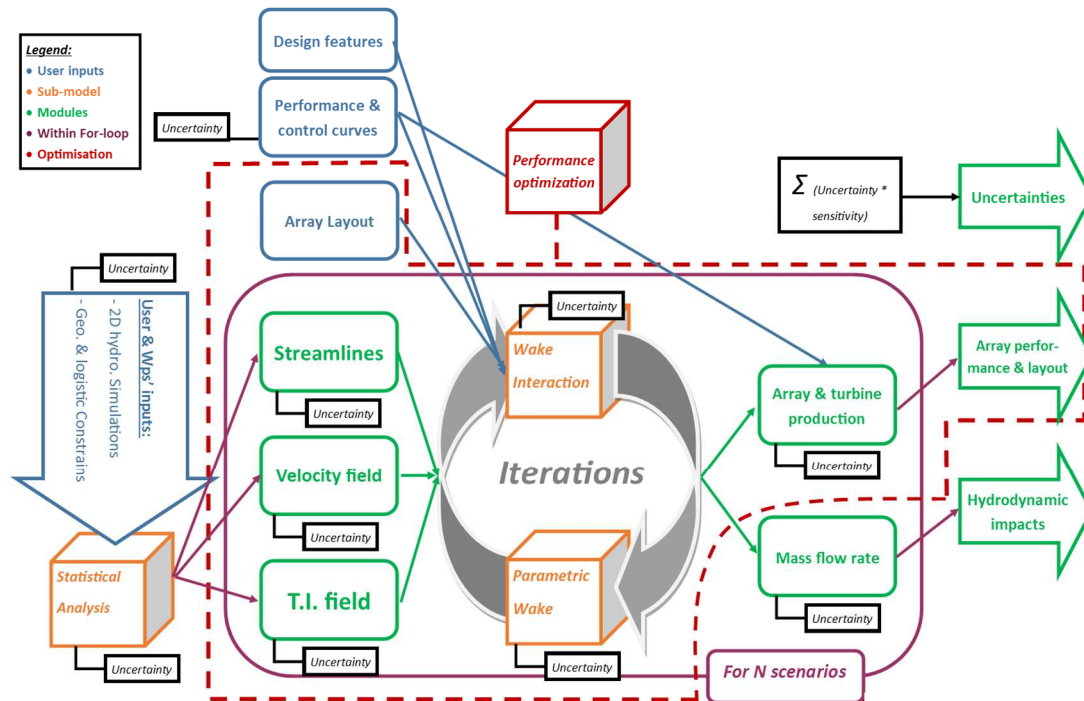


Figure 3.10: Software architecture for the WP2 Tidal model - conceptual diagram

Sandia's wake module, described below, was incorporated into the model as a lookup table of velocity deficit in the region around and behind the turbine. Sandia's lookup table is formed of a 2D array of the Coefficient of Thrust (Ct) vs. Turbulence intensity (TI). This raises the possibility of increasing the granularity of the lookup table and this will be investigated in the coming months.

The entire framework is articulated around "classes" which comprise of "attributes" and "methods" or, by extension, inputs, modules and sub-models.

3.3.3.1 CLASSES OVERVIEW

So far the framework possesses 3 classes, namely "Hydro", "Array" and "WakeInteraction":

Hydro class:

The Hydro class input is a pickle file gathering velocity field data for now (i.e. x, y, U, V). Ultimately, this class will retrieve its inputs from the data-hub as described in the In/Out (I/O) list below.

The Hydro attributes are:

- X: coordinates along x axis (1D array, in meters and assuming a regular grid)
- Y: coordinates along y axis (1D array, in meters and assuming a regular grid)
- U: depth averaged velocity component along x axis (2D array, in m/s and assuming a regular grid)
- V: depth averaged velocity component along y axis (2D array, in m/s and assuming a regular grid)
- `_bounding_box`: area defined by the outer boundaries of the grid (shapely.geometry.Polygon object and assuming a regular grid)

Optionally, this class can also plot flow velocity arrows and a contoured colour map.

Array class:

The Array class inputs are two pickle files, respectively gathering the turbines positions (i.e. x, y, z) and the turbine design features (i.e. cut-in & cut-out speeds, Ct & Cp curves, rotor diameter), as well as a Hydro object (i.e. initialised from Hydro class).

The Array attributes are:

- N is the number of turbines in the array.
- Positions: Turbine positions: x, y, z.
- Features: design features (Cp and Ct) for each turbine.
- streamline: streamline trajectory for each turbine
- distances: relative distances (across and along streamline) of all turbines downstream of each the turbine
- velHub: U, V velocity components at hub location for each turbine

In order to compute the streamline of each turbine, the “streamline” module is used. This module simulate numerical Lagrangian drifter at each of the device location and computes their trajectories by using steady-state advection. In this case, the code has been adapted from Raymond Speth’s code (43).

The relative distances to the streamlines were computed by finding the perpendicular vectors to the streamlines passing through the downstream turbines. This is achieved by using the following theorem: the scalar product of two perpendicular vectors is equal to zero.

The velHub is extracted from the velocity field at each turbine location.

WakeInteraction class:

The WakeInteraction class inputs are a Hydro object and an Array object respectively initialised from Hydro and Array class.

The WakeInteraction attributes are:

- indMat: 2D array (N,N) gathering relative induction factor to each and every one turbines.
- Induction: 1D array (n) gathering the “cumulative” induction factor for each turbine.

- wake: wake parametric sub-model unique to each turbine and each design parameters
- wakeShape: parametric wake shape

The WakeInteraction methods are:

- solv_induction: Using the “indMat” and “wake” attributes, this method iteratively resolves the inter-dependent induction factors, and thus the array velocity interaction, until reaching a convergence criteria (here, maximum cumulative discrepancy between two iterations < 0.01 m/s). After convergence the “velHub” attribute of the “Array” object is updated
- solv_wake: this method is still under development but will ultimately computes, after induction convergence, the overall wake shapes for each turbine. This will be used to compute the turbine induced velocity field and thus perform hydrodynamic assessments for environmental impact, mooring, structure as well as any other WP in need of this type of data.

3.3.3.2 STATISTICAL ANALYSIS

Selection of a representation current time series

The user provides 2D current fields $U(x,y,t)$ with a duration of at least 30 days and a time resolution of a least 1 hour.

The user is invited to pick the location of the point that he believes to be representative of the hydrodynamics of the site of interest (we may alternatively propose the centre of the wave farm for instance).

Our python tool will then perform interpolation to extract the corresponding time series $U_0(t)$. $U_0(t)$ is a vector with components $(u(t), v(t))$ that we will refer to as (u, v) in the rest of the document. We shall further use a time series extracted from ADCP measurements, gathered over a French tidal site for illustration.

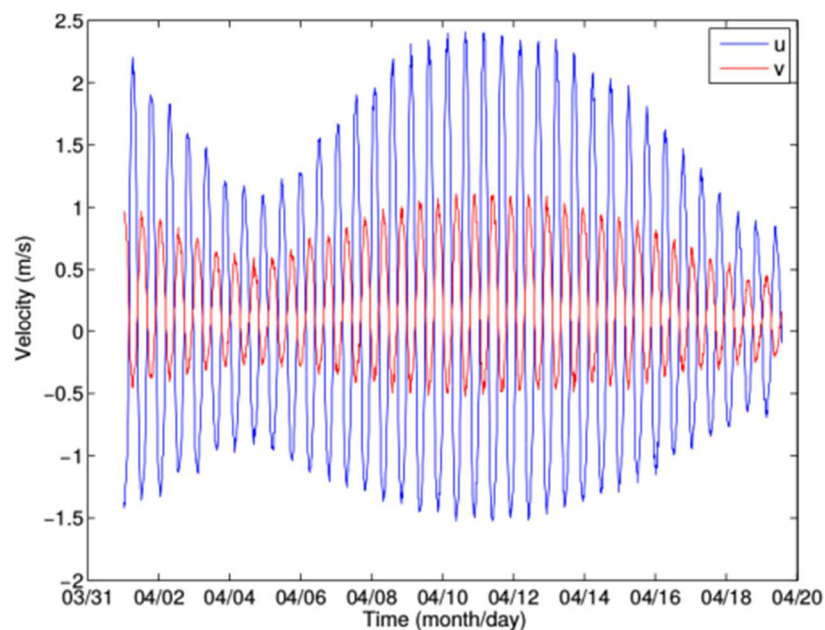


Figure 3.11: u and v time series (18.55 days) from ADCP data collected over a French tidal site.

Computation of the 2D probability function: $p(u,v)$:

The 2D probability function of u and v is computed based on the initial time series of the two components (see Figure 3.11). The u and v data is binned into N_u and N_v elements from the definition that follows:

$$N_u = \text{length}([1.1 * \min(u): du: 1.1 * \max(u)]) = \text{length}([u1: du: u2]) \quad (3.30)$$

$$N_v = \text{length}([1.1 * \min(v): dv: 1.1 * \max(v)]) = \text{length}([v1: dv: v2]) \quad (3.31)$$

The increments du and dv will be set to 0.1 m/s here.

A double loop is then performed over (u,v) to fill the $p(u,v)$ matrix (see Figure 3.12).

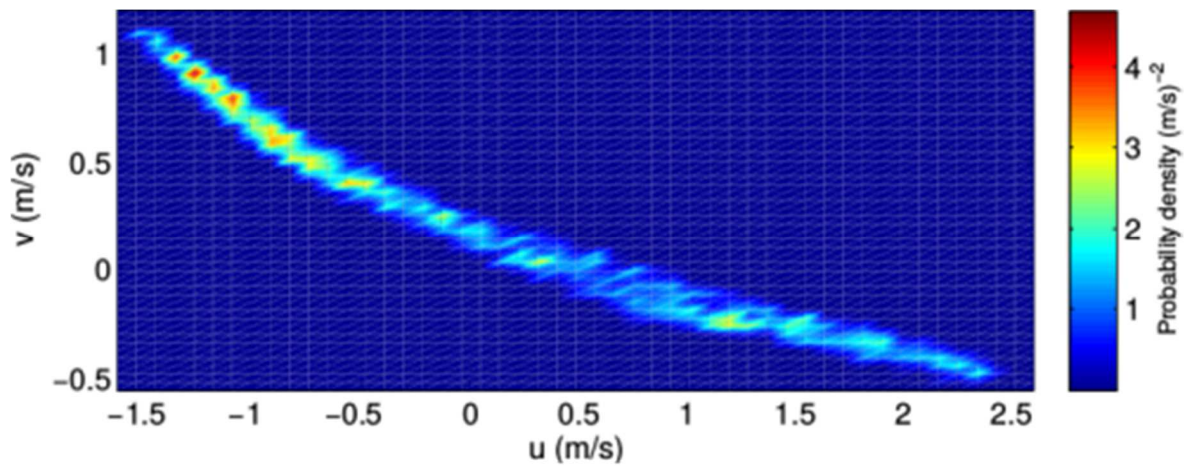


Figure 3.12: Probability density function $p(u,v)$ corresponding the time series displayed in Figure 3.11.

Determination of N_s scenarios:

We first determine the velocity components with the largest variance to capture correctly the ebb/flood features. In our case, the component u shows the largest variance (see Figure 3.12) and is therefore selected for the next step. The u -axis is then binned into N_s elements u_s regularly spaced. For each of the N_s elements, the 1D pdf $p_{us}(v)$ is computed, with i an integer varying from 1 to N_s . Then the v -velocity of the scenario is v_s , estimated based on:

$$v = \frac{\int_{v1}^{v2} v p(u_s, v) dv}{\int_{v1}^{v2} p(u_s, v) dv} \quad (3.32)$$

In our illustration, N_s was set to 10 and the 10 $p_{us}(v)$ are displayed in Figure 3.13.

We now have N_s scenarios, made of N_s couples (u_s, v_s) . Each scenario has the probability of occurrence P given by:

$$P(s) = \int_{v_{s1}}^{v_{s2}} \int_{u_{s1}}^{u_{s2}} p(u, v) du dv \quad (3.33)$$

With u_{s1} , u_{s2} and v_{s1} , v_{s2} are integral bounds varying for each scenario.

Selection of the corresponding 2D field in the initial data set:

We shall extract N_s velocity fields from the user's dataset. For this, we propose to pick the N_s time steps t_s that minimize the difference:

$$d_s = |u_s - u(t_s)| + |v_s - v(t_s)| \quad (3.34)$$

The N_s extracted velocity fields, $U(x, y, t_s)$ is assumed to have the probability of occurrence $P(s)$. This subset of data can be used to estimate e.g., the average power output of the farm.

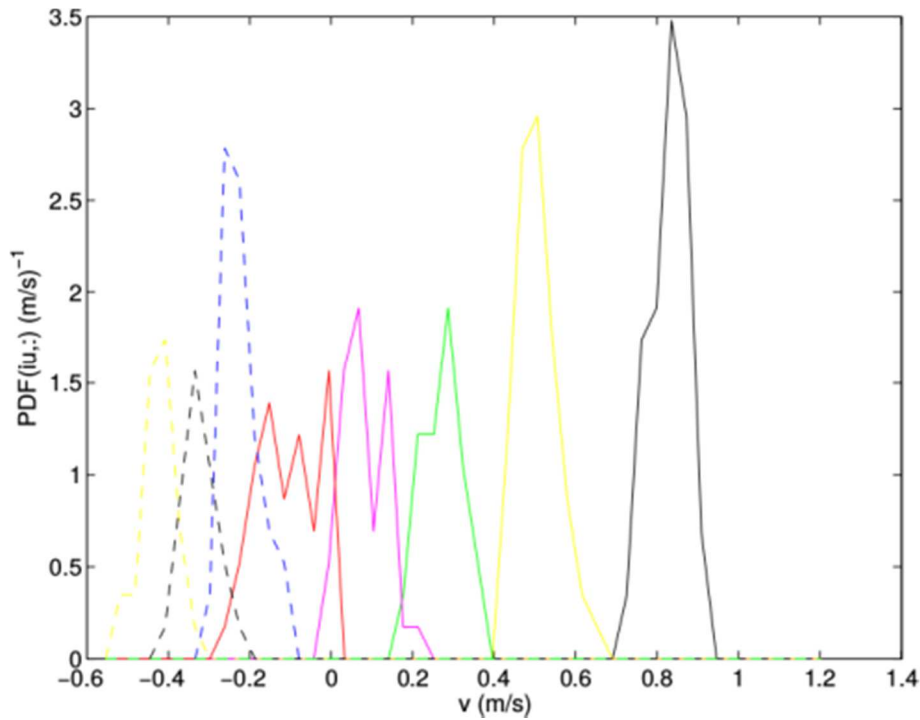


Figure 3.13: The 10 probability density functions $p(u, v)$ used to estimate the velocity v_s as described in.

3.3.3.3 PARAMETERIZATION METHODOLOGY

Describes the parametrization methodology for the last remaining model features.

Vertical profiling of flow velocity

The current model does not resolve the vertical velocity profile per se but assumes its shape based on power-law formulas. The classical power-law formula for flow velocity (44) can be expressed as follows:

$$u(y) = u_r \left(\frac{y}{a} \right)^{\frac{1}{m}} \quad (3.35)$$

where:

- y is the distance along the vertical axis from bottom-up (m)
- u_r is the reference velocity (m/s)
- a height of the layer (m)

According to Lee, 2003 (45), the exponent m can be derived the Reynolds number Re of the considered flow and the Manning coefficient n related to the geological nature of the bottom of the water column as such:

$$m = k \sqrt{\frac{Re^{\frac{1}{3}}}{n^2 * g}} \quad (3.36)$$

where:

- k is the Von Karman constant
- g is the gravitational constant for the Earth

Assuming that the reference velocity u_r is equal to the depth averaged velocity U and that height of the layer a can be expressed as the total water column height H multiplied by a yet-unknown coefficient, C , equation (3.35) can be re-written as follows:

$$u(y) = U \left(\frac{y}{C * H} \right)^{\frac{1}{m}} \quad (3.37)$$

In the context of open-channels, the Reynolds number, Re , is:

$$Re = \frac{U * H}{\nu} \quad (3.38)$$

where ν is the water's kinematic viscosity (m²/s).

Assuming that averaging the velocity vertical profile $u(y)$ over the entire water column is to be equal to the depth averaged velocity, U , gives:

$$\frac{1}{H} \int_0^H U \left(\frac{y}{C * H} \right)^{\frac{1}{m}} dy = U \quad (3.39)$$

Resolving this equation allows the remaining unknown coefficient, C , to be expressed as a function of known parameters. From equation (3.39):

$$\frac{1}{C * H^2} \left[y^{\left(\frac{1}{m}+1\right)} \right]_0^H = 1 \quad (3.40)$$

And thus:

$$C = \frac{H^{\left(\frac{1}{m}-1\right)}}{\frac{1}{m} + 1} \quad (3.41)$$

Consequently, given that U , H and n are known, the velocity vertical profiles can be evaluated at any given point of the model's domain by using, in order, equations (3.36), (3.41) and (3.37).

3.3.3.4 TURBINE WAKE SUBMODULE

The purpose of the DTOcean project is to develop a fast-running, easy to use Current Energy Capture (CEC) array spacing tool that considers tidal array performance vs. efficiency. As such this section describes the development of the device wake modelling submodule that determines the properties of the wake generated by tidal turbines (i.e. wake growth and dissipation). Initial efforts were focused on implementing simple analytic models, which have been historically used for wind turbine wakes. While these methods are very simple and quick to run, they lack the fidelity desired to adequately describe the complex features of physical turbine wakes. CFD models were then explored due to their ability to accurately capture wake structure in detail. While CFD is more capable than simplified analytic models, the cases are not always easy to set up and can be very time consuming to perform.

In an attempt to merge the benefits of each method, a hybrid type model was developed. This model consists of a CFD simulation database from which interpolated solutions can be obtained instantly. A test matrix of CFD simulations using non-dimensionalised inflow and turbine diameter conditions as well as spanning a wide range of thrust coefficients and inflow turbulent intensities was populated, and an algorithm to interpolate intermediate points was developed. The result is a fast-running tool with the capability to produce high-level, detailed wake flow results as a function of incident velocity, incident turbulence intensity, turbine diameter, and turbine thrust. Additional parameters that effect tidal turbine wakes, such as yaw angle to incident flow and vertical blockage ratio have been incorporated into the model in the form of transformations to the baseline database wake result.

CFD wake modelling

Simple algebraic models have been proposed for fast modelling of turbine wakes such as those of Jensen (46) and Larsen (47). These models are analytical equations for turbine wake velocity as a function of spatial location, resulting in a fast representation of a wake field. While these models can be run very quickly, they typically require input information which is not always known *a priori*. In addition, initial research efforts by Sandia investigated these methods, however found them to be deficient

in accurately representing wake flow parameters. For these reasons it was decided to go with a more robust method of modelling turbine wakes.

While it is much more computationally expensive, CFD modelling is not subject to the same limitations as the analytical models. To validate the use of CFD models, Sandia has run CFD simulations of the SAFL experiments using actuator disks to model the CEC turbine.

Although the standard version of OpenFOAM contains an actuator disk model, it requires the user to know the turbine coefficient of power, and to declare an upstream “infinity” point where reference values are to be obtained. It solves the following equations for the force term of the momentum equation.

$$F = 2\rho AU_{\infty}^2 a(1 - a) \quad (3.42)$$

where a is the induction factor, which is calculated as follows:

$$a = \frac{C_P}{C_T} \quad (3.43)$$

As shown by Roc (48), the same force equation can be written as:

$$F = \frac{1}{2}\rho \left(4 \frac{1 - \sqrt{1 - C_T}}{1 + \sqrt{1 - C_T}} \right) AU_d^2 \quad (3.44)$$

This formulation takes advantage of the definition $C_T = 4a(1 - a)$ in order to drop C_P from the equations. Writing force in this manner means that the only information required about the turbine is the coefficient of thrust.

This formulation also uses the relationship between U_d and U_{∞} to eliminate the need for “infinity” values. The benefit of this is that in complex flows, it can be difficult to find an undisturbed spot in the flow from which to acquire reference values. By writing the force equation only in terms of values at the disk location, the need to identify such a location is eliminated.

The above representation of the actuator disk force was implemented into OpenFOAM and the following CFD calculations were run using that model. The flow conditions for these models were chosen to be as close as possible to the experiments in order to validate the CFD method. The domain dimensions used for the SAFL simulation were 2.75m wide by 1.15m deep and were chosen to match the experiment. The simulation was started 2.0m (4 diameters) upstream of the turbine and the outflow was placed 6.0m (12 diameters) downstream of the turbine. The turbine hub centre height was placed at 0.425m as was done in the experiment. The inflow velocity of 0.4 m/s was chosen to correspond with the experiment and the thrust coefficient of 0.9975 was chosen to match the very low wake velocity seen in the experimental data (thrust coefficient was not measured for the SAFL tests). Wall boundary conditions were used to represent the channel sides and bottom and a no slip wall condition was used on the free surface boundary. The CFD results appear to match the data very well. The results are shown below in Figure 3.14.

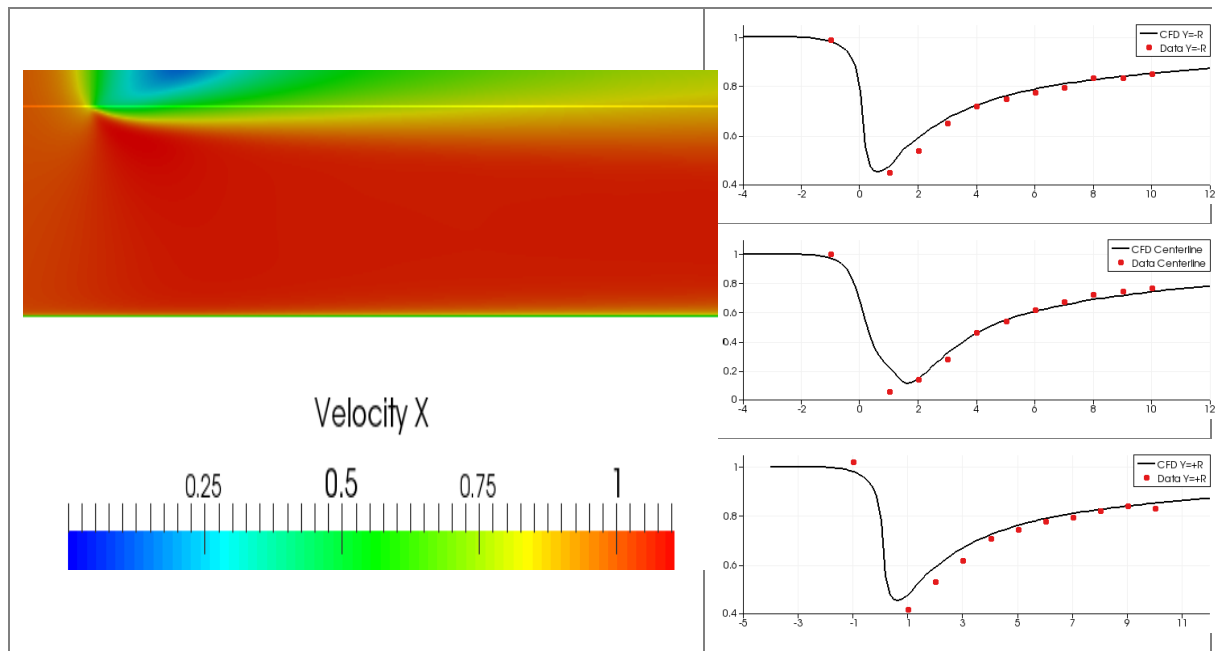


Figure 3.14: CEC wake results from OpenFOAM.

On the left is a top down contour plot of relative velocity, and on the right are axial direction relative velocity plots at $Y=R$, $Y=0$, and $Y=-R$ (top to bottom) compared to SAFL data.

As a second validation, the CFD model was compared to the experiments of Maganga (49). Maganga ran two sets of experiments and CFD simulations were run to compare to both of these. Case A was a CEC turbine with a thrust coefficient of 0.70 and an incoming turbulent intensity of 0.046. Case B was a CEC turbine with a thrust coefficient of 0.62 and an incoming turbulent intensity of 0.14.

The comparisons to both cases are shown below.

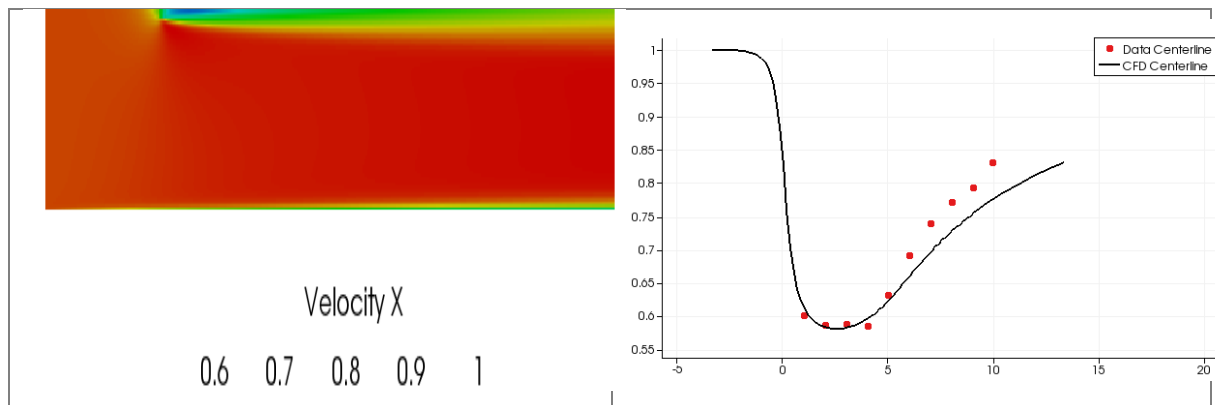


Figure 3.15: CEC wake results using OpenFOAM.

On the left is a top down contour plot of relative velocity, and on the right is a relative velocity plot at the wake centreline compared to Maganga data $C_T=0.70$, $TI=0.046$.

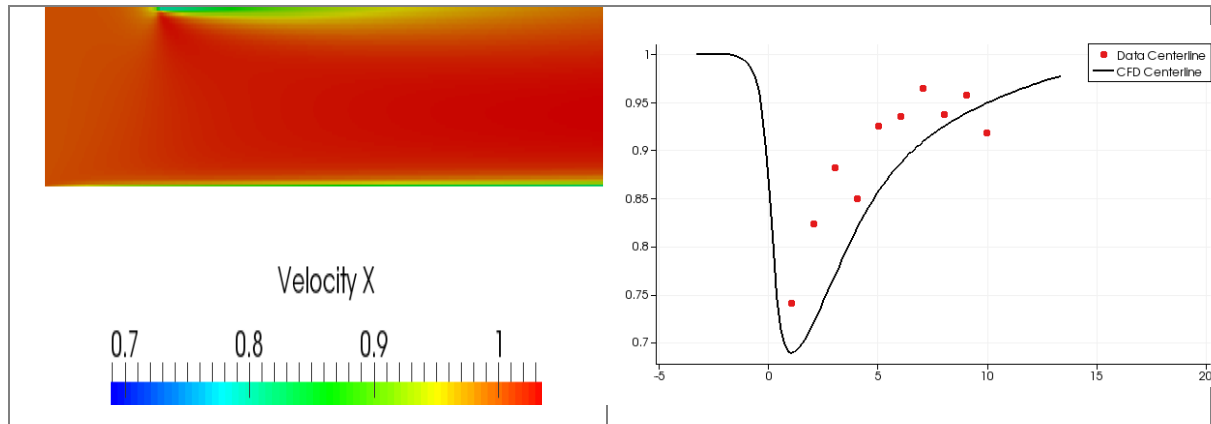


Figure 3.16: CEC wake results using OpenFOAM.

On the left is a top down contour plot of relative velocity, and on the right is a relative velocity plot at the wake centreline compared to Maganga data $C_T=0.62$, $TI=0.14$.

Note that the wake velocity centreline recovers much quicker for the case with larger incident turbulent intensity. Again the actuator disk CFD model appears to match the experimental data very well, and capture the different traits of the two experiments.

CFD populated empirical model

The above sections show the benefits of the analytical modelling approach (speed and simplicity) as well as the benefits of the CFD modelling approach (robustness and accuracy). The wake modelling approach employed here is a hybrid model consisting of high fidelity CFD wake solutions combined with an interpolation scheme and lookup table. By running a matrix of CFD cases it is possible to create a database of CFD solutions which span the parameter space of interest. By using a barycentric interpolation scheme, wakes corresponding to points within this parameter space can be inferred from the solutions at the nearest defined points in the parameter space.

Sandia has run a series of axisymmetric CFD solutions on a test matrix of 100 test conditions. Ten different thrust coefficients, and ten different turbulent intensities were simulated in preparation of this database. Ten thrust coefficient values were distributed evenly between 0.1 and 1.0, and ten turbulent intensity values were distributed between 0 and 0.3 with increased discretization between 0.05 and 0.2. The parameter space is illustrated below.

$$C_T = [0.1, 0.2, 0.3, 0.4, 0.5, 0.6, 0.7, 0.8, 0.9, 1.0]$$

$$TI = [0.000, 0.050, 0.075, 0.100, 0.125, 0.150, 0.175, 0.200, 0.250, 0.300]$$

In order to perform these calculations, a custom version of the open-source CFD software package, OpenFOAM was created. The modifications to OpenFOAM involved adding a volumetric force opposing the flow (a momentum sink) which was calculated using the following formulation previously developed by Roc, 2013 (50).

$$F = \frac{1}{2} \rho \left(4 \frac{1 - \sqrt{1 - C_T}}{1 + \sqrt{1 - C_T}} \right) A U_d^2$$

This formulation takes advantage of momentum theory and the relations $C_T = 4a(1 - a)$ and $U_d = (1 - a)U_\infty$ in order to drop U_∞ from the typical drag equations. Writing force in this manner means that the only information required about the turbine is the coefficient of thrust.

This formulation also uses the relationship between U_d and U_∞ to eliminate the need for “infinity” values. The benefit of this is that in complex flows, it can be difficult to find an undisturbed spot in the flow from which to acquire reference values. By writing the force equation only in terms of values at the disk location, we eliminate the need to identify such a location.

The above representation of the actuator disk force was implemented into OpenFOAM and the following CFD calculations were run using that model.

With the database of cases populated, a Barycentric interpolation routine was written. Given any value for C_T or TI the nearest three points on the test matrix are located. Barycentric linear interpolation is performed from those three points to the target point, resulting in an interpolated flow-field which is a function of the closest solutions available.

By using interpolation between the database entries, it should be possible to represent the basic flow conditions for any device parameters inside of the simulated range. However, multiple wake interactions and blockage effects due to the ground or riverbed walls will need to be included separately as an additional model.

Figure 3.17 below shows an interpolated solution for $C_T=0.82$ and $TI=0.09$. The results are a weighted average using the table below.

Table 3.4: Weighting values for Figure 3.17

Thrust Coefficient	Turbulent Intensity	Weighting Factor
0.8	0.075	0.4
0.8	0.100	0.4
0.9	0.100	0.2

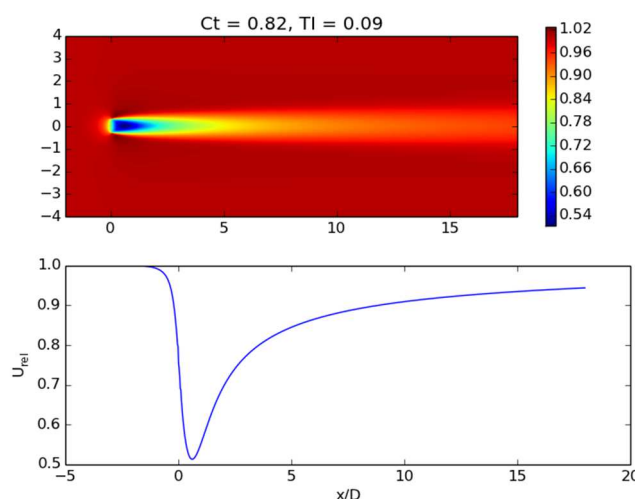


Figure 3.17: Example of the parametric interpolated solution.

At the top is the interpolated wake velocity contour plot, and at the bottom is the centreline wake velocity.

The parametric CFD model was then tested against the Maganga data (51). Note that this is not a direct CFD calculation of the Maganga experiment. This is an interpolated solution from nearby results in the CFD database.

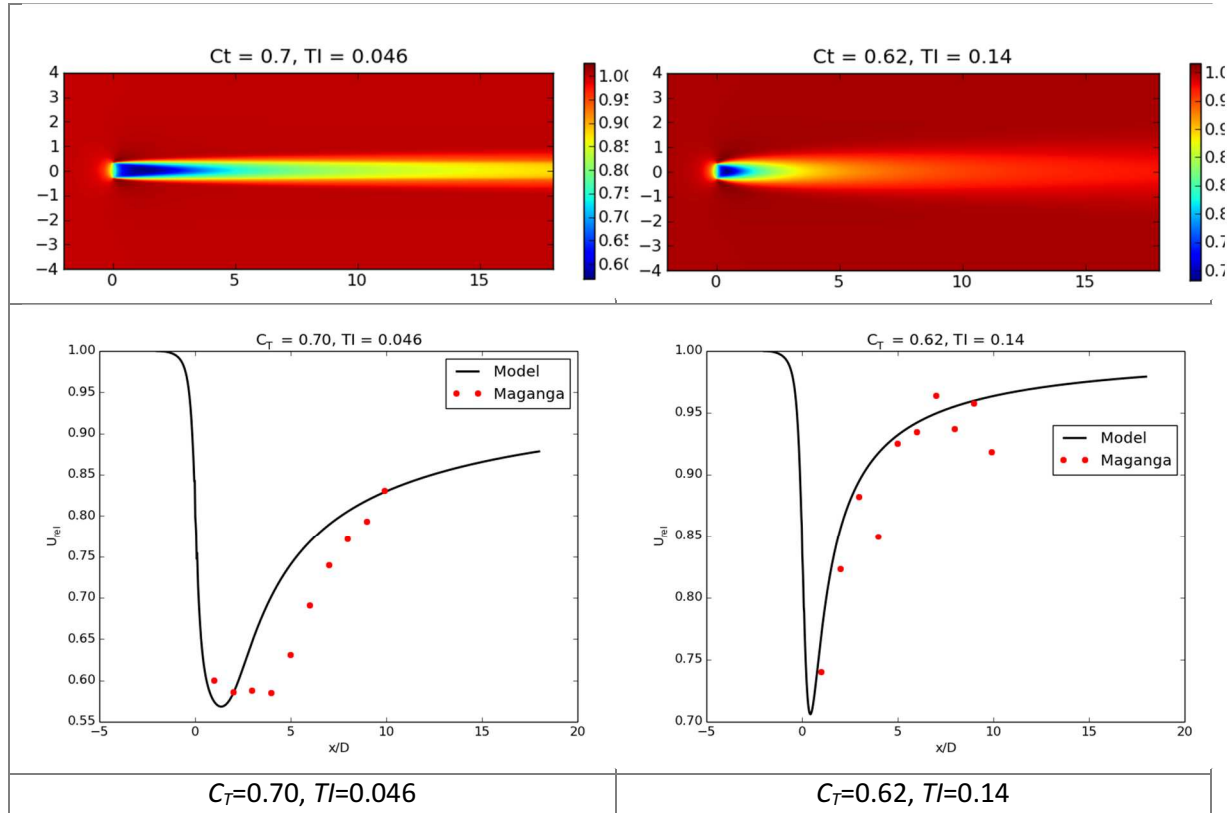


Figure 3.18: Parametric CFD model results.

At the top is the interpolated wake velocity contour plot, and at the bottom is the centreline wake velocity compared to the Maganga data.

The interpolated solutions from the database fit the data quite well; especially considering the high blockage ratio's present in the flume experiments that were not modelled within the CFD database.

It should be noted that while Sandia's database was populated using the above discretization in parameter space, the DTOcean utility will allow for an arbitrary parameter space defined by the user.

C_T calculation

All of the above models depend on knowing the coefficient of thrust of the CEC to be modelled. Most of the time this is given by the experimentalists; however this is not always the case. For cases where this value is unknown (for the example the SAFL dataset), it is inferred from the flow characteristics. Momentum theory gives us the relationship between wake velocity and thrust coefficient, as shown in (48).

$$U_w = (1 - 2a)U_\infty \quad (3.45)$$

$$C_T = 4a(1 - a) \quad (3.46)$$

Working from this you can get an expression for C_T in terms of U_w . This relation is expressed below along with a plot in terms of U_w/U_{inf} and U_{def} .

$$a = \left(1 - \frac{U_w}{U_{\infty}}\right)/2 \quad (3.47)$$

$$C_T = \left(1 - \frac{U_w}{U_{\infty}}\right)\left(1 + \frac{U_w}{U_{\infty}}\right) \quad (3.48)$$

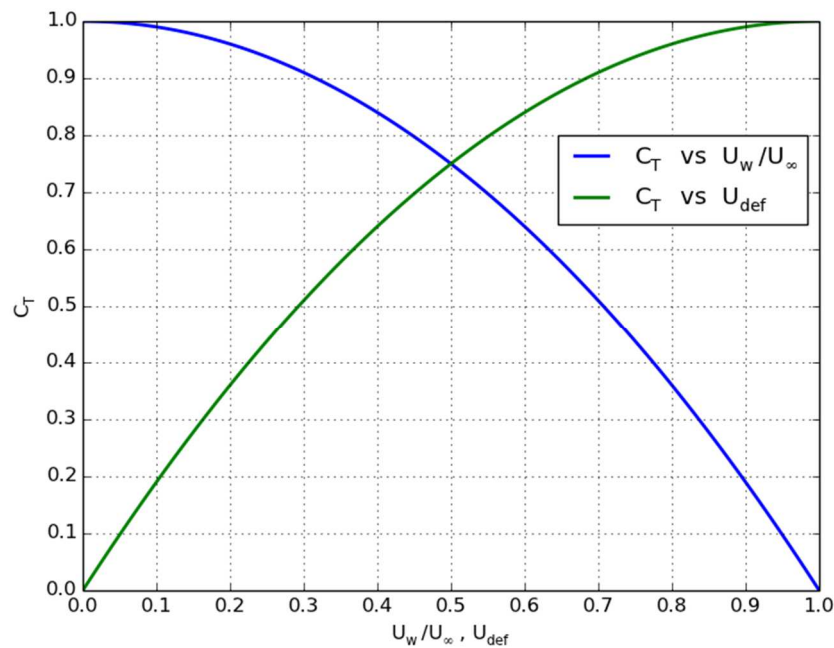


Figure 3.19: C_T vs. wake velocity/velocity deficit according to momentum theory.

For cases where the coefficient of thrust is unknown, the above relation is used to infer this value. The table below shows a comparison of the thrust coefficient inferred from momentum theory and the value given by the experimentalists. It should be noted that this chart represents a crude estimate based on the minimum wake velocity reported in the experiments. Often, velocities cannot be measured at locations less than 2-3 diameters downstream.

Table 3.5: Thrust coefficients measured by experimentalists compared to the velocity backed out value.

Case	Given C_T	Min U_w/U_{inf}	Inferred C_T
Maganga A (49)	0.70	0.584	0.659
Maganga B (49)	0.62	0.74	0.452
SAFL	NA	0.05	0.9975
Chilworth three-disc (52)	0.91	0.41	0.83

Table 3.5 above shows a comparison of the thrust coefficient value given by the experimentalists as compared to the value derived from wake velocity. The table shows that the inferred value is generally lower than the measured value. This may be due to turbulent mixing of the free stream into the wake velocity making the absorbed momentum appear to be lower. Indeed, in Case B of the Maganga data, where the turbulent intensity is very high, we see a difference of over 25%, however for the other, less turbulent cases, we see agreement of within 10%. For cases where a thrust coefficient is unknown, this table would indicate that the wake velocity approximation is typically within 10% of the measured value.

Vertical Blockage

In an attempt to model blockage effects, Sandia has run both axi-symmetric and 3D CFD calculations of turbine flow under varying levels of constraint.

Figure 3.20 shows contour lines of velocity at 95 percent of the inflow velocity for axi-symmetric simulations run with different blockage ratios. For each run an inviscid wall was placed at a specific distance from the centreline such that the percent of flow obstructed by the actuator disk was between 1% and 70%. The plot clearly shows that as the blockage ratio increases, the wake reduces in length. This is explained by the fact that the increased blockage forces a faster flow around the periphery. The sped up flow mixes with the wake flow results in a faster wake recovery.

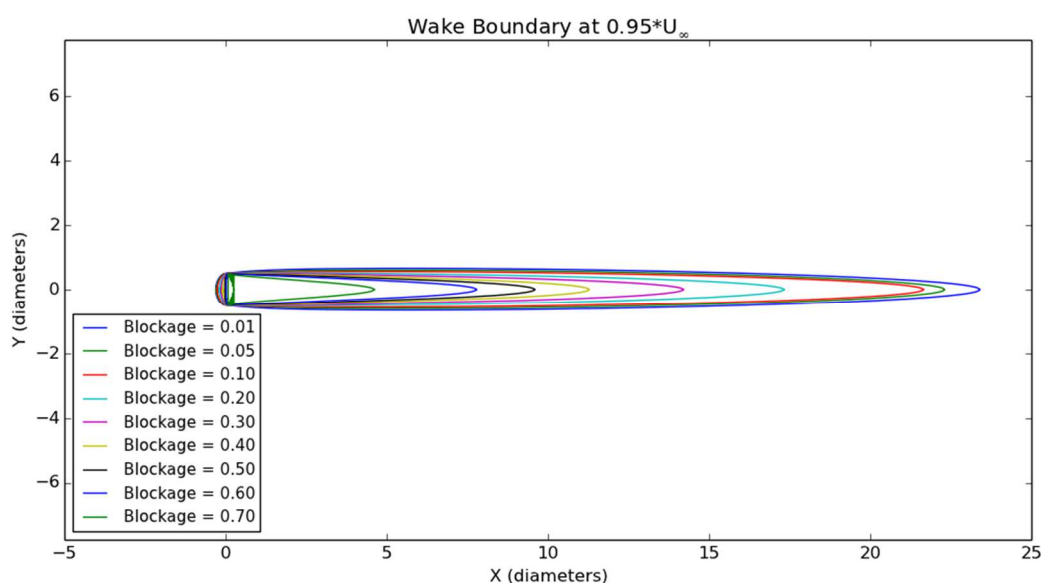


Figure 3.20: Iso-lines where wake velocity equals 95% of inflow velocity from axi-symmetric CFD simulations.

Figure 3.21 shows the 95% recovery distance along the centreline, plotted against blockage ratio, for the cases shown above. These results have been fit with a second order curve for modelling purposes. Figure 3.22 shows this same plot normalized by the Y-intersect of the curve fit. In effect, the curve fit in Figure 3.22 shows the ratio of wake length of a blocked flow to that of an unblocked wake. From the current investigation, this ratio is shown to be approximately:

$$0.489B^2 - 1.472B + 1.0$$

where B is the blockage ratio. The wake solution obtained from the database lookup is scaled in the stream wise direction by this quantity. This is the blockage model algorithm implemented in the tidal model.

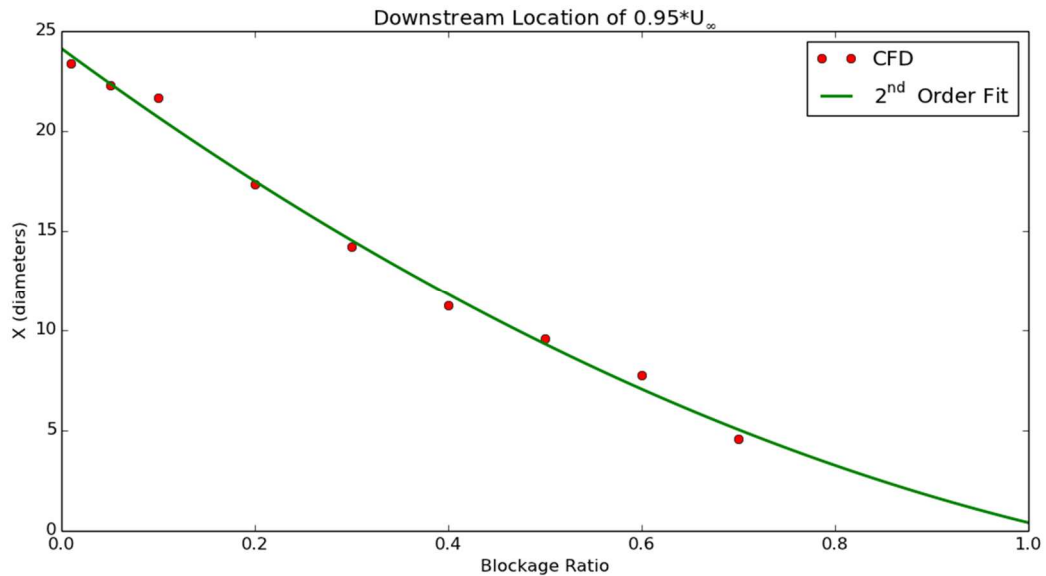


Figure 3.21: Second order curve fit for 95% recovery distance vs. blockage ratio.

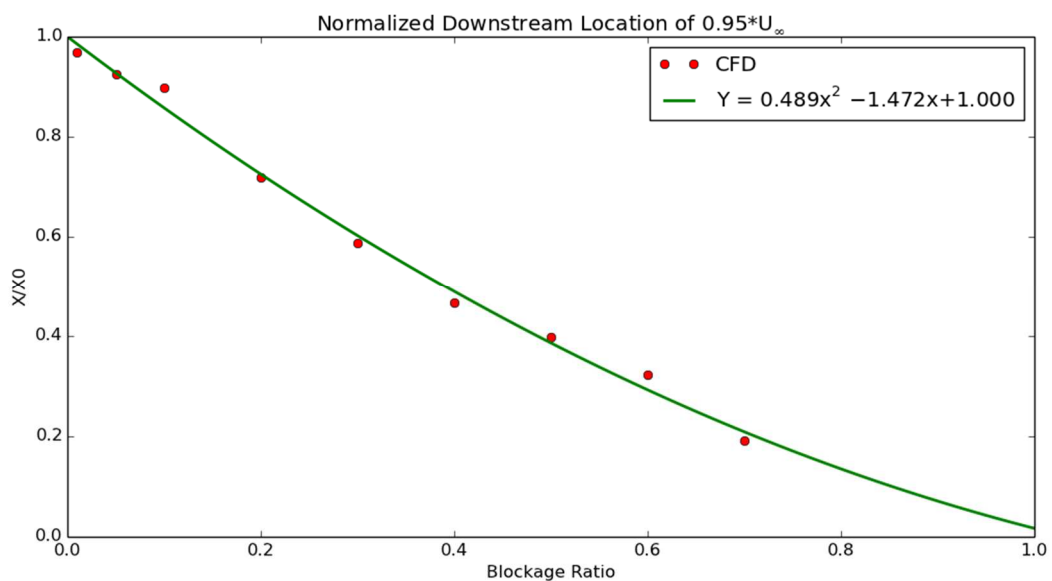


Figure 3.22: Normalized second order fit of 95% recovery vs blockage ratio.

While the effects of total blockage have can be quantified the isolated effects of vertical blockage are not so easily understood. Figure 3.23 shows iso-lines of wake velocity equalling 90% of the inflow speed for a series of 3-dimensional calculations. To simulate vertical channel blockage with negligible horizontal blockage, the following boundary conditions were used. A viscous wall was used as the floor

condition, while an inviscid wall was used for the top boundary. The top and bottom boundaries were placed such that the turbine diameter was 10%, 20%, 30%, 40%, 50% or 60% of the total domain height, and the turbine was centered between them. Both sides of the simulation were modelled as outflow boundary conditions, allowing for unconstrained flow in the horizontal direction.

The figure shows that as of 18 diameters downstream, there is no noticeable effect due to strictly vertical blockage. Because of this, no meaningful model for blockage in strictly the vertical direction could be developed. Further investigation may be conducted into the phenomenon of vertical blockage, and if appropriate, a more meaningful model may someday replace the current formulation.

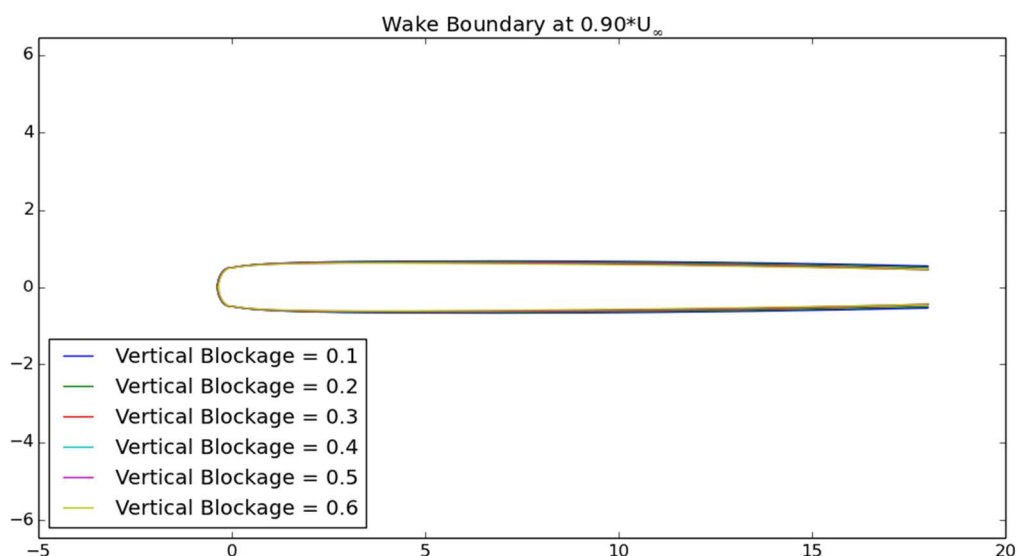


Figure 3.23: Iso-lines where wake velocity equals 90% of inflow velocity from 3D CFD simulations.

Yaw

Since the CFD database was populated using simulations run under the actuator disk assumption, the turbine is in effect treated as a continuum of resisting force. For the purposes of this application, yaw is seen as strictly affecting the cross sectional area of the turbine, and thus the resulting wake. The current model implemented for turbine yaw effects simply scale the wake in the spanwise direction by a factor of $\cos(\alpha)$, where α is the turbine yaw angle.

As with the blockage model, further studies into this effect will be performed to identify shortcomings of this representation and to quantify the uncertainty of this model. Should this model be deemed insufficient, it may be modified or replaced in the future.

3.3.3.5 ASSUMPTIONS AND LIMITATIONS

This document describes the limitations associated with the theories and assumptions implemented in the WP2 Tidal code, and hence its range of applicability. This qualitative exercise is the first step in the assessment of the tool's uncertainty.

Flow Field Modelling

A very simple algebraic axi-symmetric wake model was developed by Jensen (53) to represent the velocity deficit behind a (wind) turbine. This model was further developed to incorporate a radial velocity profile by Larsen (47). These wake models are fairly primitive and neglect many wake flow field characteristics such as upstream effects, and surrounding flow speed up due to conservation of mass. In addition to their shortcomings in modelling these features, they both require some assumptions about the flow before they can give a result. The Jensen model requires a decay constant and the Larsen model requires the user to define a known velocity at a downstream location. The resulting flow can be drastically affected by an inappropriate assumption.

Due to the speed requirements of the DTOcean project, it is not feasible to run high fidelity CFD calculations for the turbine array flow field. The method employed by the current model is to run CFD simulations for characteristic flows and populate a lookup table from this data. By doing this, we create a simple, fast-running model which is accurate for a large array of cases.

The database is populated with wake flows for a range of turbine thrust coefficients and incoming turbulent intensities. A barycentric interpolation scheme is employed to extract data from this table for cases which lie in between parametric case points. The output of the database lookup is an axisymmetric flow field of velocity and turbulence data.

This wake model, however, is not without its own limitations. The database is limited to looking up points within its defined parameter space. There is no extrapolation algorithm. Thus for points outside of the initial database definition, more points would need to be added to the database.

Another limitation of the database method is physical storage space. As points are added to the database, or addition output variables stored, the database will grow. Currently the database stores stream-wise velocity, and turbulence intensity over a spatial field of 20 turbine diameters by 4 diameters. With spatial discretization of $0.025D$, the database takes up about 200Mb decompressed. This size will scale linearly with an increased number of variables, discretization, and domain size.

Wake interactions

The core of the wake interaction model is based on a rather simple Jensen model (53) to which the parametric expression of the wake decay has been substituted with a CFD simulation based dataset and which has been modified to follow streamlines composed the wakes' trajectories rather than straight lines. Although these two additional features make the model less approximate than a traditional Jensen model, it still has limitations in term of applicability.

Several wake superimposition schemes will be tested during the model validation phase of this project (54). Nonetheless, the model, and thus wake interaction, cannot account for non-hydrostatic effects. Consequently, the influences of turbines sitting in near wakes or upstream in the close vicinity of the rotor will not be accurately modelled in the array's performances and wake interactions. In practice however, due to avoidance zones and maintenance ships safety requirements, those configurations are unlikely to occur. Note that this theoretical limitation applies for both momentum and turbulence flow characteristics.

From a hydrodynamics point of view, turbine wakes can be considered as stream tubes (55). Accordingly, it has been assumed that wake's centre-lines follow the streamline generated at hub locations in the initial flow. This assumption permits the model to account for the influence of the flow advection on the wake expansion as well as to consider the distance between turbines relative to their wake centre-line. Nevertheless, its numerical implementation may not work in highly rotational flows with recurrent eddies. In practice however, such flows tend to be avoided as they would require complex control of the machines as well as generated "chaotic" input to the drive train and hence enhanced loading and fatigue to the entire converter.

Additionally, structure induced wakes are not accounted for in the present model. Device structure may include a pile, nacelle, foundation, floating structure or any other component apart from the blades themselves. This assumption may impact the overall energy balance assessment of the system and wake interaction characterisation which, respectively, might introduce inaccuracy in modelled impact and resource assessments.

Horizontal-boundary assumptions

Lease's horizontal/lateral boundaries/limits are considered open thus, as far as the model is concerned, no horizontal boundary effects are accounted for nor modelled. This assumption may lead to spurious results for configuration where the deployment is close to the edge of a constraint site (such as a channel) or where the upstream row of the array layout densely covers the width of the channel (e.g. approximately less than rotor-diameter lateral spacing between devices). In such case, blockage effects on the overall array performance will be under-estimated. Yet in practise, considering maintenance and environmental requirements, this type of configuration is likely to be avoided.

Whelan (56) developed a 1-d analytical solution for an infinite array permitting to investigate the influence of the blockage effects on the percentage reduction in downstream free surface elevation. Based on this model, it has been showed during the Perawatt project that the downstream impact of an infinite row of turbines at a lateral spacing of two rotor diameters can be considered negligible. Yet this assumption seems valid only when the fluid is subcritical or tranquil, that is when the Froude number $Fr < 1$, where $Fr = \frac{U}{\sqrt{gz}}$. Nonetheless, and similarly to the current code, the previous example does not address the possibility of upstream flow diversion away from the array and in situations where, for example, an array is situated between an island and the main land, the upstream effect of the array should be considered (57).

Vertical-dimension assumptions

The current model does not resolve the velocity vertical profile per se but assumes its shape based on power-law formulas (see Section 3.3.3), therefore, one should expect increased discrepancies in non-ideal sites with, for instance, reverse shear and abnormal vertical stratification due steep density and/or temperature gradients. In addition, wake influences on vertical profiles are not accounted for.

As discussed earlier and due to the open horizontal-boundary assumption, Whelan's correction method for blockage effects cannot be used in this model yet its Froude limit (i.e. $Fr < 1$) still applies. Potential-flow approach should applied as suggested by the Perawatt project (57), however, for the

sake of computational time, a purely empirical approach has been chosen. Accordingly, based on Sandia's CFD model series of various vertical blockage ratios (i.e. rotor-diameter divided by the water column height), either a C_t or wake-shape correction formula will be developed.

Device yawing

The current model accounts for yawing of devices from both the performance and wake points of views yet with two different approaches. The influence of yawing on performance is accounted for by correcting the actuator disc surface area to be the "apparent" rotor surface area. This apparent surface can be defined as the projection of the actuator disc surface onto the plane perpendicular to the inflow velocity vector. The influence of yawing however shall be accounted for in a similar fashion to the vertical blockage effects, that is, through an empirical correction of the C_t and/or turbine diameter. The axi-symmetric wake from the CFD database will be scaled in the span-wise direction to represent the narrower cross section of a yawed turbine and the resulting narrower wake.

Consequently, in the case of performance, limitations will occur for turbines with ducted design and/or yaw-specific control. In the case of the wake, the main assumption here is that the hydrodynamic behaviour and relative shape of the wake shall stay the same and that only its dimensions would change accordingly to C_t and/or turbine diameter. Extensive CFD simulations, experiments and/or in-situ measurements are required to either infirm or confirm such assumptions.

3.3.4 FUNCTIONALITY TESTING AND VERIFICATION

The verification of WP2 tool is carried out by comparing the results with WAMIT and Nemoh.

3.3.5 NOTE ON THE LOSSES ACROSS WP3-6 TO APPLY ON THE RESULTS FROM WP2

When running the DTOcean software, the energy production estimates suffer sequential updates as the simulation moves from one computational module to the next one. As it was explained before, the computational module WP2 initiates the annual energy production calculation by considering the influence of the hydrodynamic interactions.

Once the electrical network is defined, in WP3, it will have an associated value of transmission losses that will reduce the energy output from the devices. The WP3 module aims to meet the power losses recommendations as defined by the European public consultation on the Treatment of Electricity Losses by Network Operators, which set a total network power loss upper limit of 4% (58).

From WP5 and WP6 comes the other reduction on power output: downtime losses. The downtime can be related to the devices or to other components of the array (cables, moorings, etc.). When a fault occurs, or even when preventive maintenance is being conducted, a device or component will stop operating. Depending on the device or component, and on the fault type, other array components may also be affected in a way that reduces the power transmitted.

The determination of when the faults occur is done in the WP6 module, using the outputs of the Reliability theme. With this information, a maintenance schedule is compiled, which includes corrective and preventive maintenance operations. From WP5, the required logistics are assessed, including the duration of the operation, and the waiting time related with weather windows. The downtime is then the result of the percentage of power not generated during:

- the time the component is not working
- the time it takes to get a maintenance team there, including the waiting time to get an appropriate weather window
 - or conversely to take the component to harbour for maintenance, also subject to weather windows
- the time it takes to repair or substitute the faulty component
- in the case the maintenance is performed on shore, the time it takes to re-install the repaired component (also subject to weather windows).

Although the data inputs in work package 2 are time series, the output of energy production that is passed on to subsequent work packages is the resulting statistical analysis. Thus, the downtime calculated in WP6 will be an average value that will be applied to the energy production.

However, depending on the type of maintenance, it can be assumed that there are different values of downtime:

Unplanned maintenance has a higher associated downtime: lead times, mobilization/demobilization and waiting times all occur when the component is not working.

For planned maintenance, the only element of downtime is when the component is being repaired⁹. Furthermore, the maintenance can be scheduled for periods of low energy production, not only to decrease the loss of power, but also because less energetic weather conditions/sea states are necessary for maritime operations.

Downtime is one of the areas in the marine energy sector that is the focus for cost of energy reduction, due to its impacts on the LCOE. From Table 2.2, the target availability¹⁰ for second arrays is between 85% and 98%. First arrays are expected to have a significant lower availability than the first commercial projects, and current projects have a very low value (5; 24).

For the purpose of the analysis on the next section, however, the values of energy output used will be those that result from the calculations on the WP2 module.

⁹ Hotswitching (i.e., direct substitution in one unique operation) can reduce greatly the downtime for both planned and unplanned maintenance.

¹⁰ Availability is the inverse of downtime losses (Availability = 1-[downtime losses])

4 SIMPLIFIED ANALYSIS OF ENERGY OUTPUT AND LCOE VARIATION WITH ARRAY CHANGES

The following section details two case studies used to demonstrate the applicability of WP2 module. These case studies are based on the Scenarios defined within DTOcean, which will be used for validation of the final tool.

4.1 WAVE: SCENARIO 3: AEGIR SHETLAND WAVE FARM

4.1.1 SCENARIO DESCRIPTION

4.1.1.1 TECHNOLOGY SPECIFIC DATA

Description

The machine used for this scenario is the Pelamis WEC, produced by Pelamis Wave Power. The figure below shows the device in operation at the EMEC test site.

The machine is composed by five cylindrical sections of equal length, interconnected by four universal joints, which allow the rotation in pitch and yaw of each section.

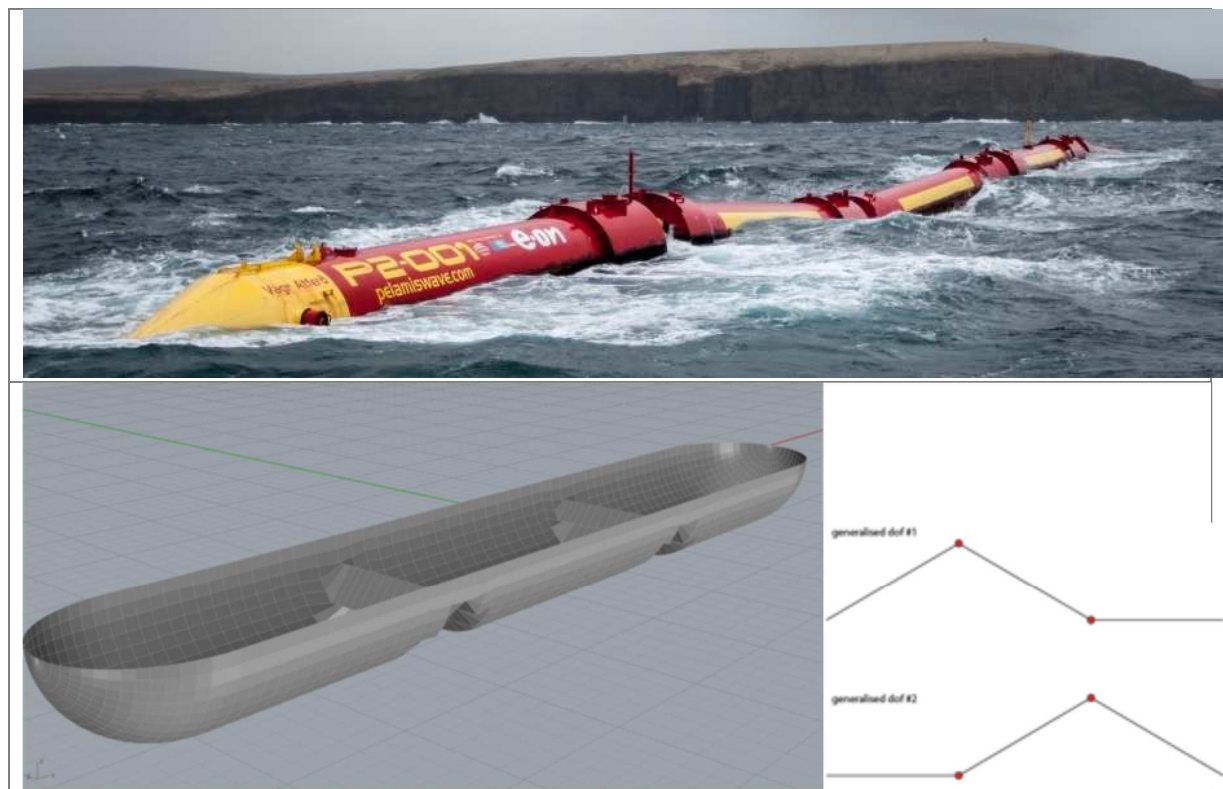


Figure 4.1: (Top) Pelamis in operation at the EMEC test site. (Bottom) simplified model of the Pelamis with description of the generalised degree of freedom.

Dimensions

The device is approx. 195 m long and 5.5 m wide. The dimensions are indicative for a 4 joints machine as shown in Figure 4.1 (Top) (59). For the sake of simplicity, a three section machine is used for the case study (see Figure 4.1 Bottom).

Table 4.1: Pelamis dimensions

Dimensions	Pelamis (59)	Simplified Pelamis
Length	195 m	60 m
Diameter	5.5 m	5 m
Number of joints	4	2

Watch circle

The minimum distance between devices depends on the water depth and on the internal grid network solution. As an indicative solution, it is possible to use the following watch area dimensions:

- Across row spacing – column width: 500 m
- Between row spacing – row width: 400 m

Additional requirements

The Pelamis is designed to be moored in waters approximately 50-70 m in depth (60).

Performance of isolated device

The Pelamis' power matrix is reported in the next table. The colour map indicates in green the low power regions and in red the high power regions.

Table 4.2. Power produced in kW by the Pelamis for different sea state conditions defined by T_e and H_s . (59)

Power Matrix (kW) for the Pelamis																	
$H_s(m) \backslash T_e(s)$	5	5,5	6	6,5	7	7,5	8	8,5	9	9,5	10	10,5	11	11,5	12	12,5	13
0,5	0	0	0	0	0	0	0	0	0	0	0	0	0	0	0	0	0
1	0	22	29	34	37	38	38	37	35	32	29	26	23	21	0	0	0
1,5	32	50	65	76	83	86	86	83	78	72	65	59	53	47	42	37	33
2	57	88	115	136	148	153	152	147	138	127	116	104	93	83	74	66	59
2,5	89	138	180	212	231	238	238	230	216	199	181	163	146	130	116	103	92
3	129	198	260	305	332	340	332	315	292	266	240	219	210	188	167	149	132
3,5	0	270	354	415	438	440	424	404	377	362	326	292	260	230	215	202	180
4	0	0	462	502	540	546	530	499	475	429	384	366	339	301	267	237	213
4,5	0	0	544	635	642	648	628	590	562	528	473	432	382	356	338	300	266
5	0	0	0	739	726	731	707	687	670	607	557	521	472	417	369	348	328
5,5	0	0	0	750	750	750	750	750	737	667	658	586	530	496	446	395	355
6	0	0	0	0	750	750	750	750	750	750	711	633	619	558	512	470	415
6,5	0	0	0	0	750	750	750	750	750	750	750	743	658	621	579	512	481
7	0	0	0	0	0	750	750	750	750	750	750	750	750	676	613	584	525
7,5	0	0	0	0	0	0	750	750	750	750	750	750	750	750	686	622	593
8	0	0	0	0	0	0	0	750	750	750	750	750	750	750	750	690	625

4.1.1.2 SITE DATA CHARACTERISATION

Deployment area

The lease area for the array deployment is shown in Figure 4.2. The vertex location is detailed below. The data is provided in UTM coordinates starting from point A and moving forward.

Table 4.3. Coordinates of the 5-nodes delimiting the lease area for Scenario 3.

Vertex	N (°,'')	W (°,'')
A	60 2 54.373	-1 32 23.707
B	60 2 48.142	-1 23 48.911
C	59 58 33.547	-1 22 19.204
D	59 56 59.436	-1 22 48.290
E	59 57 6.113	-1 32 20.175

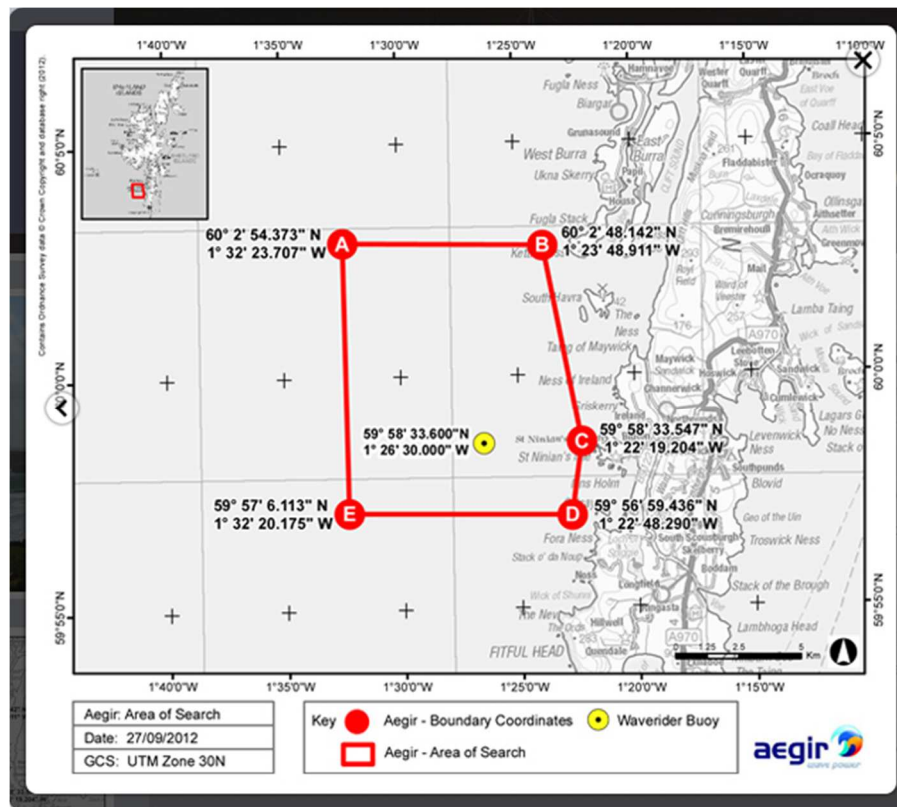


Figure 4.2: Lease area for Scenario 3. The lease area corresponds to the inner region delimited by the red line.

Bathymetry

The bathymetry around the lease area is presented in the figure below (61).

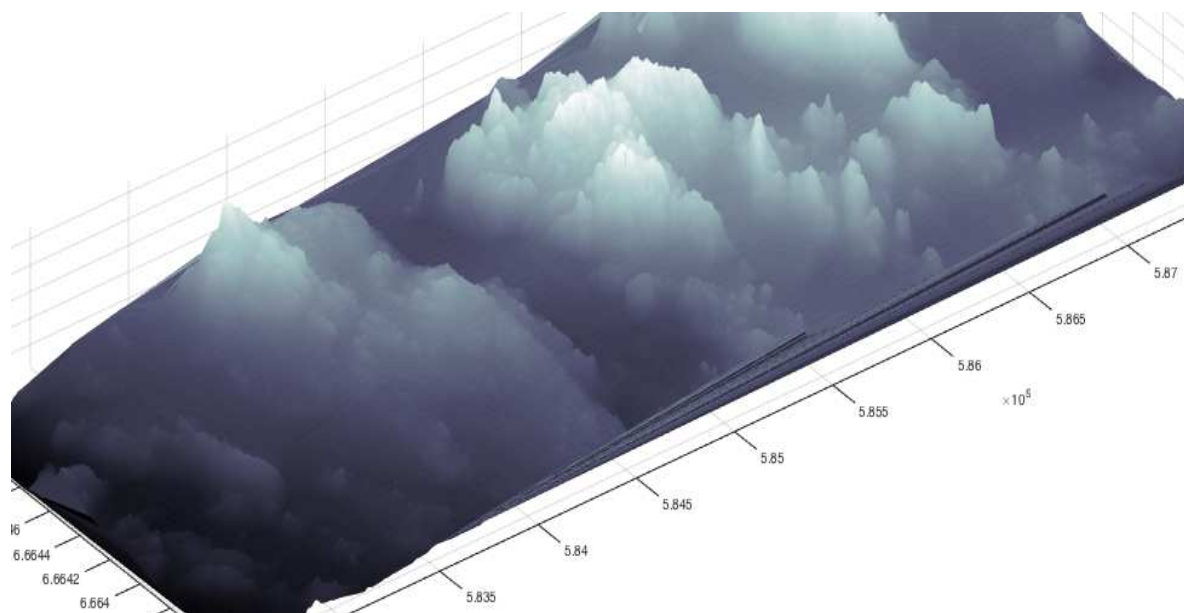


Figure 4.3: Bathymetry for Scenario 3. 3D representation of the seabed surface.

Metocean conditions

The time series of H_s , T_e and dir are available but they can currently not be used due to the absence of a satisfactory non-disclosure agreement.

In order to overcome the unavailability of the metocean condition, the data from West Lewis (scenario 1) is used instead.

The data presents a main wave direction of 270° , with most of the wave energy located in the range 220° - 320° .

4.1.2 ENERGY OUTPUT VARIATIONS DUE TO ARRAY CHANGES

This scenario was run¹¹ for 5 cases, by changing the number of WECs across the lease area:

- 2 devices
- 5 devices
- 10 devices
- 20 devices
- 50 devices

¹¹ It's important to note that while these values have been computed using the WP2 module, this was done before said module has been verified.

The array layout is presented on Figure 4.4 below.

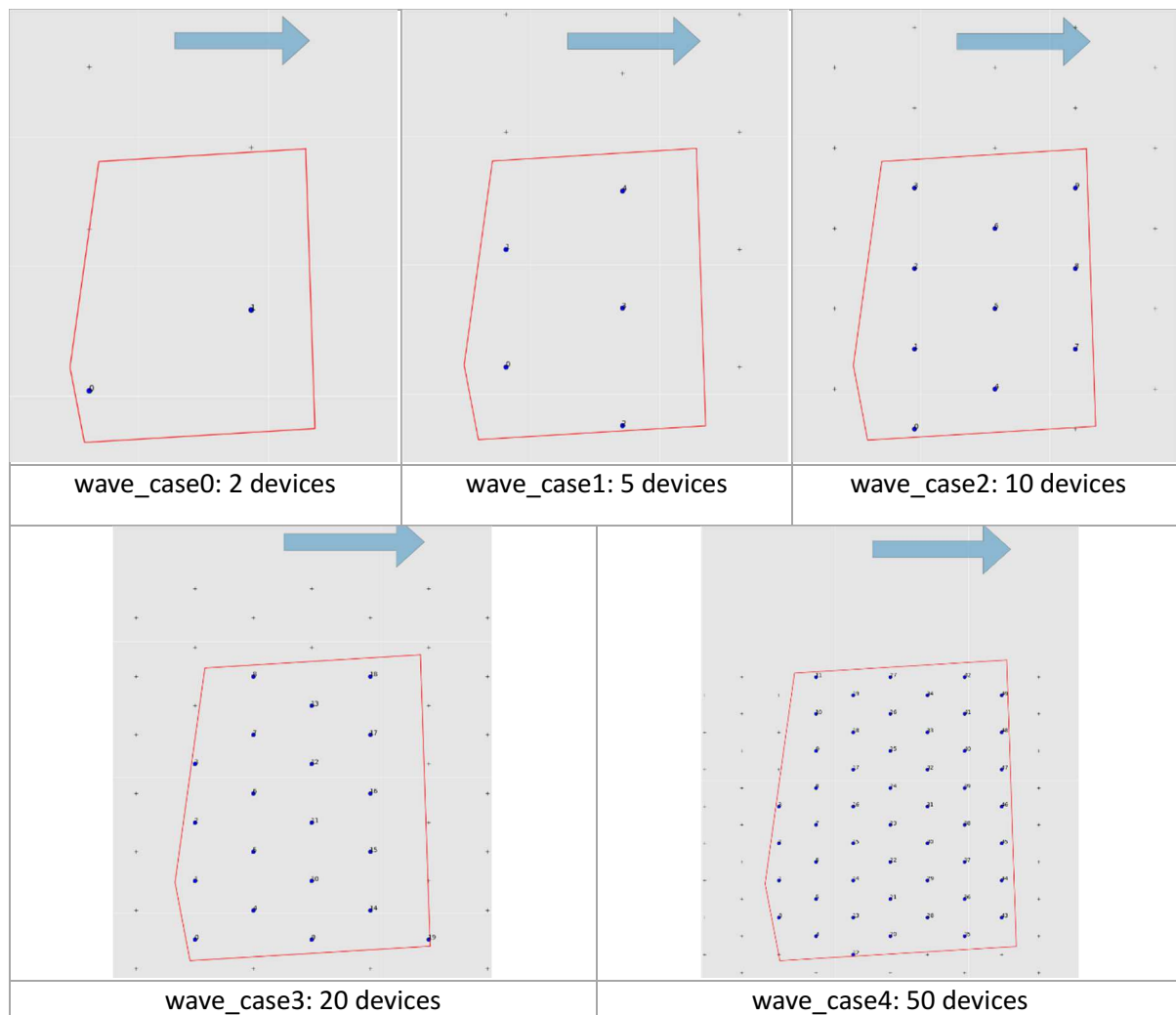


Figure 4.4: Array layouts for Scenario 3
Blue arrow indicates wave direction

In terms of energy production, the WP2 module outputs the AEP by device. For all 5 cases, the results are presented on the figure below, normalized to the average production by case. The graph shows that there is interaction between devices; more strongly felt the more devices are fitted in the same area.

Device Production Variation

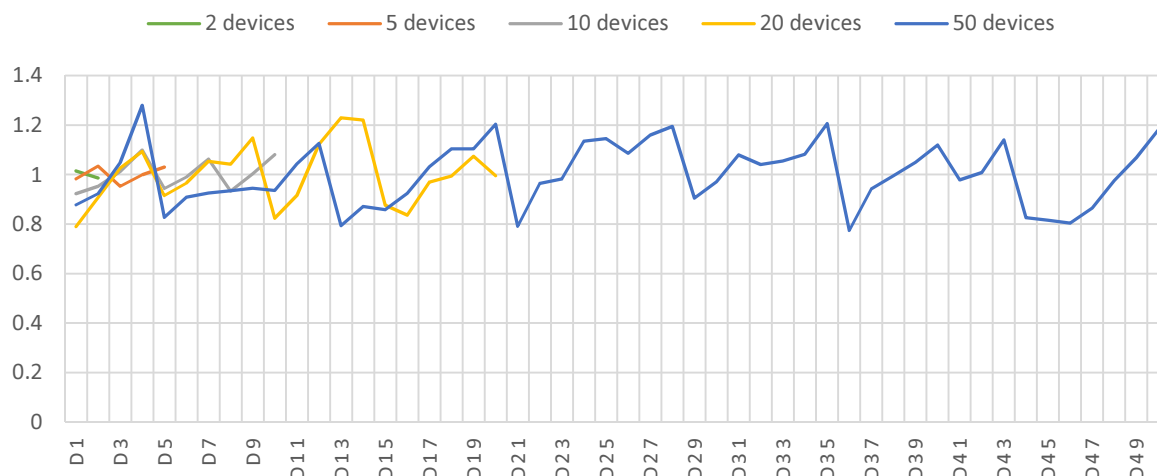


Figure 4.5: Device Production Variation, normalized to the average production

The AEP for each case is detailed in the table below, and the representation of what it means in terms of average output per device is shown in Figure 4.6.

Table 4.4: Energy output for all cases in Scenario 3

Case	Number of devices	Project Capacity (MW)	AEP ¹ (GWh)
wave_case0	2	1.5	10.51
wave_case1	5	3.75	25.34
wave_case2	10	7.5	47,96
wave_case3	20	15	104,62
wave_case4	50	37.5	263,80

¹ This figure doesn't include PTO efficiency, transmission or downtime losses

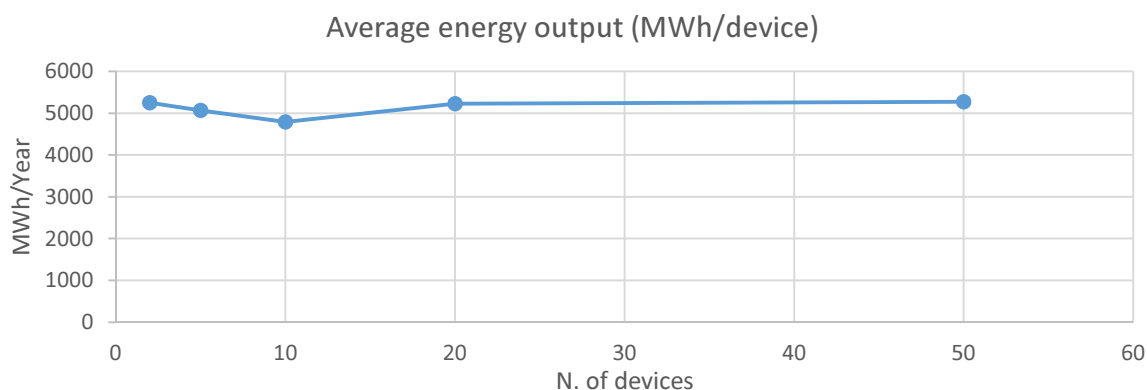


Figure 4.6: Average energy output per device

Device interactions for the case of 5 and 10 devices reduce the average power of the farm, in the order of 5 to 10% reduction. For the other cases the average production is almost equal, with the case of 50 devices producing slightly more energy on average. However, taking into consideration Figure 4.5, this case present more variability between devices.

4.1.3 SIMPLIFIED LCOE VARIATIONS DUE TO ARRAY CHANGES

Using the data from (5) for first arrays, the total lifecycle costs¹² for the different cases was calculated (Figure 4.7). How the CAPEX and OPEX influence these costs is presented on Figure 4.8.

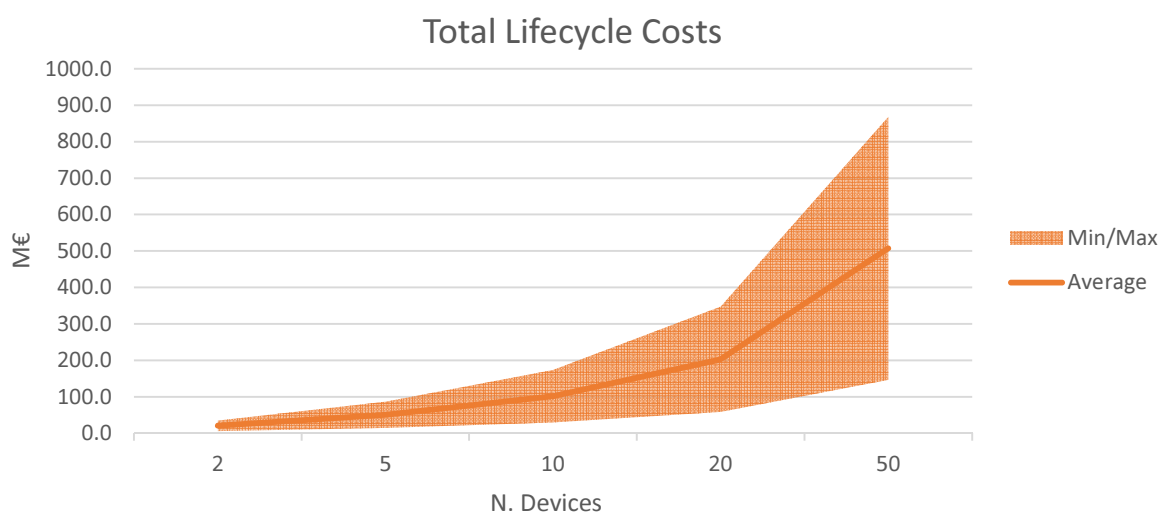


Figure 4.7: Total lifetime costs for Scenario 3

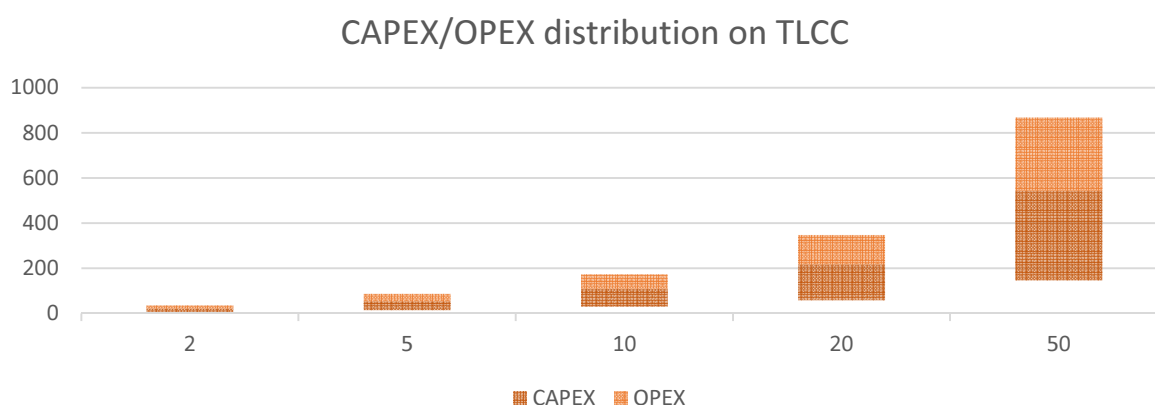


Figure 4.8: Capex and Opex distribution for Scenario 3

¹² Assuming a discount rate of 10%, in a 20 year project

Using the total lifecycle costs, and the energy output, the LCOE can be calculated, following Equation (3.1). The graph below shows the simplified LCOE, which assumes no losses beyond those calculated on WP2, for the Total Lifecycle Costs ranges. The lowest value of LCOE is in line with the highest energy output – the case of 50 devices. However, there are other solutions with a similar value, meaning that the developer could make the choice of starting small, to eventually build up to bigger arrays.

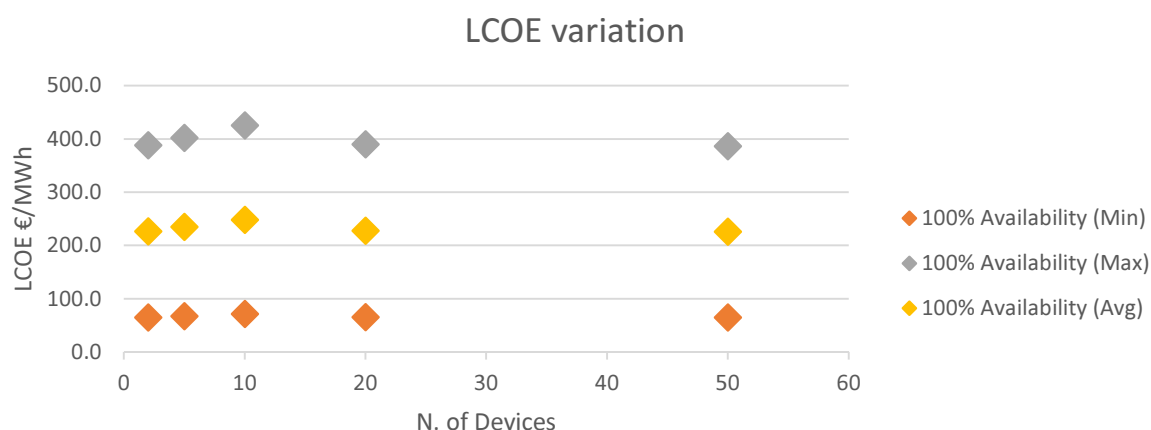


Figure 4.9: LCOE variation

To further look into the impact of energy output on the LCOE, Figure 4.10 compares the LCOE using average cost figures and different availability figures to the maximum LCOE of the previous graph. It is important to note that an availability of 50%¹³ can drive the LCOE up more than the case where the maximum costs are assumed.

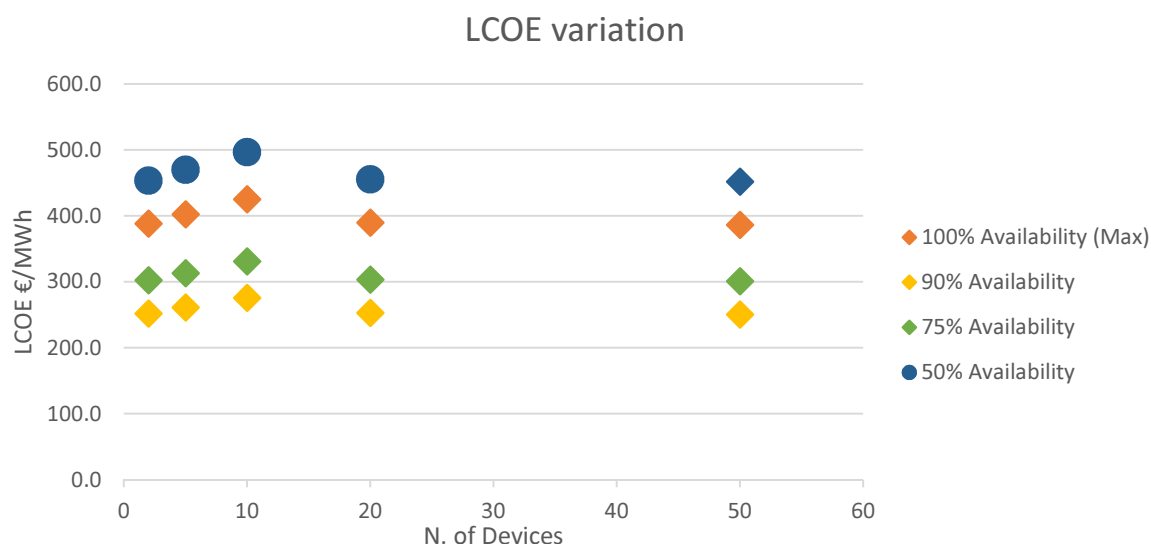


Figure 4.10: LCOE variation for different availability/energy output cases

¹³ Which in this case can be also made to include other losses such as transmission and PTO.

4.2 TIDAL: SCENARIO 5: SOUND OF ISLAY

4.2.1 SCENARIO DESCRIPTION

Scenario 5 corresponds to a tidal energy converter array located in the Sound of Islay, between the islands of Islay and Jura on the west coast of Scotland. The technologies under consideration are seabed mounted horizontal axis turbine. Moreover, the power production of the overall array is estimated at 10 MW.

4.2.1.1 TECHNOLOGY SPECIFIC DATA

Description

The turbine considered for this scenario is the HS1000, developed by Andritz Hydro Hammerfest (see Figure 4.11). The device is rated at 1MW and is variable pitch, fully submerged and seabed mounted tidal turbine.

The HS1000 model has a nacelle that can rotate 180° to better face oncoming tide and blades that can reverse their pitch to work with both flood and ebb tides. The 26m diameter rotor is supported via a sloping tower and tripod structure fixed to the seabed using gravity ballast in the legs. (62)

The lease area is near Port Askaig and seabed cables will connect the devices to a substation south of Port Askaig at Traigh Bhan.

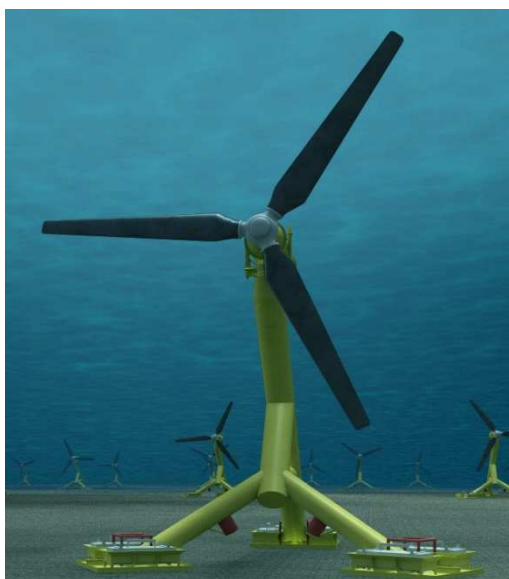


Figure 4.11: Andritz Hydro Hammerfest HS1000

Dimensions

The dimensions for the HS1000 turbine are reported in the following table:

Table 4.5. HS1000 turbine's dimensions. (62)

Dimensions and clearances	Andritz Hydro Hammerfest HS1000
Hub height	26m
Rotor diameter	26m
Tip height	39m

Watch circle

The maximum width of the Andritz Hydro Hammerfest HS1000 device is equal to the rotor diameter (i.e., 26m). At maximum yaw angle the rotor plane will be aligned with the downstream length of the support structure. As such the maximum length of the device is 35m (22m long tripod plus 13m rotor radius and assuming the rotor is centred over the front two legs of the tripod) (62).

Devices are being spaced 1.5 diameters laterally and 20 diameters downstream (62).

Additional requirements

The HS1000 is restricted to water depth larger than 52.6 m. Additional requirement on the under keel clearance for the HS1000 device which needs to be at least 13.6 m (62).

Performance of isolated device

No performance data is available for either device. However the same generic power curve and considerations provided for Scenario 2 can also be utilised for this scenario.

4.2.1.2 SITE DATA CHARACTERISATION

Deployment area

The site boundaries are shown in red in Figure 4.12. The UTM coordinates of the boundary corners are given in Table 4.6. These coordinates can be found in OS National Grid and WGS84 DD format in the nontechnical statement (2010 Version) (62).

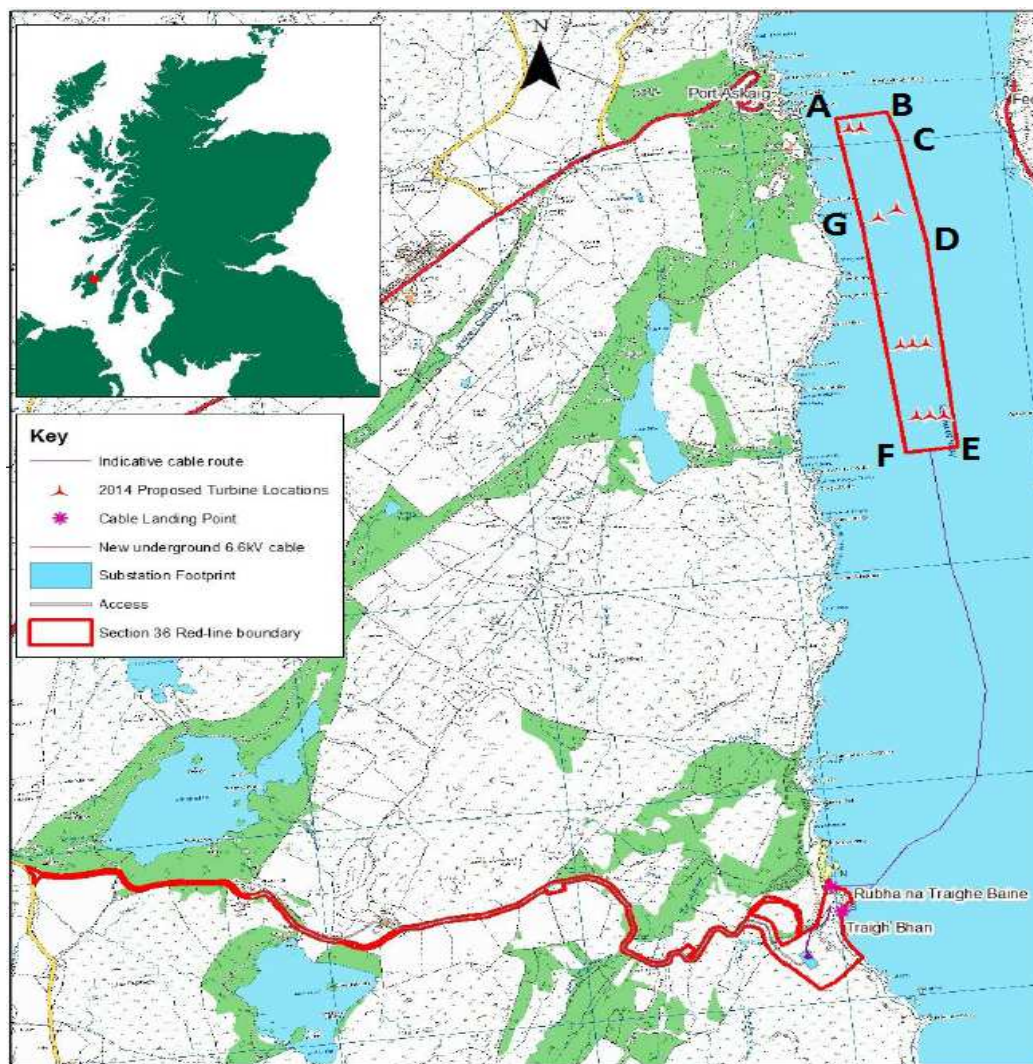


Figure 4.12: Sound of Islay lease area.

The lease area corresponds to the inner region delimited by the red line.

Table 4.6. Coordinates for the 5-nodes delimiting the lease area for Scenario 5.

Boundary	WGS84 UTM 29N	
	Easting	Northing
A	681462.72	6192834.6
B	681664.39	6192867.5
C	681708.52	6192753.95
D	681819.34	6192258.89
E	681940.52	6191294.31
F	681741.16	6191269.42
G	681570.02	6192328.32

The ratio between the lease area and the channel area is set to one because the lease area covers most of the passage area.

Bathymetry

The coverage of the bathymetry data is shown in Figure 4.13 whilst the surrounding coast can be seen in Figure 4.12. The coastline is predominantly rocky and steeply sloping down to the water line. The seabed is predominantly bedrock, boulders and gravel (63).

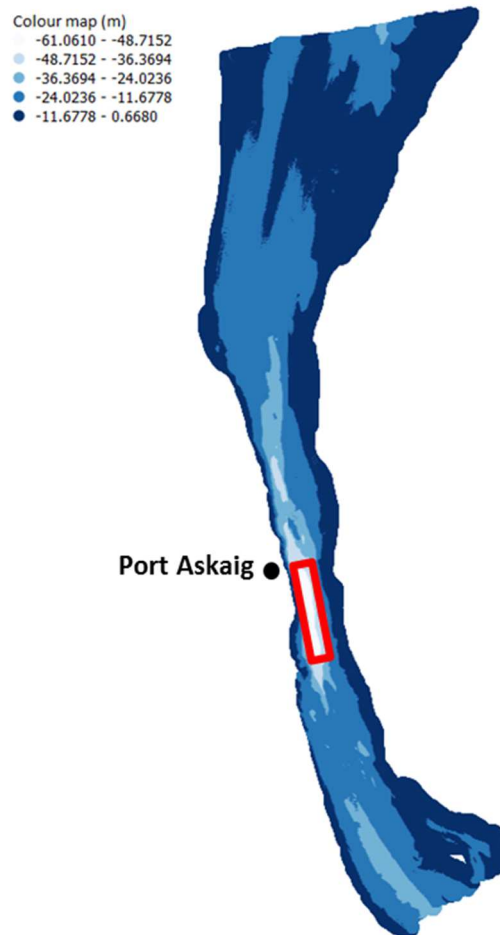


Figure 4.13: Sound of Islay lease area.

The lease area corresponds to the inner region delimited by the red line.

Metoccean conditions and other site parameters

Data on the metoccean conditions has been successfully collected. However the data is covered by a Non-Disclosure Agreement in place between Scottish Power Renewables and IT Power.

For the time being, an average stream of 1.5m/s parallel to the long side of the lease area is considered. Both positive and negative direction are used with homogeneous probability of occurrence.

The turbulence intensity is assumed to be 0.1 for the whole area.

The sea surface elevation is assumed to be +3meter, with respect to the bathymetry for the whole area.

The Velocity Shear exponent used the velocity power law for the estimation of the vertical velocity profile is assumed to be 7; in addition the Manning number of the whole area is assumed to be 0.003.

As stated above all these parameters are estimated based on general consideration, due to the absence of site data.

4.2.2 ENERGY OUTPUT VARIATIONS DUE TO ARRAY CHANGES

Based on the previously presented scenario, the WP2 module was run¹⁴ to determine the energy production across a small number of cases, to illustrate the influence of array changes on energy output. An average flow velocity of 1.65 m/s was used for this scenario.

Like in the wave scenario, the tidal submodel was run for 5 cases:

- 2 devices
- 5 devices
- 10 devices
- 20 devices
- 50 devices

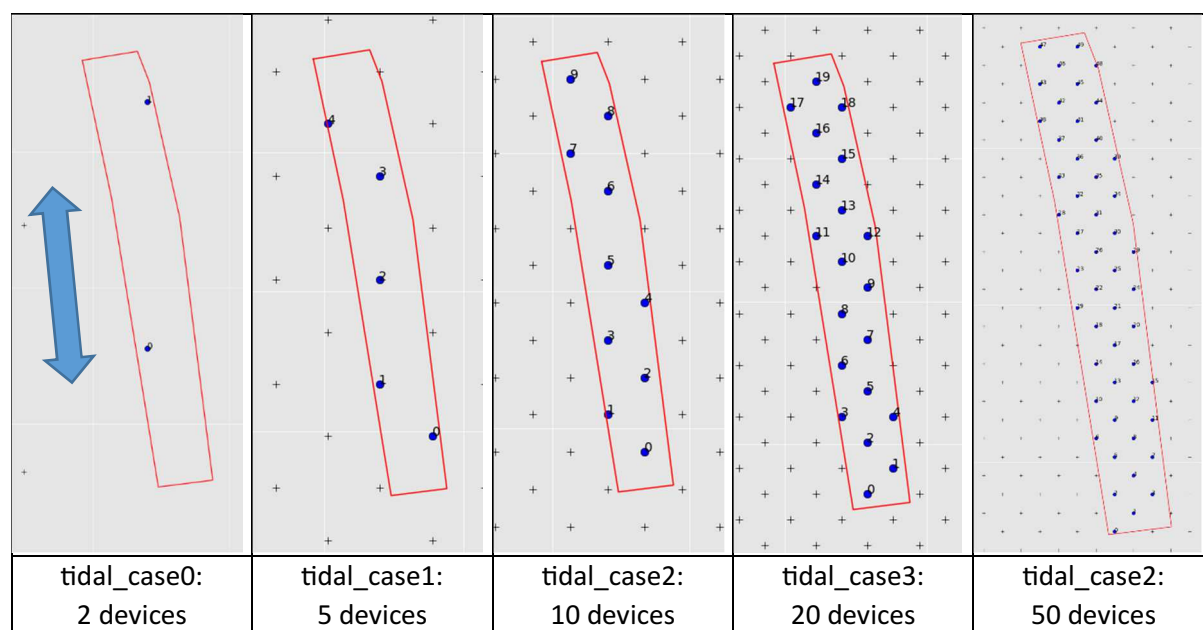


Figure 4.14: Array layout for Scenario 5

The blue arrow indicates flow direction

The figure above shows the device distribution for all the cases – how they are distributed in the lease area. The blue arrow shows the direction of the flow.

¹⁴ It's important to note that while these values have been computed using the WP2 module, this was done before said module has been verified.

The wake effects were also analysed, and Figure 4.15 (left) shows how they align for the 20 devices case. Still using the array layout for the 20 devices case, the representation of the energy production of each device is represented on the right – bubble size representative of AEP.

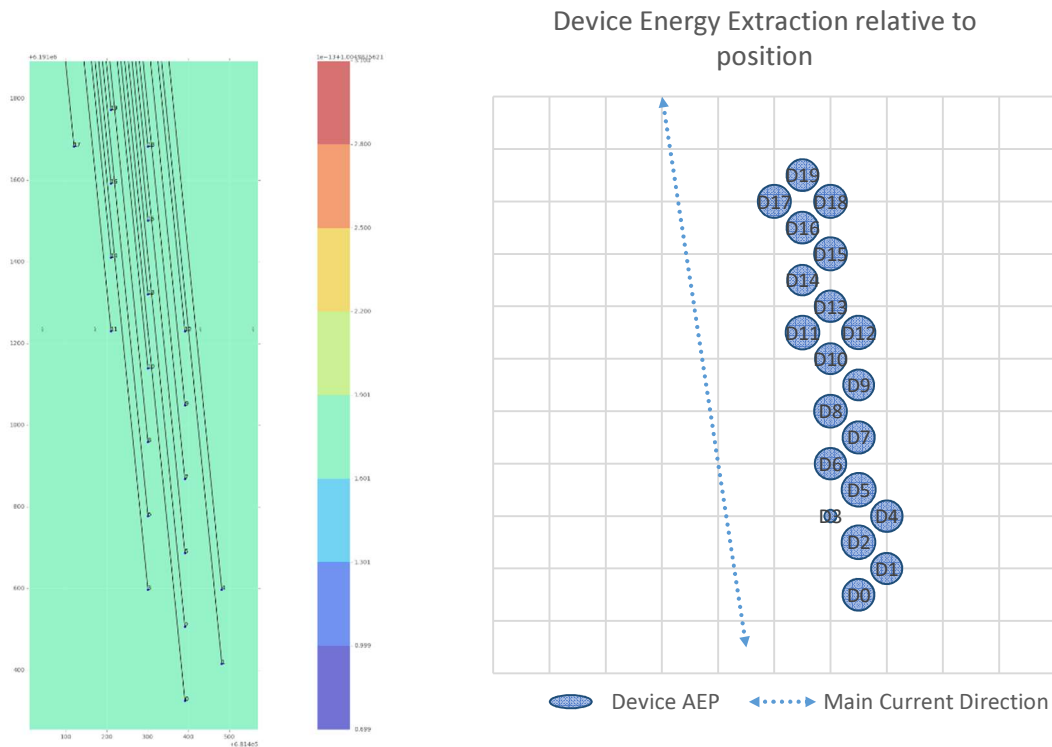


Figure 4.15: Wake distribution (left) and energy production per device (right), with layout representation for Scenario 5, case 20 devices

The aggregated results for all cases, i.e. the energy production by device for each case, is presented on Figure 4.16, normalized to the average production by case., to show the interaction for tidal energy, as the direction of the flow and whether there are turbines upstream have a big influence on the final output. The 0 values on the graph below correspond to devices with are aligned with the wake of another, and are assumed to not be producing.

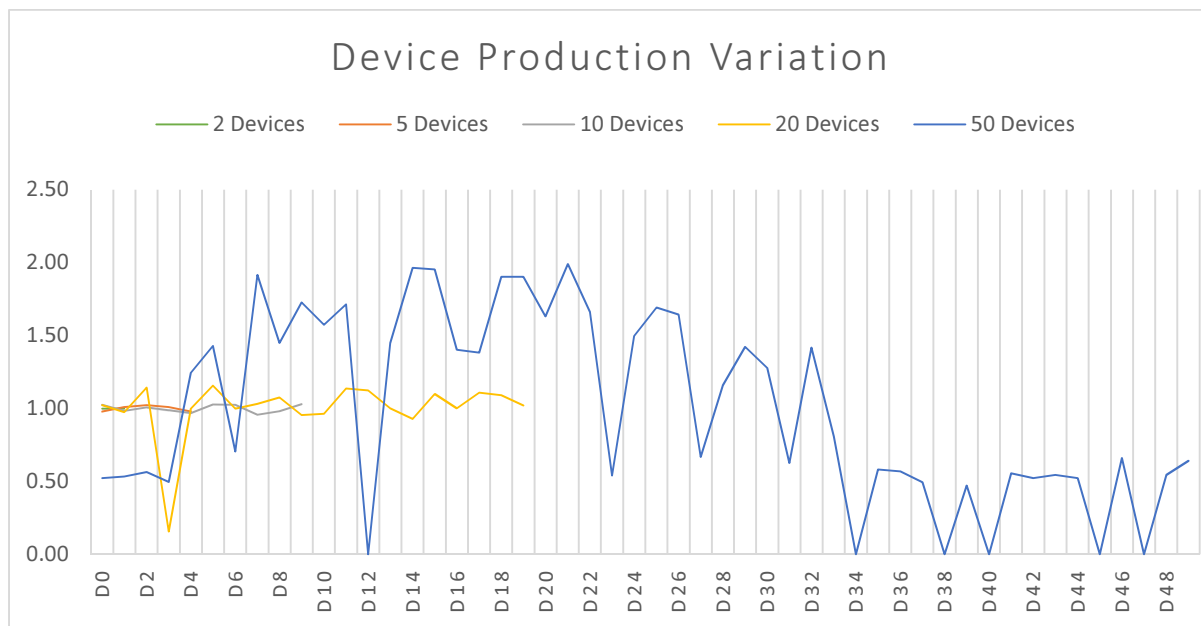


Figure 4.16: Device Production Variation, normalized to the average production

Based on this variability, the average energy output by device (Figure 4.17), shows that the case of 20 devices produces more energy than the other cases.

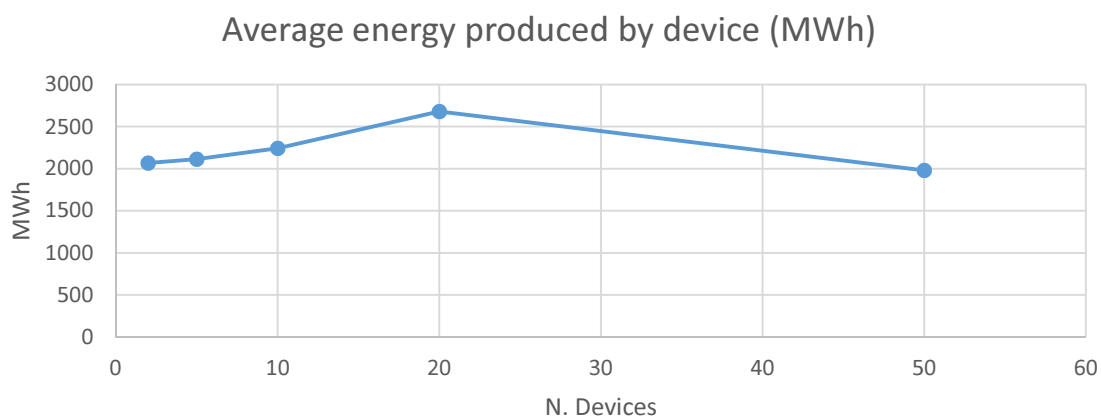


Figure 4.17: Average energy output per device

The following table summarizes the results of energy output for Scenario 5.

Table 4.7: Energy output for all cases in Scenario 5

Case	Number of devices	Project Capacity (MW)	AEP ¹ (GWh)
tidal_case0	2	2	4,14
tidal_case1	5	5	10,57
tidal_case2	10	10	22,42
tidal_case3	20	20	53,58
tidal_case4	50	50	98,93

¹ This figure doesn't include transmission or downtime losses

4.2.3 SIMPLIFIED LCOE VARIATIONS DUE TO ARRAY CHANGES

A simplified LCOE analysis was also conducted for the Scenario 5, also using the data presented on Table 2.2 for first arrays.

The total lifecycle costs¹⁵ for each case in Scenario 5 are presented on Figure 4.18 and the contribution of CAPEX and OPEX on Figure 4.19, which are similar to that of wave energy.

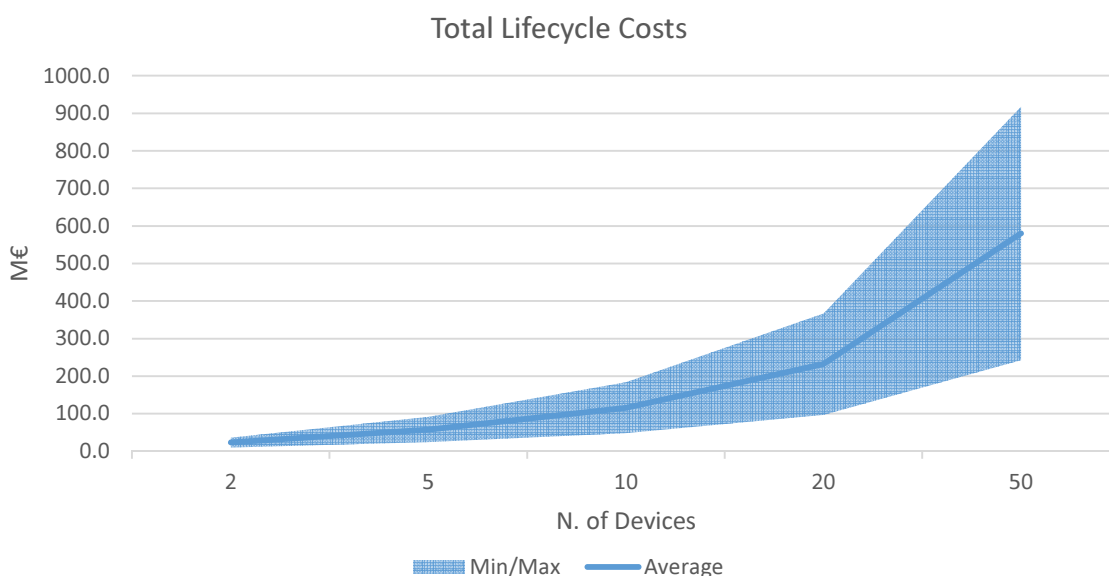


Figure 4.18: Total Lifecycle costs for Scenario 5

¹⁵ Assuming a discount rate of 10%, in a 20 year project

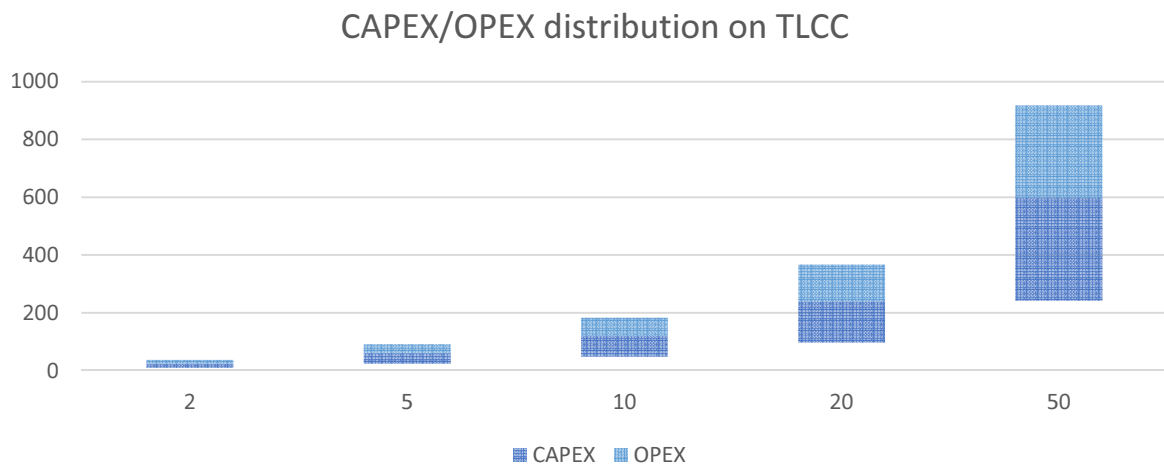


Figure 4.19: Capex and Opex distribution for Scenario 5

However, when combined with a different energy output profile, the results for LCOE also differ (Figure 4.20). The difference between different cases is more strongly felt for the maximum cost analysis, which indicates that the energy output has a big impact on the LCOE. To further illustrate this, the analysis for different levels of output (with the introduction of a broad availability factor) was compared to the maximum cost scenario, showing that having an availability of about 60% has the same effect on LCOE of rising the costs from the average scenario to the maximum.

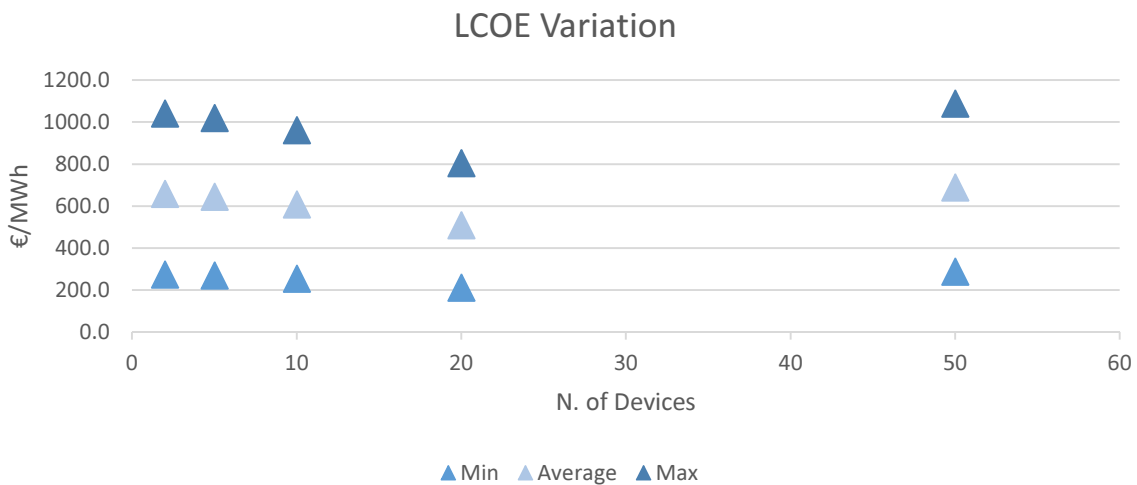


Figure 4.20: LCOE variation

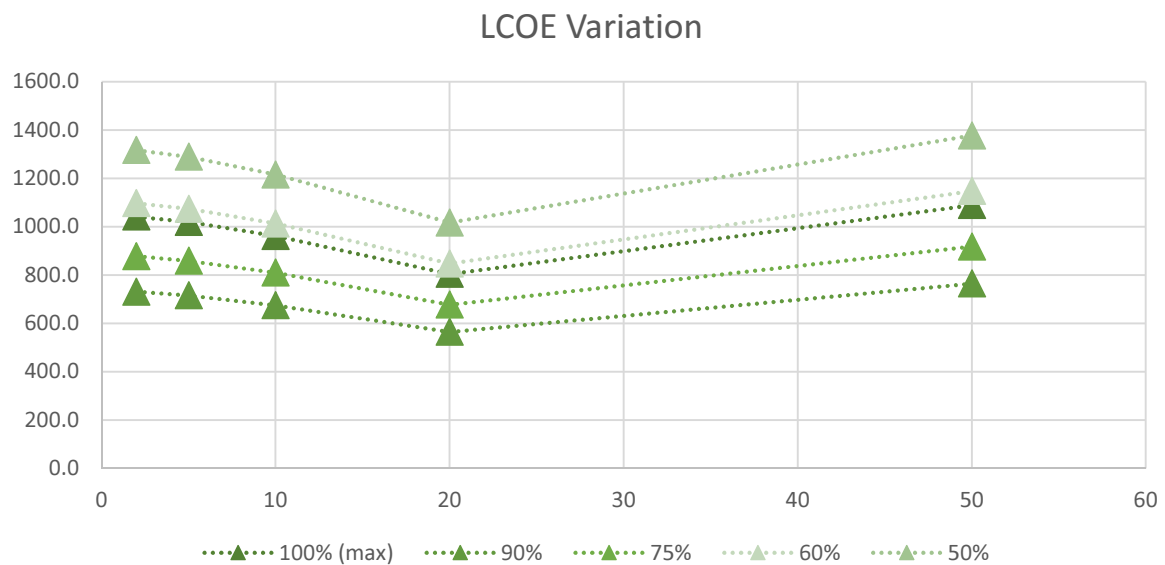


Figure 4.21: LCOE variation for different availability/energy output cases

Like in the wave energy scenario, the optimal case in regards with LCOE corresponds to the higher energy production one. However, in this case it's not the maximum amount of devices that could be fitted in an area – the case for 50 devices shows a big decrease in energy capture, due to some turbines being directly in line with the wake of upstream ones.

5 SUMMARY

This deliverable provided an overview of the economics of marine energy arrays, approaching the two sides of the equation: costs and energy production.

While the costs of marine energy devices and associated projects are still subject to high uncertainty, DTOcean aims to develop a suite of tools that can be used to assess the economic viability of projects and to aid developers in designing a project that will have a low Levelized Cost of Energy. The methodology that is used in the tool to determine costs and LCOE is in line with standard practises in the industry. Although costing is done at a work package level, the final economic indicator – LCOE – is calculated taking into consideration the system-wide costs and impacts on electricity generation.

On the cost side, and with regards to the elements that are outputs of work package 2, there is not an impact on the cost of the devices, beyond that of a linear relationship with the number of devices. Cost savings from serial production are bound to occur. But within the context of DTOcean devices are treated as another component in the project – with an associated commercial price and unchanging characteristics, so if these savings are transferred to the project developer, it will be up to the end user to update this cost value.

Although there is no effect on device costs, the outputs of work package 2 in terms of array layout will constrain the decisions made downstream the tool workflow. This means that while a certain layout may look promising from a hydrodynamic point of view – with low hydrodynamic losses, it may imply extra costs on other subsystems that can negate the gains from extra energy output.

The hydrodynamic models used to assess the interaction between devices and determine the best layout have been detailed in this document. The two submodels were then used to generate case studies for two scenarios, in order to illustrate the impact of costs and of energy output on the Levelized cost of energy.

REFERENCES

1. **IEA; NEA.** *Projected Costs of Generating Electricity*. 2010. Vol. 118 Suppl. ISBN: 978-92-64-08430-8.
2. *A Manual for the Economic Evaluation of Energy Efficiency and Renewable Energy Technologies*. **Short, Walter and Packey, Daniel J.** March, 1995.
3. **Carbon Trust.** *Future Marine Energy*. 8th Floor, 3 Clement's Inn, London WC2A 2AZ. : s.n., 2006. Tech. rep.
4. —. *Accelerating Marine Energy: The Potential for Cost Reduction*. Carbon Trust. 2011. pp. 1-64, Tech. rep.
5. **OES.** *International Levelised Cost of Energy for Ocean Energy Technologies*. Ocean Energy Systems - International Energy Agency. 2015. pp. 1-48, Tech. rep.
6. **EC JRC.** *2014 JRC Ocean Energy Status Report*. 2015. ISBN: 978-92-79-44611-5.
7. *Levelised costs of Wave and Tidal energy in the UK: Cost competitiveness and the importance of "banded" Renewables Obligation Certificates*. **Allan, Grant J., et al.** 1, #jan# 2011, Energy Policy, Vol. 39, pp. 23-39. ISSN: 03014215 DOI: 10.1016/j.enpol.2010.08.029.
8. *Quantifying the uncertainty of wave energy conversion device cost for policy appraisal: An Irish case study*. **Farrell, Niall, Donoghue, Cathal O' and Morrissey, Karyn.** 2015, Energy Policy, Vol. 78, pp. 62-77. DOI: 10.1016/j.enpol.2014.11.029.
9. **Carbon Trust.** *Cost Estimation Methodology*. Carbon Trust. 2006. Tech. rep.
10. **Oxera.** *Discount rates for low carbon and renewable generation technologies*. Committee on Climate Change. 2011. Tech. rep. 00000.
11. **Ernst & Young; Black & Veatch.** *Cost of and financial support for wave, tidal stream and tidal range generation in the UK*. 2010.
12. **SQWenergy.** *Economic Study for Ocean Energy Development in Ireland*. 2010. pp. 116-116, Tech. rep.
13. *Factors affecting LCOE of Ocean energy technologies : a study of technology and deployment attractiveness*. **Andrés, Adrián De, et al.** pp. 1-11.
14. **SI Ocean.** *Ocean Energy: Cost of Energy and Cost Reduction Opportunities*. s.l. : SI Ocean Project, 2013.
15. **DOE; EIA.** *Annual Energy Outlook 2015 : With Projections to 2040*. 2015. Tech. rep.
16. **Intergovernmental Panel on Climate Change.** *Renewable energy sources and climate change mitigation: special report of the Intergovernmental Panel on Climate Change*. 2012. Vol. 49. ISBN: 978-1-107-60710-1.
17. **IRENA.** *Renewable Energy Technologies: Cost Analysis Series: Wind Power*. 2012.
18. **European Commission.** *A Roadmap for moving to a competitive low carbon economy in 2050*. 2011. Tech. rep.

19. **US EIA.** *Levelized Cost and Levelized Avoided Cost of New Generation Resources in the Annual Energy Outlook 2014.* 2014. pp. 1-12, Tech. rep.
20. **IEA.** *Experience Curves for Energy Technology Policy.* 2000. ISBN: 92-64-17650-0.
21. **Carbon Trust; Black & Veatch.** *UK Tidal Current Resource and Economics Study.* 2011. p. 53, Tech. rep.
22. **Carbon Trust; Amec.** *UK Wave Resource Study.* 2012. Tech. rep.
23. **IEA.** *IEA Scoreboard 2009.* 2009. ISBN: 978-92-64-06377-8.
24. **Magagna, Davide, et al.** *Wave and Tidal Energy Strategic Technology Agenda.* 2014. Tech. rep.
25. **DTOcean.** *D3.4: Prediction of reliability and economics of the offshore electrical infrastructure with recommendations and guidelines for the environmental impacts of the proposed array configurations.* 2015.
26. —. *D4.6 Framework for the prediction of the reliability, economic and environmental criteria and assessment methodologies for Moorings and Foundations.* 2015.
27. —. *D5.6 Report on Logistical model for ocean energy array and considerations.* 2015.
28. **Douglas Westwood.** *Offshore Wind Assessment for Norway.* 2010. Tech. rep.
29. **DTOcean.** *D2.2 Pre-evaluation of array layouts, identified key parameters and their relevant ranges.* 2014.
30. *Tidal turbine array optimisation using the adjoint approach.* **Funke, Simon W, Farrell, Patrick E and Piggott, MD.** s.l. : Elsevier, 2014, Renewable Energy, Vol. 63, pp. 658-673.
31. *Optimal configurations of wave energy device arrays.* **Child, BFM and Venugopal, Vengatesan.** 16, s.l. : Elsevier, 2010, Ocean Engineering, Vol. 37, pp. 1402-1417.
32. *Layouts for Ocean Wave Energy Farms: Models, Properties, and Heuristic.* **Snyder, Lawrence V, Moarefdoost, M Mohsen and others.** 2014.
33. *Surrogate Based Design of a Mooring System for a Self-reacting Point Absorber.* **Ortiz, Juan P, et al.** 2015. International Society of Offshore and Polar Engineers.
34. *Layout Optimization of Wave Energy Converters in a Random Sea.* **Jia, G, et al.** 2015. International Society of Offshore and Polar Engineers.
35. *Wave Energy Converter Array Optimization: A Review of Current Work and Preliminary Results of a Genetic Algorithm Approach Introducing Cost Factors .* **Sharp, Chris and Dupont, Bryony.** s.l. : ASME/IEEE International Conference on Mechatronic and Embedded Systems and Applications (MESA), 2015.
36. *Wind turbine layout optimization using multi-population genetic algorithm and a case study in Hong Kong offshore.* **Gao, Xiaoxia, et al.** s.l. : Elsevier, 2015, Journal of Wind Engineering and Industrial Aerodynamics, Vol. 139, pp. 89-99.
37. *Distributed Genetic Algorithm for optimization of wind farm annual profits.* **Hou-Sheng, H.** 2007. pp. 418-423.

38. *Offshore wind farm layout optimization using mathematical programming techniques*. **Pérez, Beatriz, Mínguez, Roberto and Guanche, Raúl**. s.l. : Elsevier, 2013, Renewable Energy, Vol. 53, pp. 389-399.
39. *Interactions among multiple three-dimensional bodies in water waves: an exact algebraic method*. **Kagemoto, Hiroshi and Yue, Dick KP**. s.l. : Cambridge Univ Press, 1986, Journal of Fluid Mechanics, Vol. 166, pp. 189-209.
40. *A novel method for deriving the diffraction transfer matrix and its application to multi-body interactions in water waves*. **McNatt, J Cameron, Venugopal, Vengatesan and Forehand, David**. s.l. : Elsevier, 2015, Ocean Engineering, Vol. 94, pp. 173-185.
41. **Abramowitz, Milton and Stegun, Irene A**. *Handbook of mathematical functions: with formulas, graphs, and mathematical tables*. s.l. : Courier Corporation, 1964.
42. *A limited memory algorithm for bound constrained optimization*. **Byrd, Richard H, et al**. 5, s.l. : SIAM, 1995, SIAM Journal on Scientific Computing, Vol. 16, pp. 1190-1208.
43. **Speth, Raymond**. *mpl-streamlines*. [Online] copyright 2011, 2011. <https://github.com/speth/mpl-streamlines>.
44. *Viskosimetrische Untersuchungen an Lösungen hochmolekularer Naturstoffe. I. Mitteilung. Kautschuk in Toluol*. **Reiner, Markus and Schoenfeld-Reiner, R**. 1, 1933, Kolloid-Zeitschrift, Vol. 65, pp. 44-62.
45. *Power Law Exponents for Vertical Velocity Distributions in Natural Rivers*. **Lee, Hae-Eun, et al**. 2013, Engineering, Vol. 5, pp. 933-942.
46. **Jensen, N.O**. *A Note on Wind Generator Interaction*. Roskilde : Risø M-2411. Risø National Laboratory, 1983. 87-550-0971-9 / 0106-2840.
47. **Larsen, Gunner C**. *A Simple Wake Calculation Procedure*. Roskilde : Risø M-2760. Risø National Laboratory, 1988. 87-550-1484-4 / 0418-6435.
48. **Roc, Thomas, Conley, Daniel C. and Greaves, Deborah**. Methodology for Tidal Turbine Representation in Ocean Circulation Model. *Renewable Energy*. 2013, Vol. 51.
49. **Maganga, Fabrice, et al**. Experimental Characterisation of Flow Effects on Marine Current Turbine Behaviour and on its Wake Properties. *Iet Renewable Power Generation*. 2010, Vol. 4, 6.
50. *Methodology for tidal turbine representation in ocean circulation model*. **Thomas Roc, Daniel C. Conley, Deborah Greaves**. 2013, Renewable Energy Volume 51.
51. *Experimental characterisation of flow effects on marine current turbine behaviour and on its wake properties*. **F. Maganga, G. Germain, J. King, G. Pinon, and E. Rivoalen**. 2010, IET Renewable Power Generation, Volume 4, Issue 6, pp. P.498–509.
52. **Myers, Luke and Bahaj, A.S**. Experimental Analysis of the Flow Field around Horizontal Axis Tidal Turbines by Use of Scale Mesh disk Rotor Simulators. *Ocean Engineering*. 2010, Vol. 37, 2.
53. *A simple model for cluster efficiency*. **Kaltic, I., Hostrup, J. and Jensen, N**. 1986. Proceedings of the BWEA Conference.

54. *Comparison of different Wake Combination methods for Offshore wake modelling*. **Habenicht, Gerd**. Dansk : s.n., 2008. Forskningskonsortium for Vindenergi Program.
55. **Burton, Tony, et al.** *Wind Energy Handbook*. Chichester : John Wiley & Sons Ltd, 2008.
56. *Modelling of free surface proximity and wave induced velocities around an horizontal axis tidal stream turbine*. **Whelan, J., et al.** Porto : s.n., 2007. 7th European Wave and Tidal Energy Conference.
57. **Thomson, M. D. and McCowen, D.** *WG3WP4 D1 GH BLOCKAGE MODELLING*. s.l. : Garrad Hassan and Partners Limited, 2010.
58. **DTOcean.** *D3.3 Electro-mechanical aspects of components and offshore substation design/cost optimisation tool*. 2015.
59. *Evaluation of Various Technologies for Wave Energy Conversion in the Portuguese Nearshore*. **Silva, Dina, Rusu, Eugen and Guedes Soares, Carlos**. 2013. *Energies*. Vol. 6, pp. 1344-1364.
60. **Power, Pelamis Wave.** *Pelamis P-750 Wave Energy Converter*. US6476511, AU754950, ZA20012008, EP1115976B; other patents pending 104 Commercial Street, Edinburgh EH6 6NF, UK.
61. **The Scottish Government.** *Lewis Bathymetry*. *The Scottish Government*. [Online] [http://www.scotland.gov.uk/Topics/marine/science/MSInteractive/datatype/Bathymetry/data/Lewis bathymetry](http://www.scotland.gov.uk/Topics/marine/science/MSInteractive/datatype/Bathymetry/data/Lewis_bathymetry).
62. **Scottish Power Renewables.** *Sound of Islay Demonstration Tidal Array. Environmental Report. Non-Technical Summary*. [Online] http://www.scottishpowerrenewables.com/pages/sound_of_islay.asp.
63. **United Kingdom Hydrographic Office.** *INSPIRE Portal*. [Online] <http://aws2.caris.com/ukho/mapViewer/map.action>.
64. **Institute of Shipping Economics and Logistics.** *Offshore Wind Logistics as a competitive factor*. 2012.
65. *Planning Sustainable Maritime Logistics Concepts for the Offshore Wind Industry: A newly developed decision support system*. **Lange, Kerstin, Rinne, André, Haasis, Hans C.** Hamburg, Germany : s.n., 2012. 3rd International Conference on Computational Logistics.
66. **Neary, Vincent S., et al.** *Near and Far Field Flow Disturbances Induced by Model Hydrokinetic Turbine: ADV and ADP Comparison*. *Renewable Energy*. 2013, Vol. 60.
67. **Sandia National Laboratories.** *Sandia National Laboratories*. [Online] http://energy.sandia.gov/?page_id=16794.